OPTOGENETIC INVESTIGATION OF NEURONAL EXCITABILITY AND SENSORY-MOTOR FUNCTION FOLLOWING A TRANSIENT GLOBAL ISCHEMIA IN MICE

by

Yicheng Xie

Msc, The University of Missouri-Columbia, 2011

A DISSERTATION SUBMITTED IN PARTIAL FULFILLMENT OF

THE REQUIREMENTS FOR THE DEGREE OF

DOCTOR OF PHILOSOPHY

in

The Faculty of Graduate and Postdoctoral Studies

(Neuroscience)

THE UNIVERSITY OF BRITISH COLUMBIA

(Vancouver)

December 2015

Abstract

Global ischemia occurs during cardiac arrest and has been implicated as a complication that can occur during cardiac surgery. It induces delayed neuronal death in human and animal models, particularly in the hippocampus, while it also can affect the cortex. Other than morphology and measures of cell death, relatively few studies have examined neuronal networks and motor-sensory function following reversible global ischemia *in vivo*. Optogenetics allows the combination of genetics and optics to control or monitor cells in living tissues. Here, I adapted optogenetics to examine neuronal excitability and motor function in the mouse cortex following a transient global ischemia. Following optogenetic stimulation, I recorded electrical signals from direct stimulation to targeted neuronal populations before and after a 5 min transient global ischemia. I found that both excitatory and inhibitory neuronal network in the somatosensory cortex exhibited prolonged suppression of synaptic transmission despite reperfusion, while the excitability and morphology of neurons recovered rapidly and more completely. Next, I adapted optogenetic motor mapping to investigate the changes of motor processing, and compared to the changes of sensory processing following the transient global ischemia. I found that both sensory and motor processing showed prolonged impairments despite of the recovery of neuronal excitability following reperfusion, presumably due to the unrestored synaptic transmission. Interestingly, motor processing recovered faster and more completely than sensory processing. My results suggest a uniform suppression of synaptic transmission, both in excitatory and inhibitory network, despite the rapid recovery of neuronal excitability and morphology, following a global ischemia and reperfusion. This prolonged suppression of synaptic transmission might impede the recovery of sensory and motor processing with differential

severity. Besides, I extended tools for mesoscopic imaging using novel optogenetic sensors, including genetically encoded Ca^{2+} indicators - GCaMPs, and extracellular glutamate sensor - iGluSnFR. I found that iGluSnFR has fastest kinetics for reporting both sensory and spontaneous activity in the cortex, which can resolve temporal features of sensory processing that were not readily observed with GECIs. I suggest that iGluSnFR tools have potential utility in normal physiology, and neurologic pathologies in which abnormalities in glutamatergic signaling are implicated, such as stroke.

Preface

This dissertation is mainly based on works previously published:

The pioneer work was led by Shangbin Chen and was published in Journal of Neuroscience (a version of Chapter 2).

Chen, S., Mohajerani, M. H., Xie, Y., & Murphy, T. H. (2012). Optogenetic analysis of neuronal excitability during global ischemia reveals selective deficits in sensory processing following reperfusion in mouse cortex. ***The Journal of Neuroscience, 32*****(39), 13510-13519.**

Chapter 3 is based on a publication in the Journal of Neuroscience.

Xie, Y*., Chen, S*., Wu, Y., & Murphy, T. H. (2014). Prolonged deficits in parvalbumin neuron stimulation-evoked network activity despite recovery of dendritic structure and excitability in the somatosensory cortex following global ischemia in mice. ***The Journal of Neuroscience, 34*****(45), 14890-14900. (*Equal contributors).**

Chapter 4 is based on a publication in Journal of Cerebral Blood Flow & Metabolism.

Xie, Y., Chen, S., Anenberg, E., & Murphy, T. H. (2013). Resistance of optogenetically evoked motor function to global ischemia and reperfusion in mouse in vivo. ***Journal of Cerebral Blood Flow & Metabolism, 33*****(8), 1148-1152.**

A version of Chapter 5 has been accepted for publication by the Journal of Neuroscience.
Yicheng Xie, Allen W Chan, Alexander McGirr, Songchao Xue, Dongsheng Xiao, Hongkui

Zeng, and Timothy H. Murphy. Resolution of high-frequency mesoscale intracortical maps using the genetically-encoded glutamate sensor – iGluSnFR.

I conducted the majority of experimental procedures and data analysis, and wrote the draft of manuscripts for the optogenetic characterization of PV-neuronal excitability (Chapter 3) and motor mapping (Chapter 4) during a transient global ischemia, as well as mesoscopic cortical imaging with iGluSnFR (Chapter 5). I conducted experimental procedures and data analysis for the optogenetic characterization of cortical pyramidal neuronal excitability during a transient ischemia, and worked with former post-doctor Shangbin Chen to finish the submission and revision (Chapter 2). Jeff LeDue helped with microscopy set-up for imaging experiments. Pumin Wang helped with animal surgery. Cindy Jiang helped with the management of mouse colony. Dr. Jamie Boyd developed software used for operating previously designed hardware (Ayling et al., 2009). Dr. Timothy H. Murphy supervised the project, edited the published manuscripts, and provided materials and financial supports.

Approval for animal experiments was issued by the Animal Care Committee of the University of British Columbia (Protocols A09-0665 and A10-0140).

Table of Contents

List of Tables

List of Figures

List of Abbreviations

AAV: adeno-associated virus

APV: ((2R)-amino-5-phosphonovaleric acid

AMPA: a-amino-3-hydroxyl-5-methyl-4-isoxazole-propionate

ATP: adenosine triphosphate

CaMKII: Ca^{2+}/calcodulin-dependent protein kinase II

CAV2: canine adenovirus type 2

CCAO: common carotid arterial occlusion

CCD: charge-coupled device

ChR2: channelrhodopsin-2

CNS: central neuron system

COX2: cyclooxygenase 2

DAGs: diacylglycerides

DC: direct current

DNQX: 6,7-dinitroquinoxaline-2,3-dione

ECG: electrocorticography

EEG: electroencephalography

EMG: electromyogram

ET-1: endothelin-1

FL: forelimb

fMRI: functional magnetic resonance imaging

GABA: gamma-Aminobutyric acid

GCaMP: genetically encoded calcium indicator

GECI: genetically encoded calcium indicator

GEVI: genetically encoded voltage indicator

GFP: green fluorescent protein

HpHR: halorhodopsin

HEPE: (4-(2-hydroxyethly)-1-piperazineethanesulfonic acid

HL: hindlimb

ICMS: intracranial microstimulation

IL1: interleukin 1

IL6: interleukin 6

IL8: interleukin 8

iGluSnFR: intensity-based glutamate-sensing fluorescent reporter

IOS: intrinsic optical signal

iNOS: inducible NOS

LED: light-emitting diode

LFP: local field potential

M1: primary motor cortex

MCAO: middle cerebral artery occlusion

MCP1: monocyte chemoattractant protein 1

MEPs: motor evoked potentials

NMDA: N-methyl-D-aspartatic acid

NA: numerical aperture

PET: positron emission tomography

PV: parvalbumin

Thy1: thymocyte differentiation antigen 1 (promoter)

tPA: tissue plasminogen activator

TMS: transcranial magnetic stimulation

TNFα: tumor necrosis factor alpha

tTA: tetracycline-regulated trans-activator

TTX: tetrodotoxin

TTL: transistor-transistor logic

VSD: voltage sensitive dye

V1: primary visual cortex

sFL: somatosensory forelimb

sHL: somatosensory hindlimb

SNR: signal to noise ratio

Acknowledgements

I would like to thank the guidance and help from my advisor and committee members, and support from family. Without them, I could never accomplish what I have achieved during PhD study.

First of all, I would like to express deepest gratitude to my advisor – Dr. Timothy H. Murphy, for his excellent guidance, caring, patience, as well as supports with experimental ideas and materials. Moreover, I feel really grateful that Dr. Murphy has provided extra helps on my English writing. Next, I would like thank Dr. Yutian Wang, Brian MacVicar, and Kurt Haas for their valuable suggestions and criticisms on my proposal and scientific ideas during committee meetings, comprehensive exam, and private chat.

I would like to thank my colleagues – Dr. Allen Chan, Matthieu Vanni, Greg Silasi and Shangbin Chen for providing direct help to my experiments, analysis, and manuscript preparation. I would like to also thank the staffs in the lab – Jeff LeDue and Jamie Boyd for providing assistance in optical set-up, and Pumin Wang and Cindy Jiang for assistance in animal surgery and management.

Last but not least, Canadian Institutes of Health Research (CIHR) provides me excellent financial supports for experimental and living expenses (Vanier Canada Graduate Scholarship). I also want to thank the University of British Columbia for providing the Four Year Fellowship, International Tuition Scholarship, and also for providing the beautiful working environment!

Dedication

I dedicate this thesis to my family for nursing me with affections and love and their dedicated partnership for success in my life.

Chapter 1: General Introduction

1.1 Stroke

1.1.1 Etiology of Stroke and Its Complications

Stroke is the 2nd leading cause of death in the world (World health Organization 2014). It is a leading cause of serious long-term disability (Mozaffarian et al., 2014), particularly in elderly people. Stroke is caused by the interruption of blood flow to the brain (ischemic stroke) or the rupture of blood vessels in the brain (hemorrhagic stroke). The majority (87%) of stroke incidences are ischemic. Other forms of stroke include hemorrhagic stroke and transient ischemic attack (TIA) (Mozaffarian et al., 2014). The most common ischemic strokes include thrombotic stroke, in which a blood clot forms in one of the arteries that supply blood to the brain; and embolic stroke, in which a blood clot or other debris forms away from the brain – usually in the heart. In ischemic stroke, the loss of blood flow restricts the supply of oxygen and nutrition (e.g., glucose) to the affected areas in the brain, leading to the loss of synaptic connection and, eventually cell death (Dirnagl et al., 1999; Lo et al., 2003; Lai et al., 2014). Depending on the location and the severity of stroke in the brain, behavioral complications may occur, including paralysis or loss of muscle movement, difficulty talking or swallowing, emotional problems, pain or other subtle behavioral changes (Mercier et al., 2001; Murphy and Corbett, 2009; Godefroy, 2013; Mozaffarian et al., 2014).

1.1.2 The Importance of Stroke Study

In Canada, the financial costs of stroke are ~$3.6 billion a year in physician services, hospital costs, lost wages and decreased productivity (Dai et al., 2009), substantially increasing burden on communities and families (Bhogal et al., 2015). Despite stroke studies having been performed for decades, no cure has been found for stroke. Great efforts and financial investments have been put into drug development with the hope of improving stroke outcomes: the estimated cost for a stroke drug development is $14-64 billion (Howells et al., 2012). However, out of 1,026 experimental treatments in acute stroke, only 3 improved outcome in clinical trial (O'Collins et al., 2006). Four acute interventions are of proven benefit (Donnan et al., 2008), including intravenous thrombolysis, oral aspirin, patient care, and decompressive hemicraniectomy. Currently, the only FDA approved treatment for ischemic strokes is tissue plasminogen activator (tissue plasminogen activator (tPA)), which works by dissolving the clot and improving blood flow to the part of the brain with ischemia (Hacke et al., 1995; Wang et al., 1998). Unfortunately, it has to be applied within the first 4.5 hour after stroke symptom starts; as most patients do not arrive at the hospital within this window, only a minority of patients (< 5%) are eligible to receive the treatments (Lansberg et al., 2009). Rehabilitation can substantially improve post-stroke recovery by enhancing brain plasticity, in which the intact brain tissue may adopt the function of damaged brain regions (Murphy and Corbett, 2009). However, the outcome of rehabilitation following stroke is still variable (Duncan, 2013), and the underlying biological mechanisms are still not fully understood (Murphy and Corbett, 2009). Mechanistic knowledge is still missing regarding how the brain responds to stroke. Most of the current data are not acquired from *in vivo* preparations, in which the brain circuits are intact, or are lacking temporal

and spatial resolution for precise measures, making the mechanistic basis for developing stroke treatment unclear.

1.1.3 General Pathophysiology of Ischemic Stroke

The brain accounts for 2% of the total body weight, but consumes 25% of the glucose and 20% of the total oxygen budget (Attwell and Laughlin, 2001; Hofmeijer and van Putten, 2012). The majority of metabolic support for the brain is provided by oxidative metabolism. Consequently, the brain is very sensitive to disruption in its oxygen and glucose supply, making an ischemic stroke devastating to its function. This is because failure of synthesis of adenosine triphosphate (ATP) and other nucleoside triphosphates (such as cytidine triphosphate and uridine triphosphate) (Astrup et al., 1981) threatens cell survival in three ways. First, in the absence of an adequate energy source, anaerobic glycolysis is stimulated, leading to intra- and extracellular acidosis (Astrup, 1982; Levine et al., 1988; Doyle et al., 2008). This is a potential threat to the viability or recovery of ischemic tissue (Siesjö, 1988). Second, the disruption of ion homeostasis may threaten the survival of ischemic tissue (Hansen and Nedergaard, 1988; Katsura et al., 1993; Yu et al., 2001), particularly, the increases in extracellular glutamate concentration activates glutamate receptors, further leading to dramatic increases in intracellular Na^+, Ca^{2+} and Cl^- with osmotically obligated water (Astrup et al., 1977; Dirnagl et al., 1999) or swelling of neurons by opening non-aquaporin channels to water (Andrew et al., 2007). Last but not least, energy failure may threaten the structural integrity of the cell. Given high-energy phosphates are required to support resynthesis of micromolecules and macromolecular assemblies following their spontaneous or enzyme-catalyzed degradation, loss of ATP leads to the breakdown of cell

structure. For example, ATP failure leads to proteolytic cleavage of components of the cytoskeleton, such as microfilaments and microtubule, and their anchorage of the cell membrane (Lemasters et al., 1987; Molitoris, 1991; Kellerman and Bogusky, 1992; Zhang et al., 2005; Murphy et al., 2008). Moreover, ATP failure also can lead to the degradation of phospholipids, with the accumulation of breakdown products such as lysophospholipids, diacylglycerides (DAGs), and free fatty acids, including arachidonic acid (Bazan, 1976; Paller et al., 1984; Bazan et al., 1991; Schousboe, 2014). Many of the degradation enzymes are activated by Ca^{2+} signaling, thus, the breakdown of structure is due both to a loss of ATP and to an upregulation of Ca^{2+} concentration (Kristián and Siesjö, 1998; Szydlowska and Tymianski, 2010). Furthermore, high Ca^{2+}, Na^{+} and ADP levels in ischemic cells stimulate excessive mitochondrial oxygen radical production and death signaling pathways, causing further cell dysfunction and tissue damage (Dirnagl et al., 1999; Lee et al., 1999; Raha and Robinson, 2000; Lai et al., 2014). After the onset of blood vessel occlusion, ischemic injury also rapidly triggers inflammatory cascades that further amplify tissue damage (Allan and Rothwell, 2001; Macrez et al., 2011). As reactive microglia, macrophages and leukocytes are recruited into the ischemic brain, inflammatory mediators are generated by these cells or by neurons and astrocytes. Among these, inducible NOS (iNOS) (Iadecola et al., 1997), cyclooxygenase 2 (COX2) (Iadecola et al., 1999), interleukin 1(IL1) (Beamer et al., 1995), and monocyte chemoattractant protein 1 (MCP1) (Hughes et al., 2002) have crucial roles. Around 12-24 h after stroke, chemokines and cytokines are expressed (e.g., IL1, IL6, IL8, TNFα, MCP1 etc.) (Macrez et al., 2011). Inflammatory cascades stimulate both detrimental and potentially beneficial pathway after ischemia, and has been targeted as novel therapeutic strategies (Macrez et al., 2011).

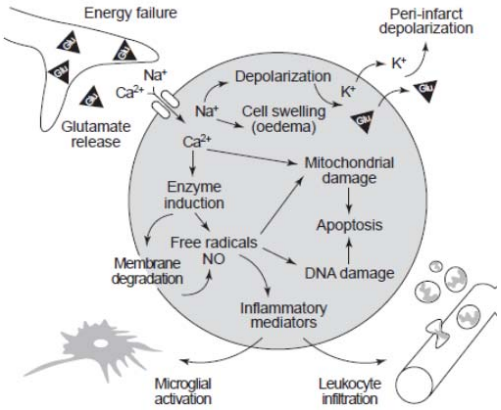

Figure 1.1 Simplified overview of pathophysiological mechanisms in the ischemic brain.

Energy failure leads to the depolarization of neurons. Activation of specific glutamate receptors dramatically increases intracellular Ca^{2+}, Na^{+}, Cl^{-} levels while K^{+} is released into the extracellular space. Diffusion of glutamate (Glu) and K^{+} in the extracellular space can propagate a series of spreading waves of depolarization. Water shifts to the intracellular space *via* osmotic gradients and cells swell (edema) (Andrew et al., 2007). The universal intracellular messenger Ca^{2+} overactivates numerous enzyme systems (proteases, lipases, endonucleases, etc.). Free radicals are generated, which damage membranes (lipolysis), mitochondria and DNA, in turn triggering mediators, which activate microglia and lead to the invasion of blood-borne inflammatory cells (leukocyte infiltration) *via* upregulation of endothelial adhesion molecules. From (Dirnagl et al., 1999), reprint with permission from Elsevier.

1.1.4 Transient Global Ischemia

1.1.4.1 Transient Global Ischemia Leads to Brain Dysfunction

Transient global ischemia occurs during cardiac arrest and has been implicated as a complication that can occur following cardiac surgery (Block, 1999). The persistence of unfavorable neurologic outcomes led the American Heart Association to recognize brain injury following transient global ischemia as an important area for clinical research (Geocadin et al., 2008). Human patients who have suffered global ischemia through cardiac arrest or cardiac surgery could putatively develop brain deficits, including memory, motor and sensory, and variable executive impairment (McKhann et al., 1997; Lim et al., 2004). Cardiac arrest or cardiac surgery-induced global ischemia could not only result in sensory and motor dysfunction (Gerlai et al., 2000; Lim et al., 2004; Madl and Holzer, 2004), but also could cause many psychiatric and cognitive disorders, including depression and cognitive decline (McKhann et al., 1997; Lim et al., 2004). Indeed, brief periods of cerebral ischemia can lead to forms of dementia that are associated with switching patients to temporary bypass (Roach et al., 1996). Other conditions with brief recurrent ischemia would be chronic sleep apnea, and transient ischemic attack, both of which are associated with progressive vascular dementia (Roach et al., 1996). However, more than 2 decades of clinical trials failed to demonstrate benefit from a number of putative neuroprotective strategies (Geocadin et al., 2008), except hypothermia (Nolan et al., 2003; Holzer et al., 2005).

When the transient global ischemia occurs, the entire brain is subjected to a transient period of complete ischemia followed by a reperfusion. Human imaging studies suggested structural

damage, particularly in the hippocampus, can be observed in the patients experienced cardiac arrest (Petito et al., 1987; Fujioka et al., 2000; Greer et al., 2011), which putatively leads to later memory impairment (Squire, 1992; Grubb et al., 1996; O'Reilly et al., 2003). In rodent models of transient global ischemia, a delayed neuronal death in the hippocampal CA1 has been confirmed (Pulsinelli and Brierley, 1979; Kirino, 1982; Zola-Morgan et al., 1986). Though the cortical neurons are relatively resistant to the global ischemia-induced cell death (Crain et al., 1988), our lab has previously shown their fine structures such as dendrites, axons, and spines could still be damaged shortly after the onset of global ischemia, but can recover following reperfusion (Murphy et al., 2008; Liu and Murphy, 2009). These morphological injuries may lead to functional disability following transient global ischemia in rodents, including deficits in motor-sensory function and cognitive function (Block, 1999). Using *in vivo* or *in situ* intracellular recording, other labs identified that the excitability of CA1 pyramidal neurons and striatal large aspiny neurons is depressed following transient global ischemia, along with the depression of their neurotransmitter release (Xu and Pulsinelli, 1994; Pang et al., 2002). While these studies have been important in demonstrating the effects of global ischemia, these techniques are difficult to conduct; and maintaining recording over a long period of time is almost impossible. Moreover, their invasiveness may confound findings.

Questions remain for continuing study of the pathophysiological processes involved in the brain damage during a transient global ischemia. Contradictory evidence suggests that brain injury following transient global ischemia is associated with reperfusion (White et al., 1996), during which a wide and complex inflammatory responses initiates, aggravating injury (Lo et al., 2003). Although we and others have shown that reperfusion is beneficial for the structural and

functional recovery (Xu and Pulsinelli, 1994; Murphy et al., 2008; Liu and Murphy, 2009), whether it can restore neuronal excitability and synaptic activity has not been tested *in vivo*. In addition to the recovery of sensory responses in the brain (Hossmann et al., 1987; Murphy et al., 2008), motor function following a transient global ischemia also has not been investigated in acute phase. On the other hand, pyramidal neurons in hippocampal CA1 have been shown to be more susceptible to damage following a transient global ischemia (Pulsinelli and Brierley, 1979; Pulsinelli et al., 1982), whereas PV neurons in the same region exhibit higher resistance (Nitsch et al., 1989). This phenomenon is known as "selective vulnerability" (this term also refers to selective spatial vulnerability in the brain). Their structural and functional susceptibility has not been tested and compared in acute phase following a transient global ischemia due to a lack of tools. The cortex also contains these two types of neurons (Celio, 1990). By adapting newly developed optogenetic tools, we will be able to monitor and compare the structural and function of cortical pyramidal neurons and PV neurons following a transient global ischemia. This new knowledge may provide a fundamental basis for a rational approach to "transient global ischemia" that will allow substantial amelioration of the often dismal neurologic outcome associated with cardiac arrest or cardiac surgery.

1.1.4.2 A Rodent Model of Reversible Global Ischemia

To study the functional consequence during and after transient global ischemia, rodent models have been established (Hossmann, 1971; Nemoto et al., 1975; Pulsinelli and Brierley, 1979; Pulsinelli et al., 1982). In mice, global ischemia is induced by occluding common carotid arteries and/or basilar artery; and reperfusion is achieved by releasing the occluding sutures (Pulsinelli et

al., 1982; Traystman, 2003). In additional to its relevance to the brain damage associated with cardiac arrest or cardiac surgery, this model is also desirable because it is convenient to incorporate with imaging and electrophysiological recording (Murphy et al., 2008; Xie et al., 2013). The susceptibility to global ischemia model in mice is strain-dependent and can be variable between individuals (Fujii et al., 1997). After induction of global ischemia in gerbils, blood flow in the cortex and hippocampal CA1 region decreases to ~10% and ~20%, respectively, and both returned to pre-ischemic level within 10 min (Kuroiwa et al., 1992). C57Black/6 mice, which are the background strain of many genetically engineered mice and the mice that are used in this body of research, are especially susceptible to global ischemia due to an incompletely formed circle of Willis (Fujii et al., 1997). In C57Black/6 mice, bilateral occlusion of common carotid arteries reduced cerebral blood flow to 10 to 20% of the pre-ischemic level (Fujii et al., 1997). Occlusion of the basilar artery, along with the bilateral occlusion of common carotid arteries, further lowered the cerebral blood flow to less than 10%. Reperfusion following 14 min of this global ischemia recovered cerebral blood flow to 80% of baseline value (Yonekura et al., 2004). Bilateral occlusion of common carotid arteries in our hands reduced > 95% blood flow in the somatosensory cortex, and reperfusion rapidly and almost completely recovered the blood flow, revealed by a measure of red blood cell velocity using two-photon imaging (Murphy et al., 2008). These results validate the usage of bilateral occlusion of common carotid arteries as a reversible global ischemia model that can be used to study the cortical neuronal excitability, synaptic function, as well as motor and sensory function associated with transient global ischemia-induced damage which could occur during cardiac arrest or cardiac surgery.

1.2 Brain Excitability and Its Alterations after Transient Ischemia

1.2.1 Assessing Brain Excitability

Neurons are electrically excitable, owing to the presence of voltage sensitive ion channels in the neuronal plasma membrane, including selective Na^+, K^+, Cl^-, or Ca^{2+} channels. The excitability of neurons is influenced by the nature of their ion channels, the density of ion channels in their surface membranes, and the location of ion channels in the different functional compartments of the cell (Catterall, 1984). The terminology of "brain excitability" is not definitive, and can be considered as a summation of neuronal excitability and network function responding to certain stimulations. Despite the uncertain definition, measures of brain excitability have been intensively used in human and animals studies, reflecting brain function following brain plasticity paradigms or brain diseases. In humans, transcranial magnetic stimulation (TMS) and transcranial direct current stimulation (tDCS) have been developed as valuable research tools and can be used to study brain excitability noninvasively when it combined with proper readouts, such as EEG, EMG, or fMRI (Ilmoniemi et al., 1998; Hallett, 2000; Antal et al., 2011; Pascual-Leone et al., 2011; Brunoni et al., 2012). In animal studies, integration of stimulations (e.g., electrical stimulation, sensory stimulation, optogenetic stimulation, etc.) and readouts (EEG, EMG, imaging, etc.) have been used to assess brain excitability following brain plasticity or brain diseases (Murphy and Corbett, 2009; Lim et al., 2013). Assessing brain excitability following brain diseases, such as stroke, is informative given the changes in the physiological responsiveness of the brain networks occur at the same time as alterations in neuronal excitability and synaptic functions, and direct measures of neuronal excitability, particularly in a

defined neuronal population (e.g., excitatory neuron or inhibitory neuron) or especially in a single neuron is difficult to be conducted in animal models and cannot be performed in human studies.

1.2.2 Brain Excitability after Transient Global Ischemia

1.2.2.1 Neuronal Excitability after Transient Global Ischemia

Transient global cerebral ischemia results in neuronal death in certain brain regions. For instance, CA1 pyramidal cells in the hippocampus and medium-sized spiny neuron in the neostriatum are highly sensitive to ischemic insults (Pulsinelli and Brierley, 1979). Although other neurons in the same regions, such as hippocampal CA3 pyramidal neurons and striatal cholinergic interneurons, are relatively resistant to transient ischemia (Pulsinelli and Brierley, 1979; Koh et al., 1996), differential alterations of neuronal excitability have been observed in particular type of neurons (Deng and Xu, 2009). Similarly, cortical neurons are also relatively resistant to the transient ischemia-induced cell death (Pulsinelli and Brierley, 1979; Pulsinelli et al., 1982); however, these neurons may still exhibit alterations of neuronal excitability that may contribute to functional deficits. Early studies suggest that a terminal depolarization in cortical steady potential and large increases in electric impedance occur following transient cerebral ischemia in the cat brain (Hossmann, 1971). Direct electrical stimulation and EEG recording in the somatosensory cortex suggest a suppression of neuronal responses in the cortex after the onset of terminal depolarization, and is reversible upon the normalization of cortical impedance and steady potential following reperfusion (Hossmann, 1971). These results have been further confirmed by *in vivo* imaging at cellular resolution, indicating that the loss of structural integrity,

and the elevation of cellular Ca^{2+} signals and mitochondria membrane potential are coincident with the occurrence of ischemic depolarization, and are reversible with the normalization of ischemic depolarization following reperfusion (Li and Murphy, 2008; Liu and Murphy, 2009). Like in the hippocampus, differential alterations of neuronal excitability responding to a transient ischemia in particular cortical neuronal population may exist. Unfortunately, current results lack cell type specificity, thereby the remaining question needs to be further investigated.

1.2.2.2 Sensory and Motor Processing after Transient Global Ischemia

Although the cognitive deficits after global ischemia are well characterized (McKhann et al., 1997; Lim et al., 2004), the motor and sensory deficits have been more difficult to quantify. None the less, it may be important to identify motor deficits (even if small or transient), because the cognitive tests in rodents (e.g., water maze) all require motor output from the animals, and previous studies have demonstrated that motor impairments can also produce deficits in these "cognitive" tests. Previously, a neurological score has been described to assess motor-sensory function following a 30 min transient global ischemia in rats (Capdeville et al., 1985). This score tests for several functions - grasping, several placement reactions, righting reflexes, two equilibrium tests, flexion reflex and spontaneous motility. Before ischemia, a normal rat will receive a total score of 20, indicating normal motor-sensory function. One hour after ischemia this score is reduced by 50%, and deficits can be observed in all the tests. At 3 h following ischemia a further reduction in this score can be observed, indicating severe impaired motor-sensory function. At 24, 48 or 72 h after ischemia no difference to the pre-ischemic score exists. Another motor score has been developed to assess the motor function following a 20 min global

ischemia (Combs and D'Alecy, 1987). It consists of three tests, including a screen test which serves as an indicator of general muscle strength, a balance beam test and a prehensile–traction test which both give a measure of equilibrium and muscle strength. Application of this motor score reveals a deficit in ischemic animals at 24 h after ischemia, but not later on (Combs and D'Alecy, 1987; Gionet et al., 1991). Based on the two neurological tests applied to animals with global ischemia, it seems that global cerebral ischemia does not result in long-lasting motorsensory deficits. More direct and presumably more precise assessments of motorsensory function following transient global ischemia consist of direct sensory stimulation and measures of cortical responses (Hossmann et al., 1987; Murphy et al., 2008), and direct electrical stimulation and measures of spinal cord or muscle responses (motor evoked potentials (MEPs)) *in vivo* (Konrad et al., 1987). Although the duration of global ischemia varies across different studies, the motor-sensory function shows a similar pattern that is suppressed during the onset of ischemia, and is more or less recovered hours after reperfusion (Konrad et al., 1987; Murphy et al., 2008). These results suggest a dynamic change of motor-sensory function following a transient global ischemia; thus the temporal and spatial resolution of functional assessment is critical to uncover the rapidly changed pattern; so that these results can be associated with the analysis of neuronal excitability. Moreover, the possible subtle and reversible changed motor function following transient global ischemia requires less invasive techniques, other than direct electrical stimulation (Konrad et al., 1987; Nudo et al., 1996), to avoid complicating findings.

1.3 Optogenetic Tools for Investigating Brain Excitability after Cerebral Ischemia

1.3.1 Optogenetic Activators and Inhibitors

The idea of using light to selectively controlling precise neuronal activity patterns within targeted brain cells was articulated by Francis Crick (Crick, 1979). The motivation behind this idea was to precisely control activity in one cell type while leaving the others unaltered, which cannot be achieved by conventional electrodes stimulation (Crick, 1979). Boris Zemelman and Gero Miesenbock first expressed drosophila rhodopsin photoreceptors for photo-activation in cultured mammalian neurons (Zemelman et al., 2002). In 2005, Karl Deisseroth's laboratory further improved the photo-activation system using channelrhodopsin (ChR), a single-component light-activatable cation channel (Nagel et al., 2002, 2003), to precisely control neuronal activity with light at millisecond level in cultured neurons (Boyden et al., 2005) and in living animals (Adamantidis et al., 2007). ChRs are from a subfamily of retinylidene proteins (rhodopsin) and were found in *Chlamydomonas reinhardtii* (Nagel et al., 2003). It has seven-transmembrane proteins like rhodopsin, and contains the light-isomerizable chromophore all-*trans-retinal* (Figure 1.2). The retinal chromophore is covalently linked to the rest of the protein through a protonated Schiff base (Kato et al., 2012). ChR2 directly form ion channels (ionotropic) that is permeable to cations (Feldbauer et al., 2009), making cellular depolarization extremely fast, robust, and useful for bioengineering and neuroscience applications. ChR2 can be light-activated at a peak excitation wavelength of ~470 nm with a unitary conductance of ~50 fS (Nagel et al., 2003; Lin, 2011).

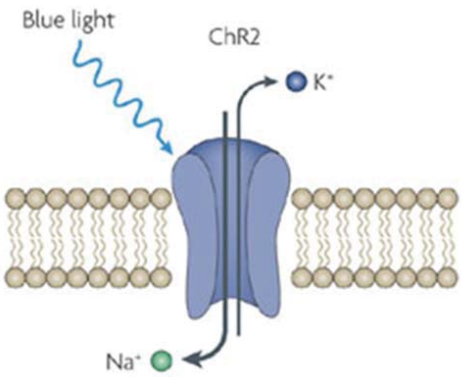

Figure 1.2 Light-gated cation channel - Channelrhodopsin-2

Channelrhodopsin-2 is a light-gated cation channel native to the green alga *Chlamydomonas reinhardtii*. It consists of seven transmembrane proteins and absorbs blue light through its interaction with retinal. Photoisomerization of retinal opens the channel to sodium ions, which have a higher concentration outside than inside the cell. From (Zhang et al., 2007a). Reprint with permission from Nature Publishing Group.

On the other hand, direct light-triggered inhibition of electrical activity (precisely timed hyperpolarization) can be achieved *via* expression of the halorhodopsin (NpHR) or microbial proton pumps *in vivo* (Han and Boyden, 2007; Zhang et al., 2007b; Chow et al., 2010). Recent modification of optogenetic tools have improved their light sensitivity, conductance (Zhang et al., 2007b), trafficking for membrane expression (Zhao et al., 2008; Gradinaru et al., 2010), broadened the selection of light wavelength for activation (Lin et al., 2013; Klapoetke et al., 2014), as well as decreased their desensitization during prolonged light illumination (Lin et al., 2009; Lin, 2011). This collection of tools, along with the development of versatile devices to

deliver light *in vivo* (Adamantidis et al., 2007; Aravanis et al., 2007; Gradinaru et al., 2007; Anikeeva et al., 2011), has enabled widespread application of optogenetics.

1.3.2 Optogenetic Sensors for Imaging Brain Activity

In contrast to synthetic dyes, genetically encoded biosensors provide ways to monitor neuronal activities at cellular and subcellular resolution over long periods of time. They can also be readily delivered to specific cell types. The most well-developed and widely used genetically encoded biosensors are calcium indicators; other biosensors include voltage indicators, pH sensors, and transmitter sensors.

Genetically encoded calcium indicators: Two types of genetically encoded calcium indicators (GECIs) were generated for monitoring the intracellular calcium signals in neurons (Mank et al., 2008; Tian et al., 2009): One is based on a calcium-induced change in the fluorescence level of a single XFP (e.g., GCaMPs). The other is based on Förster resonance energy transfer (FRET; e.g., YC3.60), in which calcium binding induces a conformational change of the calcium binding protein that brings two XFP domains close enough to allow FRET to occur. Recently, Looger's group at Janelia farm has been making great efforts to advance the field with the improved GCaMPs (e.g., GCaMP6 series) (Chen et al., 2013b). GCaMPs are generated from a fusion of green fluorescent protein (GFP), calmodulin, and M13, a peptide sequence from myosin light chain kinase. In GCaMPs, GFP is circularly permutated, creating a new terminus in the middle of the protein. Fused to the new terminus is calmodulin (CaM) and the M13 domain of a myosin light chain kinase (Figure 1.3). CaM is a symmetrical, hinge-like protein that binds to four calcium ions. When calcium is present, CaM undergoes a conformational change, and the hinge

region is able to bind helical peptide chains on M13. In the absence of calcium, the circularly permutated fluorescent proteins exist in a poorly fluorescent state due to a water pathway that enables protonation of the chromophore and poor absorbance at the excitation wavelengths. Ca^{2+} binding to the calmodulin moiety results in a structural shift that eliminates this solvent pathway, rapid de-protonation of the chromophore, and bright fluorescence (Akerboom et al., 2009; Ding et al., 2014).

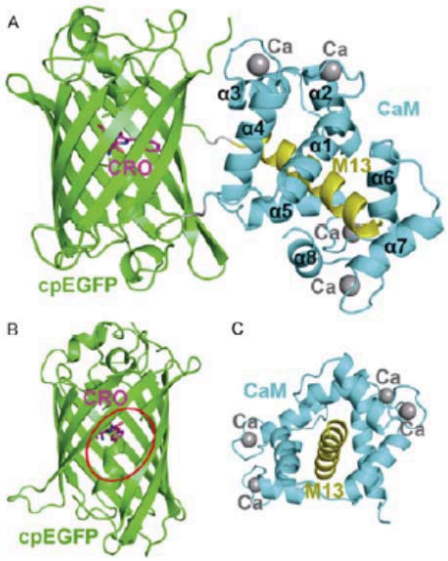

Figure 1.3 Structure of GCaMP6m monomer.

(A). Overall structure of GCaMP6m in cartoon scheme. (B). Side view of cpEGFP in GCaMP6m. the entrance on the surface of cpEGFP is highlighted in red circle. From (Ding et al., 2014) (open access).

Genetically encoded voltage indicators: Series of genetically encoded voltage indicators (GEVIs) have been generated. However, the performance of GEVIs has lagged behind that of

GECIs, due to the lower levels of signal, making these sensors more useful for wide-field imaging (Akemann et al., 2010, 2012). The most advanced version of GEVIs is the VSFP series, in which a voltage-sensitive domain is linked to a fluorescent protein or pair of proteins (FRET-based). VSFP2.3 and VSFP-Butterfly detect electrical responses in both brain slices and in vivo (Akemann et al., 2010, 2012). Moreover, alternative types of voltage-sensing fluorescent proteins have been recently developed, including PROPS (Kralj et al., 2011), Arch (Kralj et al., 2012), and ArcLight (Jin et al., 2012). However, their functionality has yet to be demonstrated *in vivo*.

Genetically encoded transmitter indicators: Other genetically encoded indicators have been developed to monitor neurotransmitter release, vesicular release, pH value, or even intracellular signaling and metabolism (Tantama et al., 2012; Huang and Zeng, 2013). We are more interested in the indicators that can monitor the neurotransmitter release given the abnormality of neurotransmitter release or uptake has been proven to induce neuronal death through excitotoxicity or prevent functional recovery during ischemia (Choi and Rothman, 1990; Clarkson et al., 2010). One recently developed glutamate sensor, iGluSnFR, has demonstrated a high SNR and amenability to fast *in vivo* imaging (Marvin et al., 2013). iGluSnFR is an intensity-based glutamate-sensing fluorescent reporter with SNR and kinetics appropriate for *in vivo* imaging. *Escherichia coli* gltI, encoding the periplasmic component of the ABC transporter complex for glutamate and aspartate, has been genetically constructed to fuse with circularly permutated (cp) iGluSnFR (Figure 1.4). iGluSnFR is superior over the previous versions of glutamate sensors (e.g., SuperGluSnFR) (Hires et al., 2008; Marvin et al., 2013), and is bright and photostable, with 4.5 $(\Delta F/F)_{max}$ in cell culture. In the presence of glutamate, conformational

changes restore the distorted cpGFP β-barrel (Figure 1.4) to make it fluorescent (Marvin et al., 2013). iGluSnFR is readily suitable to be applied in *in vivo* preparations and works robustly for long-term imaging with high sensitivity and kinetics in various species (Marvin et al., 2013). In addition, bacteria express periplasmic binding protein for GABA, acetylcholine (Nguyen et al., 2010), glycine, and a number of other relevant molecules, it is likely that sensors based on these molecules will produce the most direct read-outs. The usage of genetically encoded neurotransmitter sensor imaging enables real time monitoring of the dynamics of neurotransmitters that are associated with brain plasticity or brain diseases in living animals. Compared to conventional neurotransmitter measures, such as microdialysis or electrochemical sensors, genetically encoded neurotransmitter sensor imaging exhibits high temporal and spatial resolution. Moreover, it is inexpensive and relatively non-invasive.

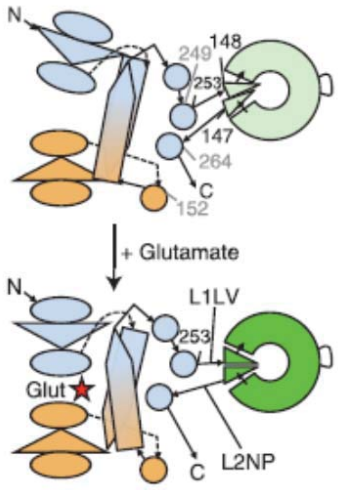

Figure 1.4 Schematic of GltI-cpGFP insertion.

Residues from both domains (blue and orange) contribute to the binding site for glutamate. The polypeptide chain starts in the N-terminal domain (blue), passes into the C-terminal domain (orange) and continues back through two β-strands (long pointed shapes) and into a series of helices (circles). After residue GltI253 (or other residues, identified in gray for 'failed' sensors), the polypeptide chain enter cpGFP at strand7 (GFP residue 148), runs through cpGFP and exits (last GFP residue 147) to region the remainder of GltI. The open (top), ligand-free state of the construct is dim, presumably because of distortion of the cpGFP β-barrel (tilted triangles). Binding of glutamate (star) induces a conformational change. The closed (bottom) state is bright, presumably owing to the restoration of the β-barrel. From (Marvin et al., 2013), reprinted with permission from Nature Publishing Group.

1.3.3 Techniques for Genetic Targeting

In neuroscience, genetic tools have the inherent potential to achieve appropriate spatiotemporal resolution and cellular molecular specificity, making it possible to observe and perturb the cellular activity and their interactions within circuits (Huang and Zeng, 2013). In combination with the newly developed markers (e.g., GFP), sensors (e.g., GCaMPs), or manipulators (e.g., ChR2) (Fenno et al., 2011; Tantama et al., 2012; Tian et al., 2012), molecular biology has made it possible to systematically design and tailor experiments to answer specific problems in the field of neuroscience, and is especially applicable for the field of stroke research/stroke recovery. Particularly, our question regarding the selective neuron vulnerability following transient ischemia can be tackled with the help of cell-population targeting for two-photon imaging of their structure, or for precise stimulation for assessing their excitability and synaptic activity.

Cell population targeting: Cell-type identification is central to the study of neural circuits (Gong et al., 2003). The debate over how to define neuronal cell types remains unresolved (Nelson et al., 2006; Bota and Swanson, 2007). A partial list of the criteria that have been used to classify neurons includes developmental genetic origin, precise location, morphology, connectivity, neurotransmitter content(s), physiological properties, and functional role in circuits and behavior (DeFelipe et al., 2013).

In vertebrate nervous systems, neurons often show stereotyped and tightly correlated lineage, location, connectivity, and function (Gong et al., 2003; Nelson et al., 2006; DeFelipe et al., 2013). However, defining cell types becomes increasingly challenging in more complex circuits, especially those of the cerebral cortex (DeFelipe et al., 2013). For example, although the basic division between glutamatergic excitatory neurons and GABAergic inhibitory neurons is well recognized, there are likely dozens of subclasses of excitatory and inhibitory cortical neurons (DeFelipe et al., 2013). Much of the current confusion may stem from our incomplete knowledge of the comprehensive properties of different cell populations (DeFelipe et al., 2013).

Genetic targeting is arguably the best strategy to establish reliable experimental access to specific cell populations (Madisen et al., 2010; Taniguchi et al., 2011). With this approach, one can operationally define cell types and then explore their biological basis within the context of the neural circuit. We now understand that unique gene expression profiles likely reflect and contribute to cell phenotypes, which can be used to distinguish different cell populations (Gong et al., 2003; Madisen et al., 2010). A combination of different genetic and viral strategies is often necessary to be combined to achieve specific targeting (Huang and Zeng, 2013). In the current

study, we have targeted cortical excitatory neurons and PV neurons with various genetic and viral strategies to achieve precision on the targeting of cell population and brain regions with high-efficiency on transgene expression.

Recombination-based gene-targeting system: The bacterial phage-derived Cre recombinase and its loxP recognition site compose the best-established binary system, allowing for versatile and efficient activation and inactivation of gene expression (Figure 1.5) (Nagy, 2000). In particular, a reporter allele can be driven by a strong and ubiquitous promoter but is interrupted by a transcription STOP cassette flanked by loxP sites. A selective Cre driver can activate the reporter in the desired cell types (Nagy, 2000). An increasing number of reporter lines, many at the Rosa26 locus, have been generated that conditionally express markers, sensors, and transducers (Madisen et al., 2010). An important advance was the invention of the Ai9 reporter and its variants, generating high level expression of tool genes sufficient for in vivo imaging and physiology studies (Madisen et al., 2010, 2012).

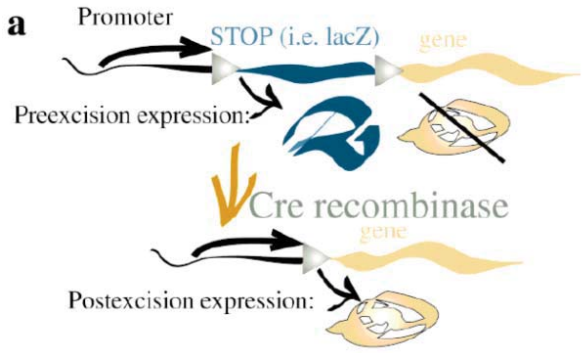

Figure 1.5 Cre recombinase conditional transgenesis.

A simple strategy for conditional transgene activation. Transgene activation region if both Cre and the conditional transgene are under the control of lineage/cell type-specific promoters. From (Nagy, 2000), reprinted with permission from Wiley.

Taking advantages of the available Cre driver lines (Madisen et al., 2010) and the Cre-dependent transgenic lines (Madisen et al., 2015), we have reproduced transgenic GCaMPs and iGluSnFR mice that highly express the genetically encoded activity indicators in the cortex with neuron population specificity. Being superior to the non-specific cell labeling during VSD imaging, the cell population specific targeting of genetically encoded activity sensors enables the direct readouts of neuronal activity from a defined neuronal population (e.g., excitatory neurons, or inhibitory neurons) during mesoscopic cortical imaging. In addition, PV-Cre transgenic mice were used for targeting ChR2 and tdTomato expression in PV neurons in the somatosensory cortex with AAV viral transduction, which allows us to assess the structure and function of cortical PV neurons following a transient global ischemia.

Viral Vector Targeting: Diverse neurotropic viruses have evolved ingenious mechanisms that hijack cellular machineries for their transduction, rapid genome amplification, high-level gene expression, and efficient transneuronal spread (Davidson et al., 2000; Peel and Klein, 2000; Callaway, 2005). Viral vectors from numerous systems have been engineered to harness these properties for the purposes of neuronal labeling and manipulation (Callaway, 2005). Until a few years ago, the most important limitation of viral vectors was the lack of sufficient cell-type selectivity for infection and gene expression. Recent advances employing engineered tropism, engineered gene expression, and axon transduction at projection sites have begun to overcome

this limitation in several widely used viral systems (Table 1.1) (Huang and Zeng, 2013). The delivery of viral vectors can be both temporally controlled and region specific (Taymans et al., 2007; Huang and Zeng, 2013). Thus, the combination of mouse genetic systems and viral vector technology has the potential to yield unprecedented cell-type specificity. In the current study, we mainly applied AAV vectors to carry the gene of interests (e.g., ChR2, iGluSnFR, tdTomato, etc.) for the transduction in the mouse cortex. Its advantage over transgenic strategy yields higher efficiency of expression, as well as convenient without the needs for breeding and genotyping for simultaneous expression of multiple genes.

Table 1.1 Recombinant viral vectors that confer cell-specific transduction and/or gene expression. From (Huang and Zeng, 2013) (open access).

	AAV	Lentivirus	Retrovirus	CAV2	Rabies virus
Genome	Single-stranded DNA	RNA	RNA	DNA	RNA
Capacity	~5 Kb	~8 Kb	~8 Kb	~30 Kb	~? Kb
Expression onset	Weeks	Weeks	Weeks	Weeks	Days
Expression duration	Years	Years	Years	Years	~10 days
Envelope	No	Yes	Yes	No	Yes
Specificity through engineered tropism	Capsid protein, serotypes	Envelope protein; pseudotyping	Envelope protein; pseudotyping	Capsid protein	Envelope protein; Pseudotyping
Specificity through engineered expression	Cre, Flp, tTA-dependent	Cre-dependent (FLEX)	Cre-dependent (FLEX)	N/A	N/A
Predominant applications	Long-term transgene expression; axonal projection mapping	Long-term transgene expression Fate	Fate mapping	Retrograde labeling	Retrograde; trans-synaptic labeling

1.3.4 Light-Based Optogenetic Mapping and Its Application in Probing Spatial and Temporal Changes in Neuronal Excitability and Motor Output

Recently, optogenetic tools have been applied to selectively manipulate and monitor neural systems (Lee et al., 2010; Lim et al., 2012, 2013; Tye and Deisseroth, 2012; Mohajerani et al., 2013). The development of another category of optogenetic tools – genetically encoded activity

sensors, allows the wide-field sensory and connectivity mapping in the cortex (Akemann et al., 2012; Mohajerani et al., 2013; Vanni and Murphy, 2014; Carandini et al., 2015). Combining these tools has enabled the mapping of functional connections between stimulated cortical targets and other brain regions. The advantages of optogenetic mapping includes the ability to arbitrarily stimulate brain regions that express opsins, allowing for brain mapping independent of behavior or sensory processing (Lim et al., 2012). The ability of opsins to be rapidly and locally activated allows for investigation of connectivity with spatial resolution on the order of single neurons and temporal resolution on the order of milliseconds (Mohajerani et al., 2013; Pala and Petersen, 2014). Optogenetic mapping have been applied in experiments ranging from *in vitro* investigation of microcircuits (Hooks et al., 2011), to *in vivo* probing of inter-regional cortical connections (Lim et al., 2012), to define the primary motor cortex (Ayling et al., 2009; Hira et al., 2009), to examine global connections within the whole brain (Lee et al., 2010).

1.3.5 Optogenetic Mapping following Stroke

One of the major functional deficits following stroke in human patients is sensory and motor disability (Murphy and Corbett, 2009). Mapping the cortex is one of the widely-used approaches to voluntarily evaluate the sensory and motor function following stroke both in animals (Zhang et al., 2005; Brown et al., 2009; Murphy and Corbett, 2009; Mohajerani et al., 2011; Harrison et al., 2013; Anenberg et al., 2014; Silasi and Murphy, 2014) and in humans (Traversa et al., 1997; Nelles et al., 1999).

Mapping the motor cortex: In humans, transcranial magnetic stimulation has been used to probe the excitability in the motor cortex (Pascual-Leone et al., 2011). In animals, ICMS has been

widely used to map the reorganization in cortical representation of the primary motor cortex following stroke (Nudo et al., 1996; Gharbawie et al., 2005). Each of these techniques has their advantages and limitations. TMS stimulation is noninvasive but has poor spatial resolution (Hallett, 2000), which limits its application in rodents. ICMS has improved spatial resolution and can be applied to map the motor cortex in mice (Tennant et al., 2011); however, it lacks selectivity for targeting neuron subtypes, has low temporal resolution, and is invasive when impalements are made. Our lab has recently developed a method of light-based motor mapping using transgenic ChR2 animals (Arenkiel et al., 2007) for mapping the motor cortex (Ayling et al., 2009) under normal physiology (Harrison et al., 2012) or following stroke (Harrison et al., 2013). Light-based motor mapping has the advantages of being faster and less invasive than electrode based mapping, which is suitable for mapping the fast changes of motor cortex during a transient global ischemia.

Mapping the sensory cortex: In humans, brain imaging (fMRI, PET) or electrical recording (e.g., ECG) can be applied to map the sensory cortex (Fox et al., 1987; Engel et al., 1994; Crone et al., 1998a, 1998b). Owing to their low temporal and/or spatial resolution, it is almost impossible to apply these techniques to map the sensory cortex in mice. Intrinsic optical signal (IOS) imaging was developed to visualize activity-dependent changes in the reflectance of brain tissue and delineate functional areas (Grinvald et al., 1986). It is suitable for longitudinal mapping the sensory cortex following brain plasticity and brain diseases, such as stroke (Zepeda et al., 2004; Harrison et al., 2013). Although IOS imaging is relatively non-invasive and requires no additional reagents, the disadvantages of IOS imaging consist of relatively low and spatial temporal resolution, as well as low SNR. During the last decade, the emergence of high

resolution and sensitive approaches, such as voltage sensitive dye (VSD) imaging, has enabled the visualization of fast sensory processing in the cortex (Shoham et al., 1999; Grinvald and Hildesheim, 2004; Mohajerani et al., 2010); however, this technique employing organic dye lacks cell specificity and cannot be used for longitudinal studies. Integration of recently developed genetically encoded activity sensors and transgenic strategies enables the longitudinal mapping of the sensory cortex with cell type specificity at high performance (Díez-García et al., 2007; Akemann et al., 2010; Minderer et al., 2012; Vanni and Murphy, 2014; Madisen et al., 2015). One can anticipate mapping the sensory cortex with genetically encoded activity sensors will enable longitudinal studies during brain plasticity or after models of brain diseases, such as stroke.

1.3.6 Using Optogenetics to Study Brain Plasticity and Diseases

The technology of optogenetics represents a step toward addressing the difficulties regarding perturbing neuronal activity with high spatial and temporal resolution. Optogenetics have provided a new way to establish causal relationships between brain activity and behavior in health and diseases. In the last decade, optogenetics have been used in dissecting circuits function in many brain regions, such as the amygdala (Haubensak et al., 2010; Johansen et al., 2010; Yiu et al., 2014), the sensory and motor cortex (Cardin et al., 2009; Harrison et al., 2012), the nucleus accumbens (Tecuapetla et al., 2010; Witten et al., 2010), the prefrontal cortex (Sohal et al., 2009), the hippocampus (Liu et al., 2012; Redondo et al., 2014), etc., further investigating their functions and the involving circuitry mechanisms in fear conditioning, sensory and motor processing, social activity, working memory, and learning and memory, etc.. Optogenetics have

also contributed to understanding the circuitry mechanisms behind brain diseases that are relevant to fear, anxiety, depression, schizophrenia, addiction, social dysfunction, Parkinson's disease and epilepsy (Tye and Deisseroth, 2012). Recently, molecular therapy that is based on optogenetics has shown the translational potentials for brain diseases. For instances, expression of ChR in retina neurons can restore the visual function in mice with retina degeneration (Lagali et al., 2008). Optogenetic activation of direct pathway medium spiny projection neurons rescue deficits in a mouse model of Parkinson's disease (Kravitz et al., 2010). On-demand optogenetic inhibition has been shown to suppress epilepsy in a mouse model (Krook-Magnuson et al., 2013). Moreover, optogenetic neuronal stimulation promotes functional recovery in a mouse stroke model (Cheng et al., 2014).

1.4 Hypothesis and Objectives

There were two general objectives for my PhD study. The first objective was to adapt the currently available optogenetic tools to establish methods that can be applied to examine rodent stroke *in vivo*. The second objective was to use these optogenetic methods to investigate the changes of neuronal excitability, synaptic transmission, network activity, motor and sensory function following a mouse model of transient global ischemia.

Based on previous *in situ*, cell culture and post-mortem studies (Xu and Pulsinelli, 1994; Bolay and Dalkara, 1998; Bolay et al., 2002; Pang et al., 2002; Liu et al., 2006), we hypothesized that a transient global ischemia could temporarily suppress cortical neuronal excitability and synaptic transmission *in vivo*. Furthermore, motor and sensory processing could also be disrupted due to the suppression of neuronal and synaptic function. Following reperfusion, the neuronal

excitability and synaptic function, as well as sensory and motor function have been shown to more or less recover; however the temporal profiles of their recovery have yet to be determined *in vivo* due to technical difficulties. It was our aim to examine these temporal changes using cell-specific targeting of excitatory or inhibitory neurons with ChR2, or using light-based motor mapping. We hypothesized that the inhibitory neurons in the cortex, particularly PV neurons, would exhibit higher resistance to the ischemic damage, owing to the Ca^{2+} buffering property of parvalbumin protein (Nitsch et al., 1989; Johansen et al., 1990). For this reason, we expressed ChR2 in PV-Cre transgenic mice for the specific stimulation of PV-neurons, and then recorded its responses following a transient global ischemia. Moreover, using optogenetic sensors to characterize glutamate signaling in the cortex, we expect to establish additional mesoscopic cortical imaging approaches that will be useful for future pathophysiological studies in stroke.

Chapter 2: Optogenetic Analysis of Neuronal Excitability during Global Ischemia Reveals Selective Deficits in Sensory Processing following Reperfusion in Mouse Cortex

2.1 Introduction

Stroke is a major cause of death and disability that results from a transient or permanent reduction in cerebral blood flow (Dirnagl et al., 1999; Hossmann, 2006; Murphy and Corbett, 2009). During stroke, neuronal structure and function are rapidly damaged (Risher et al., 2010; Mostany and Portera-Cailliau, 2011), but can in part recover during reperfusion (Zhang et al., 2005; Li and Murphy, 2008; Murphy et al., 2008). Although structure can recover after reperfusion, brain activity is depressed as measured by spontaneous cortical electro-encephalogram (EEG) activity (Murphy et al., 2008) or somatosensory-evoked potential (Astrup et al., 1981; Lesnick et al., 1986). It is unclear whether this prolonged depression is due to a lack of a hyperpolarized membrane potential (Xu and Pulsinelli, 1994) or a defect that selectively impairs excitability or synaptic transmission (Gao et al., 1998). Since ischemia can affect upstream sensory or presynaptic pathways (Pang et al., 2002; Li et al., 2009), or enhance inhibition (Clarkson et al., 2010), sensation is not always a reliable means for assessing excitability. Electrophysiological measurements involving direct antidromic neuronal stimulation may be difficult to employ and interpret *in vivo*. Here, we selectively examine neuronal excitability during the period beginning with the induction of ischemia and extending after reperfusion using transgenic mice [B6.Cg-Tg(*Thy1*- COP4/EYFP)18Gfng/J] expressing channelrhodopsin-2 (ChR2) in predominantly layer 5 cortical pyramidal neurons (Arenkiel et al.,

2007; Wang et al., 2007; Ayling et al., 2009). ChR2 is a directly light-gated nonselective cation channel, which when expressed in neurons can transduce light energy into neural activity (Nagel et al., 2003; Boyden et al., 2005; Miesenböck, 2009). With conventional EEG and multichannel local field potential (LFP) as readouts, the ChR2-based technique can optically interrogate defined circuit elements with millisecond-scale, and cell type-specific precision *in vivo* (Zhang et al., 2007b). This optogenetic approach has the advantage of being able to directly assess neuronal excitability independently of changes to synaptic activity. In addition, we use a mouse *in vivo* global ischemia model that allows us to titrate the duration of ischemia to within seconds and can rapidly alternate between the initiation of ischemia or reperfusion (Li and Murphy, 2008; Murphy et al., 2008). Using this approach within the sensorimotor cortex, we show that prolonged post-ischemic depression of sensory-evoked activity is not attributed to a loss of neuronal excitability since ChR2-mediated EEG responses are recovered following reperfusion.

2.2 Materials and Methods

2.2.1 Transgenic Mice

We have studied a total of 24 adult male *Thy1*-ChR2- yellow fluorescent protein (YFP) transgenic mice [B6.Cg-Tg(*Thy1*- COP4/EYFP)18Gfng/J; Fig. 2.1*A*, ChR2-YFP expression) (Arenkiel et al., 2007), which were obtained from Jackson Laboratories and bred at the University of British Columbia animal facilities. The mice were 2–4 months of age and ranged in weight between 26 and 32 g. All experiments used urethane anesthesia (1.25 g/kg). Body temperature was maintained at 37 ± 0.5°C using a heating pad and feedback regulation from a rectal temperature probe (FHC). Hydration was maintained by intraperitoneal injection of saline

(200–300 μl) with 20mM glucose at 1–2 h intervals. The experimental protocols were approved by the University of British Columbia Animal Care Committee and were consistent with the Canadian Council on Animal Care and Use guidelines.

2.2.2 Surgical Procedures

The surgical procedures for preparing a cranial window and the *in vivo* intrinsic optical signals (IOSs) imaging methods have been described previously (Zhang et al., 2005). Briefly, animals were fitted into a custom-made head holder. A stainless steel chamber that covered mainly the right parietal cortex was adhered to the skull with ethyl cyanoacrylate (Krazy Glue, Elmer's Products). The animal was then prepared for a global ischemia model. A 4 × 4 mm cranial window was made over the somatosensory cortex, leaving the dura intact. The cortex was covered with 1.3% low-melt agarose (at 37–38°C; Type 3-A; A9793; Sigma) dissolved in HEPES buffered artificial CSF (ACSF) and sealed with a glass coverslip (#1). For optrode recording (described below), a smaller cranial window (2 × 2 mm) was made to cover the forelimb cortex with ACSF filling a well-made of dental cement without a coverslip. A tracheotomy was performed on all animals to alleviate breathing problems, which may have been confounded by surgical manipulation of the tissue within the neck region or prolonged urethane anesthesia (Li and Murphy, 2008). After surgery, the animal was allowed to recover (under anesthesia) for at least 30 min before further experimental recording.

2.2.3 Global Ischemia Model

The common carotid arteries (CCAs) were exposed bilaterally and sutures (5-0, silk; Ethicon) were looped around each CCA. The animal was turned upright, placed in a head holder, and the

craniotomy procedure performed. To induce global ischemia, we carefully pulled on both sutures and secured them with tape to induce bilateral CCA occlusion (CCAO). Ischemia was induced 15–40 min after EEG recording, and IOS imaging (or optrode recording) was begun. For experiments using EEG recordings with forepaw or ChR2 stimulation, only animals exhibiting >8 mV of DC shift were considered as successful global ischemia models. To avoid compromising the health of the animals, we limited the ischemic period to ~5 min, and animals were reperfused by cutting the sutures. After 1–1.5 h of reperfusion, the animal was killed with an intraperitoneal injection of Euthanyl (0.10 ml) (Figure 2.1 *B*, timeline).

2.2.4 ChR2 Stimulation

Laser (CNI Optoelectronics) was used to stimulate ChR2-expressing neurons. The relatively collimated laser beam was delivered to the brain surface via an Olympus BX51 upright microscope, and the diameter measured through the objective (4×) was 43 μm at the brain surface (Fig. 2.1*A*, $n = 7$ mice). The beam was positioned over the somatosensory cortex as determined by stereotaxic coordinates. Laser output 1 mW premeasured with a power meter (Thorlabs) was triggered by a transistor–transistor logic pulse of 5 ms duration for each photostimulation (Arenkiel et al., 2007; Ayling et al., 2009). The power was ~700 mW/mm^2 at brain surface. Based on previous work addressing light spreading and scattering in brain tissue (Aravanis et al., 2007; Kahn et al., 2011), the laser power at the depth of layer 5 (800 μm, where most ChR2-YFP-labeled neuronal cell bodies were found) was expected to be 6 mW/mm^2; however, light levels at superficial dendrites were likely much higher. Laser power for ChR2 stimulation was adjusted (1–5 mW) following one to two pilot trials to obtain a ≥ 0.5 mVpeak EEG response, which was measured with a surface electrode.

2.2.5 Forepaw Stimulation

Two metal pins were inserted into the left forepaw, and a 1–5 mA 1 or 2 ms electrical pulse was delivered. The electrical pulse was generated by a constant current stimulus isolator (A385, World Precision Instruments) triggered 5 s after ChR2 laser stimulation by a 1322A Digidata system (Molecular Devices).

2.2.6 EEG Recording

For EEG recording, a Teflon-coated chlorided silver wire (125 μm; World Precision Instruments) with an exposed tip (1 mm) was placed on the cortical surface within the agarose. For EEG recording combined with optrode recording, the EEG electrode was placed in the ACSF and the reference electrode was placed on the nasal bone under the skin (Murphy et al., 2008; Mohajerani et al., 2010). The cortical signal was amplified and filtered (gain 100×, 0–1000 Hz) using a differential amplifier (DAM50, World Precision Instruments) and digitized (1000 Hz) using the 1322A Digidata. The output from the DAM50 amplifier was also sent to a USB-based device (MiniDigi 1A, Molecular Devices) then acquired by an Axoscope 9.2 (Molecular Devices) for continuous recording. In our experiment, Clampex software was used as the central controller for timing the experimental system.

2.2.7 Optrode Recording

To obtain information from different cortical depths, a silicon optrode (A1x16-3 mm-50-413-Op16, NeuroNexus Technologies) was used for recording LFP and multiunit activity (MUA) and ChR2 stimulation in eight mice (Kravitz et al., 2010; Kahn et al., 2011). The optrode contained 16 413 _m2 recording sites (0.7–1.2 MΩ impedance at 1 kHz), arranged linearly with 50 μm

spacing between each site. A 473 nm laser (IKE-473-100-OP, IkeCool) was coupled to the optrode using a fiberoptic patch cord (FC-x.x-NNC, NeuroNexus Technologies). Based on the atlas of mouse cortex from the Allen Institute for Brain Science, the optrode probe was inserted into the forelimb somatosensory cortex to a depth of 800 μm (bregma 0.3 mm, lateral 2.0 mm) to target layers 1–5. Here, ChR2 stimulation was performed with an optrode-integrated laser fiber (105 μm diameter). The fiber tip was positioned ~50 μm above the uppermost recording site near the cortical surface. Based on previous work with a similar probe (Kravitz et al., 2010), laser power was adjusted to yield 0.5–2 mW at the fiber tip to obtain clear LFP deflections from the deepest recording site. In one preliminary experiment, laser power of 0.5–5 mW was systematically varied. The quantified LFP deflection showed a hyperbolic tangential increase with laser power (data not shown). By fitting to the tangential function, 0.5–2 mW laser power was found to evoke 72–99% of the maximum response. LFP recordings were performed from the optrode using a portable 16-channel data acquisition system (USB-ME16-FAI-System, Multi Channel Systems). After 1000× amplification, all 16-channel LFP signals were sampled at 25 kHz with a bandwidth of 1–5000 Hz.

2.2.8 Pharmacology

Seven ChR2 mice were used for pharmacological experiments. For experiments (n = 4) involving glutamate receptor antagonists, DNQX (200 μM) and APV (500 μM) (Sigma) were dissolved in ACSF and applied to the craniotomy. Experiments (n = 3) using tetrodotoxin (TTX; 30 μM, Sigma) used local microinjection within the craniotomy, and were performed under

ketamine-xylazine anesthesia using a similar collimated laser delivery system (Ayling et al., 2009) with 10 ms laser pulses.

2.2.9 Electrophysiology Analysis

Since CCAO caused a DC shift during the recording (Murphy et al., 2008; Tran et al., 2011), linear fitting was used to remove the shifting baseline of EEG signal. The continuous EEG recording from the Axoscope was performed routinely with off-line highpass filtering (0.1 Hz, Bessel filter, 8 pole) to exclude the slow DC shift. EEG power of 0.3–3 Hz was calculated from the filtered EEG signal (only 4.5 s of data between ChR2 and forepaw stimulation in each period were used to avoid stimulation interference) with the frequency domain filtered to 0.3–3 Hz (Murphy et al., 2008). The amplitude from ChR2 stimulation was defined as the minimum EEG signal within 40 ms after onset of ChR2 stimulation. To reduce the photoelectric artifact (Ayling et al., 2009), the ChR2 responses were corrected by subtracting ChR2 responses obtained 10 min after the death of the animal. For forepaw electrical stimulation, the evoked potential was extracted from linear corrected EEG data by determining the minimum value within 20 ms after stimulation. Forepaw-evoked potentials were averaged over 1 min. Only the amplitude of the large primary cortical wave was determined (Lesnick et al., 1986), which corresponded to the N1 wave (Fujioka et al., 2004).

For 16-channel optrode recording, 50 ms columnar ChR2 and sensory-evoked LFP responses were segmented to display data from baseline, during occlusion, and after reperfusion. To quantify the ChR2- mediated LFP responses, the minimum voltage value of 8–12 ms after the ChR2 stimulation onset was extracted. For sensory-evoked LFP responses, the minimum of 10–20 ms after the forepaw stimulation onset was calculated. Since the bandwidth of LFP recording

was 1–5000 Hz, the mean power of 1–3 Hz was calculated as previously (Mohajerani et al., 2010). Only LFP data from 500 μm depth (beginning in layer 5) were quantified for group data. To resolve spikes from LFP recording, off-line bandpass filtering (600–6000 Hz, elliptic filter) was performed to acquire MUA (Kahn et al., 2011). Automated amplitude thresholding (four times the SD of the background noise) was used to detect spikes from the filtered data (Quiroga et al., 2004). Relatively large laser stimulation artifacts were removed by setting another upper-bound threshold (40 times SD). To reduce possible false-positive spikes, a principal component analysis was used to extract features of spike shapes that were used for excluding outliers (Bokil et al., 2010). The selected spikes were presented in a raster plot. The open source program Wave Clus (Quiroga et al., 2004) was used for this analysis.

2.2.10 Statistics

In the 17 animal experiments for global ischemia, 15 of the animals permitted successful recording of both consistent ChR2 and forepaw stimulation responses (DC shift >8 mV). Two of the 17 animals did not show a typical DC shift after CCAO. Only data from 15 animals that produced clear DC shifts were used for statistical analysis. Except for DC potential, the other statistical variables (e.g., EEG power and ChR2 peak amplitude) were based on normalized relative values. The mean baseline level values before CCAO 15 min from each animal were used to normalize the absolute measurements. All group data were expressed as the mean ± SEM. Phase plots were created by plotting the mean values for forepaw and ChR2-mediated EEG amplitude on the *y*-axis and DC potential on the *x*-axis for each point in time (Ba et al., 2002). A Student's *t* test was used for testing whether the group data showed significant changes at

different time points relative to the baseline level 100%. Values were considered statistically significant at $p > 0.05$.

2.3 Results

2.3.1 EEG Analysis of Cortical Excitability during Global Ischemia Using ChR2

Here we adapt a mouse model of global ischemia (Murphy et al., 2008; Tran et al., 2011) for direct optogenetic activation of subpopulations of cortical neurons from B6.Cg-Tg(Thy1-COP4/EYFP)18Gfng/J ChR2 transgenic mice before, during, and after global ischemia. These mice express ChR2 in predominantly cortical layer 5 (Arenkiel et al., 2007; Ayling et al., 2009; Harrison et al., 2012) (Fig. 2.1A). Given the diffuse labeling that is also present, we cannot rule out that a minority of expression occurs in other layers. The global ischemia model permits the induction of ischemia and reperfusion while retaining access to the cortical surface for light stimulation of ChR2 or imaging (Fig. 2.1A). ChR2 was used to assess neuronal excitability independent of sensory stimulation every 10 s during baseline, ischemia, and reperfusion in combination with electrophysiological methods. During periods of baseline activity in pre-ischemic animals, we observed a regular EEG signal consisting of ~0.3–3 Hz activity, which is expected with urethane anesthesia (Barth and Mody, 2011; Mohajerani et al., 2011). Bilateral CCAO (5 min) resulted in a rapid suppression of EEG activity within 20 s, consistent with previous reports (Murphy et al., 2008) (n=7 mice; Fig. 2.1Ci). Following the EEG depression with an ~2 min delay, an ischemic depolarization characterized by a shift in DC potential was observed (amplitude: ~8–18 mV; duration: 7–10 min) (Fig. 2.1Ci). There was a small transient hyperpolarization (1–2 mV) of DC potential before the negative DC potential shift

(depolarization), consistent with previous work (Xu and Pulsinelli, 1994). Given these robust EEG changes, the loss of a normal cortical EEG was used as a marker of ischemic onset. Following reperfusion, the DC potential partially recovered within 10 min (to ~5.7 ± 1.2 mV, n = 7) (Fig. 2.1Ci). However, spontaneous EEG power quantified over 0.3–3 Hz showed relatively slower recovery. Even 1 h after CCAO, EEG power was ~40% of baseline levels.

While simultaneously monitoring the spontaneous EEG and forepaw sensory response, ChR2 stimulation was used to assess neuronal excitability by measuring the depolarizing (negative going) EEG response to light (Fig. 2.1Cii). Brief 5ms pulses of 473nm light produced a depolarizing EEG response that contained components expected from rapid (within 15–25 ms) direct ChR2 activation (Murphy et al., 2008), as well as delayed responses that may reflect secondary activation of neurons through synaptic transmission (Harrison et al., 2012). During baseline EEG recordings (15–40 min before CCAO), the ChR2 response peak from each 5 ms 473 nm laser stimulation pulse was 0.5–2 mV and occurred ~15–25 ms after stimulation. Forepaw stimulation (1 ms electrical pulse)-evoked EEG responses had a peak amplitude of ~0.05–0.10 mV that occurred ~15–20 ms after electrical stimulation in animals before ischemia. The peak ChR2-mediated EEG response was used as a measure of neuronal excitability. Within 1 min after occlusion, the forepaw-evoked response was blocked, while the ChR2-mediated response was preserved (Fig. 2.1Cii). Surprisingly, neuronal excitability as monitored by ChR2 and EEG was intact during the first 2 min of global ischemia despite strong suppression of spontaneous EEG activity. The ChR2-mediated EEG response actually increased 1 min following occlusion before ischemic depolarization (Fig. 2.1Cii). Both ChR2 and forepaw-evoked responses were markedly suppressed within 3 min of CCAO. During reperfusion after 5

min of ischemia, the ChR2-mediated EEG response showed faster recovery than the forepaw-evoked response (Fig. 2.1D).

Relationship between DC potential and excitability assessed using ChR2

To examine the relationship between neuronal excitability (measured by forepaw- or ChR2-mediated responses) and ischemic depolarization, phase plots were constructed (Fig. 2.1E). Specifically, the phase plots were used to graphically display how changes in the ChR2-mediated or sensory-evoked EEG response were related to DC potential during ischemia and reperfusion in group data. By setting a 15% level of excitable response as a threshold, a three-phase relationship was observed: phase 1, initiation of ischemia and suppression of response to 15% of baseline; phase 2, maximum inhibition; and phase 3, recovery during reperfusion. The forepaw-evoked EEG response showed a rapid decrease even before a change in DC potential was observed during phase 1, while the ChR2 measure of EEG excitability was relatively unaffected. Interestingly, during phase 1 the ChR2-mediated EEG response was gradually attenuated in proportion to the loss of DC potential. The use of linear regression indicated that the loss of DC potential and the ChR2 response were strongly correlated ($r = 0.93$, $p < 0.01$), while DC potential and forepaw response were not ($r = 0.05$, $p < 0.05$). During phase 3, DC potential gradually recovered and an approximately proportional return of the ChR2-mediated response was observed ($r = 0.91$, $p < 0.01$). However, the recovery of the forepaw-evoked response during phase 3 was significantly delayed and incomplete despite the recovery of DC potential (Fig. 2.1E). The use of phase plots indicates that changes in excitability assessed by the ChR2-mediated EEG response are strongly correlated with the DC potential, while the forepaw-evoked

or spontaneous EEG response shows defects that precede the loss of DC potential and are still apparent even after the DC potential has appreciably recovered (Fig. 2.1E).

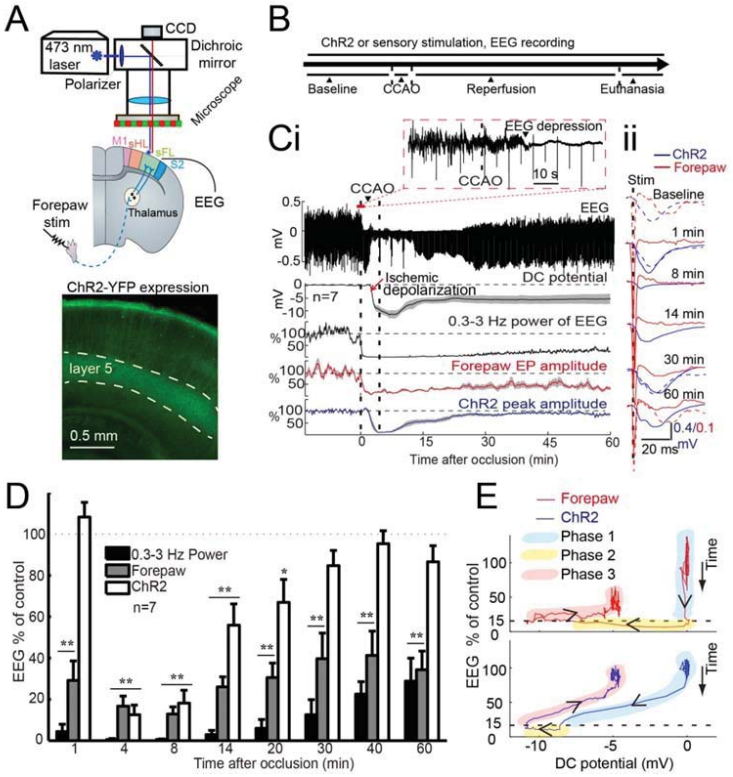

Figure 2.1 EEG recording reveals selective deficits in sensory processing and rapid recovery of ChR2 response following reperfusion.

A, Schematic drawing of experimental system. EEG recording, IOS imaging, photo-stimulation, and electrical forepaw stimulation were coordinated with synchronized trigger signals. ChR2 and sensory stimulation were interleaved and repeated every 10 s. Coronal brain slice indicates that ChR2 is predominantly expressed in layer 5 of cortex. B, Experimental timeline: ChR2 and sensory stimulation were performed during baseline, CCAO, reperfusion, and after the animal was killed (~3 h for the timeline). Ci, Changes of spontaneous EEG (example mouse), DC potential (n = 7 mice), 0.3–3 Hz EEG power (n = 7 mice), forepaw-evoked potential (EP) (n = 7

mice), and ChR2 peak amplitude (n = 7 mice) are shown from top to bottom. In the EEG record, an enlarged view shows EEG depression within 20 s after CCAO (inset). Ischemic depolarization is indicated with an arrow over the DC potential record. Except for EEG and DC potential, the other statistical data were based on relative values, which were normalized with baseline level as 100%. The shaded band indicates SEM. Spontaneous EEG power and forepaw-evoked EEG response were depressed immediately after CCAO and recovered relatively slowly. However, ChR2 peak amplitude is transiently increased 1–2 min after occlusion, followed by a decrease in response and relatively rapid recovery with reperfusion. Cii, Six time segments of ChR2-/forepaw-evoked EEG data. The vertical dashed line indicates the onset of ChR2 or forepaw stimulation (a stimulus artifact is present during forepaw stimulation). The baseline responses of ChR2/forepaw stimulation are shown with dashed lines and superimposed over selected records. ChR2-mediated response shows a larger amplitude than the baseline (blue dash line) at 1 min after CCAO (trace 2), and relatively faster recovery at 30 min after CCAO. The forepaw-evoked potential shows prolonged suppression at 60 min after CCAO compared with the baseline response (red dash line). D, Statistical analysis of 0.3–3 Hz EEG power, forepaw-, or ChR2-mediated EEG responses during global ischemia at select time points. *$p < 0.05$; **$p < 0.01$. E, Forepaw/ChR2-mediated EEG responses are shown in phase plots for comparison to DC potential (n = 7 mice). By setting a 15% level of excitable response as a threshold, a three-phase relationship was observed: phase 1 (shadowed with cyan), initiation of ischemia and suppression of response to 15% of baseline; phase 2 (shadowed with yellow), maximum inhibition; phase 3 (shadowed with pink), partial recovery of DC potential and excitable response. The primary motor cortex (M1) and hindlimb (sHL), forelimb somatosensory cortex (sFL), and secondary somatosensory cortex (S2) are indicated. Stim, Stimulation.

LFP characterization of ChR2- and sensory-evoked responses during global ischemia

Although surface EEG recording showed robust changes in both sensory and ChR2 responses following global ischemia, it was not clear whether these effects were present throughout the depth of cortex. Using a 16-channel optrode, we monitored spontaneous, sensory, and ChR2-mediated changes in LFP within cortical layers 1–5 (Fig. 2.2A). Before CCAO, we observed a robust spontaneous LFP signal, consisting primarily of relatively low-frequency ~1–3 Hz activity. After 1 min of CCAO, the forepaw-evoked and spontaneous LFP signals were suppressed, but the ChR2- mediated peak LFP response was preserved across cortical depth (Fig. 2.2Bi, Bii). Analysis of ChR2-mediated response recovery (during reperfusion), using LFP sweeps that were stacked to form images, indicated that all depths exhibited relatively faster and

more complete recovery than the forepaw-evoked response (Fig. 2.2C). Since the ChR2 was expressed predominantly in layer 5, we selected the LFP signal from the 500 μm depth recording site to quantify the changes during global ischemia within the group data (Fig. 2.2D). Plotting the ChR2 response from layer 5 indicated nearly full recovery of the ChR2-mediated response after 7–10 min of reperfusion (>90% of baseline level), but only minimal recovery of the sensory-evoked LFP response (Fig. 2.2D). In additional longer term recording experiments (n = 4 mice) with stronger forepaw stimulation (2 ms), we found greater recovery of the forepaw-evoked LFP response 2 h after reperfusion (77 ± 21% of baseline level, n = 4, p = 0.36), consistent with previous data examining sensory maps (Murphy et al., 2008). Using stronger sensory stimulation, we were also able to better match the amplitude of the optogenetic and sensory responses (0.67 ± 0.19 mV optogenetic *vs.* 0.52 ± 0.07mV forepaw, n = 4, p = 0.53), and confirmed that the sensory response was consistently depressed at 30 min after reperfusion (36 ± 7% of baseline level, n = 4, $p < 0.01$), while the optogenetic response recovered to 103 ± 5% of baseline level at 30 min (n = 4, p = 0.60).

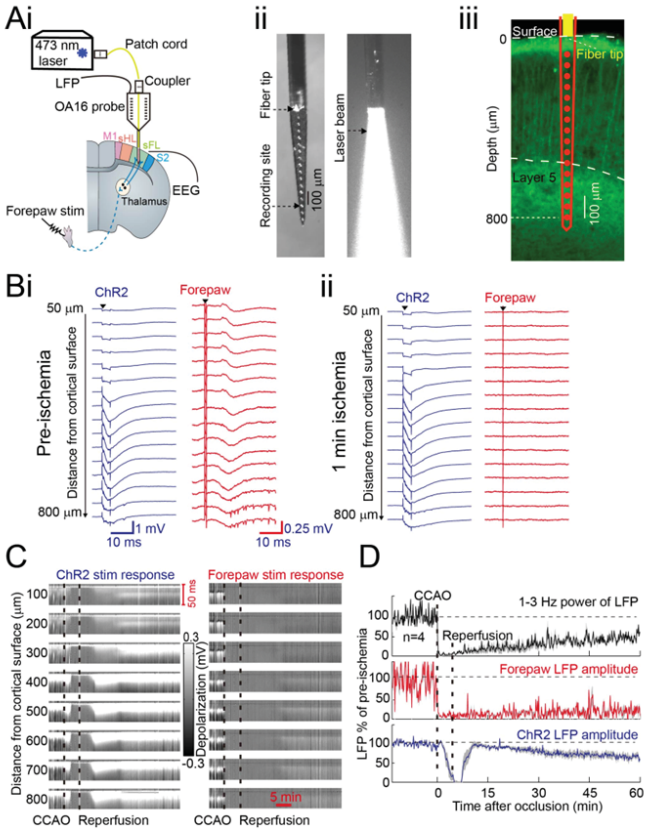

Figure 2.2 LFP-based electrophysiology confirms selective deficits in sensory processing after global ischemia.

Ai,A16-channel optrode (OA16, NeuroNexusTechnologies) was used for LFP recording and ChR2 stimulation. Aii, Laser light exits from the fiber tip (50 µm above the first recording site). Aii shows the laser distribution before implantation in cortical tissue.Aiii shows the approximate location of the optrode in cortical layers 1–5. Bi, Bii, Representative LFP data from pre-ischemia (Bi) and 1 min after ischemia (Bii) from cortical layers 1–5 (up to 800 µm depth from the brain surface). Compared with pre-ischemia results, the data from 1 min after ischemia show preservation of ChR2-mediated response and a lack of forepaw-evoked response. C, ChR2-mediated LFP responses from 8 recording sites (half of all 16 sites) to a depth of 800 µm below the cortical surface, which are visualized as 50 ms columnar time sweeps. Preserved ChR2 responses are seen in the period between CCAO and ischemic depolarization. ChR2 responses are suppressed at all measured sites following ischemic depolarization and recover faster in deeper layers compared with more superficial layers of cortex. Sensory responses are suppressed

following CCAO and slowly recover during reperfusion. D, Group data of 1-3 Hz LFP power, forepaw-evoked LFP amplitude, and ChR2-mediated LFP amplitude. stim, Stimulation.

To investigate the nature of the ChR2-evoked response, we performed additional LFP analysis and parallel pharmacological experiments. Data obtained from all 16 channels were bandpass filtered (600–6000 Hz) to isolate spike activity that spontaneously occurred or was evoked in response to ChR2 or sensory stimulation (Fig. 2.3A, B). Despite the laser entering at the brain surface, we detected an increase in spikes evoked by ChR2 stimulation from electrodes within layer 5. Although ChR2 is expressed at highest density within layer 5 neuron cell bodies, laser stimulation is likely to predominantly activate superficial dendritic tufts. The spiking is consistent with a direct activation of ChR2-expressing neurons (Kahn et al., 2011). Consistent with a component of light-stimulated signals being dependent on action potentials, locally applied TTX led to a 67% reduction in ChR2-evoked EEG signal (Fig. 2.3C). To assess the contribution of synaptic transmission, we applied DNQX and APV locally and observed a complete blockade of the depolarizing forepaw-evoked signal, but no significant effect on the ChR2-evoked peak EEG response (Fig. 2.3D).

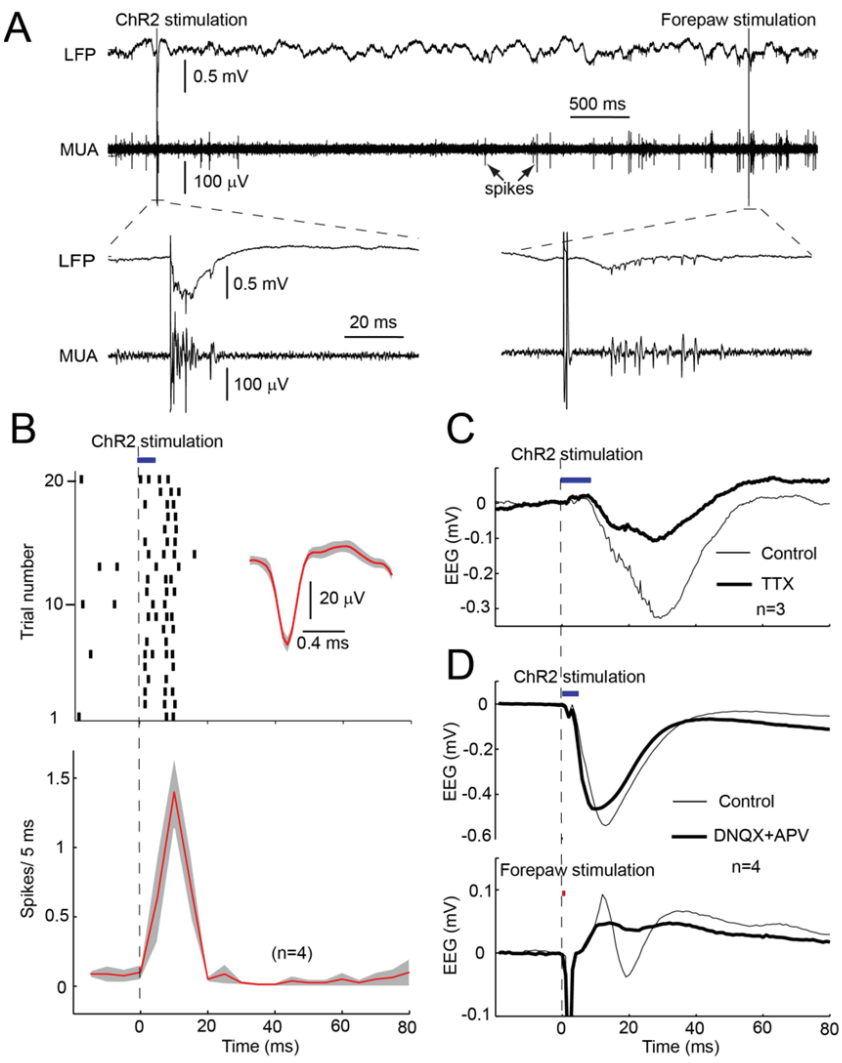

Figure 2.3 Role of spiking and synaptic activity in ChR2-mediated responses

A, LFP responses (top) during ChR2 or forepaw stimulation filtered to resolve MUA (middle). Representative spikes are indicated with arrows. Two segments of ChR2 or forepaw stimulation response are shown in enlarged views (bottom). ***B***, Quantification of spiking with 5ms of laser stimulation. Top, Raster plot of spikes during 20 trials and average spike waveform (example mouse shown). Bottom, Plot of spiking rate with 5ms bin size ($n = 4$ mice). The shaded area indicates the SEM. ***C***, Effect of locally applied TTX 30 μM on ChR2-mediated EEG responses; average response from $n = 3$ mice is shown. ***D***, Antagonists of glutamate receptors (DNQX 200

μM and APV 500 μM) block sensory-mediated, but not ChR2-mediated, EEG response; average from $n = 4$ mice is shown.

2.4 Discussion

2.4.1 ChR2-Based Assessment of Neuronal Excitability during Global Ischemia

Preservation of neuronal excitability is critical for functional recovery after stroke (Bütefisch et al., 2003; Murphy and Corbett, 2009; Clarkson et al., 2010). Previous data have shown that synaptic transmission is depressed during ischemia and following reperfusion (Gao et al., 1998). This effect can be measured using cortical EEG recordings (Astrup et al., 1981) that presumably reflect synaptic activity. However, it has been a challenge to directly assess neuronal excitability *in vivo* while EEG activity is depressed during ischemia and within 1 h after reperfusion. Conventional recording of sensation-evoked potentials has revealed hyper-excitability from time points 1–6 h after focal ischemia (Fujioka et al., 2004). Neuronal excitability can be assessed indirectly *in vivo* after stroke or trauma using paired-pulse sensory stimulation (Fujioka et al., 2004; Ding et al., 2011). However, previous work has shown that the cortical sensory evoked potential is abolished after global ischemia (Lesnick et al., 1986). We have used ChR2 to directly depolarize neurons and extend the previous measurement of cortical excitability with embedded stimulating electrodes (Lesnick et al., 1986). We expect ChR2 to be predominantly expressed in layer 5 cortical pyramidal neurons (Arenkiel et al., 2007; Wang et al., 2007; Ayling et al., 2009). Therefore, the changes in neuronal excitability we observe during acute phases of global ischemia are relatively specific to these neurons. With optogenetics, we show that it would be feasible to study the excitability of select cell populations, such as large aspiny neurons (Pang et

al., 2002; Li et al., 2009) or GABAergic interneurons (Redecker et al., 2002; Boyden et al., 2005; Clarkson et al., 2010), during ischemia.

The global ischemia model used here is clinically related to cardiac arrest or cardiac surgery (Hofmeijer and van Putten, 2012). Although this model does not recapitulate more clinically relevant middle cerebral artery occlusion models (Dirnagl et al., 1999), we can precisely control the duration of ischemia to within seconds and can rapidly alternate between the initiation of ischemia or reperfusion. The methods used here could be extended to a focal ischemia model, but it would be difficult to monitor excitability within the first minutes of occlusion since these models are not necessarily compatible with continuous recording (Li and Murphy, 2008). Since it is possible to perform scanning stimulation (Ayling et al., 2009), we may be able to complete a spatial optogenetic analysis of a focal photothrombotic model (Mohajerani et al., 2011). This would distinguish changes in excitability within specific regions such as the infarct, penumbra, and normal tissue. Additionally, it would be possible to study neuronal excitability with the recently developed hippocampal ischemia model (Barth and Mody, 2011) using *in vivo* fiber optic activation of ChR2. Given its wide applications, ChR2-based assessment of neuronal excitability could be a mouse analog of transcranial magnetic stimulation, providing background for translational stroke studies (Bütefisch et al., 2003)

2.4.2 The Nature of the ChR2-Mediated Electrophysiological Signal

The ChR2-mediated EEG or LFP response can reflect both direct ChR2-mediated and indirect synaptic activation and can last longer than the duration of the light stimulus (Harrison et al., 2012; Lim et al., 2013). Given the relatively long deactivation time for ChR2 (Fenno et al., 2011),

even the response to direct activation should be on the order of 10–15 ms in duration, consistent with the peak responses we observe. Some of the indirect effects from light stimulation may be attributed to ChR2 directly gating channels on axons that produce neurotransmitter release (Petreanu et al., 2007; Schoenenberger et al., 2011). However, the initial peak component of the ChR2-mediated response (within 10–20 ms) was relatively insensitive to glutamate receptor antagonists and is likely derived from direct channel activation and secondary action potential firing given its sensitivity to tetrodotoxin. Therefore, ChR2-mediated peak EEG or LFP signals may predominantly reflect subthreshold activity and poorly synchronized firing among populations of neurons.

2.4.3 Selective Deficits in Sensory Processing following Reperfusion

Previous studies have shown that ischemia can profoundly change synaptic transmission and neuronal excitability (Pang et al., 2002; Fujioka et al., 2004; Zhang et al., 2006; Liang et al., 2009; Clarkson et al., 2010; Paz et al., 2010). However, the results were not always consistent between models. Using assessment of forepaw stimulation-evoked cortical potentials, we find that forepaw sensation-dependent cortical synaptic transmission was inhibited even 1 h after reperfusion from CCAO. This finding was consistent with previous work (Astrup et al., 1981; Murphy et al., 2008) and may reflect a persistent synaptic transmission defect (Bolay and Dalkara, 1998). In contrast to synaptic responses, the use of ChR2 stimulation revealed that neuronal excitability was recovered with reperfusion. These results suggest that the selective deficits in sensory processing following reperfusion in mouse cortex are not necessarily attributed to a loss of direct neuronal excitability. The absence of forepaw-evoked and

spontaneous EEG or LFP responses is indicative of a loss of synaptic activity. This fact, combined with the ability to depolarize neurons with light in ChR2 transgenic mice, argues for a long-term selective block in synaptic transmission during the post-reperfusion period.

The mismatches between changes within sensory processing and neuronal excitability after transient global ischemia may be due to a block of conduction within white matter (including thalamus) (Lesnick et al., 1986). The short-latency forepaw response (within 20 ms of forepaw stimulation) we quantified is likely to be directly related to thalamocortical activity (Wu et al., 2012). Further research may focus on functional changes within thalamocortical projections during stroke (Paz et al., 2010) by performing direct thalamic recordings (Ding et al., 2011). Moreover, it is also possible that postsynaptic cortical mechanisms are involved in the ischemia-induced loss of synaptic activity such as glutamate receptor endocytosis (Man et al., 2000).

2.4.4 Ischemic Depolarization Is Associated with a Loss of Neuronal Excitability

Previous work has shown that ischemic depolarization is the major trigger of neuronal structural damage (Obeidat et al., 2000; Murphy et al., 2008; Risher et al., 2010) during stroke. Here we show that ischemic depolarization is directly related to the loss of neuronal excitability measured by ChR2-mediated EEG responses. Ischemic depolarization is initiated at the edge of the ischemic core by elevated [K]o and glutamate (Nedergaard, 1996; Lee et al., 1999; Strong and Dardis, 2005). Since both K and glutamate may excite neurons, this could be why we observed a transient increase in neuronal excitability within 1 min after CCAO. In our experiments, 5 min of CCAO would induce a DC shift of ~10 min in duration, about three times longer than normoxic spreading depression (Leo, 1944) induced in healthy brain. The prolonged collapse of ion

gradients during ischemic depolarization could initiate a cascade of damaging events (Dirnagl et al., 1999) that lead to prolonged inhibition of forepaw sensory responses. The dependence of ChR2 responses on an intact resting membrane potential (Nagel et al., 2003) is consistent with its strong inhibition during ischemic depolarization and rapid recovery during reperfusion.

Although the DC potential did not completely return to baseline levels after reperfusion, the ChR2 peak amplitude recovered nearly fully when compared with the ischemic depolarization process. It is possible that this reflects hyper-excitability that is observed after stroke, which enhances the ChR2 response despite incomplete recovery of membrane potential (Fujioka et al., 2004). This may be related to a reduction in GABAA receptor expression after stroke (Schiene et al., 1996; Redecker et al., 2002). More work is also needed to determine whether GABAA receptor-mediated tonic inhibition plays a role (Clarkson et al., 2010). In both experimental and clinical studies, recurring ischemic depolarization or spreading depression waves have been associated with an exacerbation of damage after stroke (Dirnagl et al., 1999; Jarvis et al., 2001; Dreier et al., 2006; Shin et al., 2006; Strong et al., 2007; Risher et al., 2010). In vitro data indicate that ischemic depolarization can alter the balance between excitation and inhibition (Berger et al., 2008). Our study supports the idea that agents that reduce ischemic depolarization are potential therapeutic targets for stroke (Douglas et al., 2011; Risher et al., 2011). Reducing ischemic depolarization will help to maintain excitability and may prevent prolonged loss of sensory processing, leading to better outcomes following reperfusion.

In summary, our results indicate that neuronal excitability recovers much faster than sensory-evoked synaptic activity in vivo following ischemia and reperfusion. This delineates a time

window following ischemia where synaptically silent, yet excitable neurons are present. We anticipate that optogenetically stimulated ChR2 will allow investigators to further examine the excitability of unique cell populations during ischemic damage and reperfusion.

Chapter 3: Prolonged Deficits in Parvalbumin Neuron Stimulation-Evoked Network Activity Despite Recovery of Dendritic Structure and Excitability in the Somatosensory Cortex Following Global Ischemia in Mice

3.1 Introduction

Global ischemia occurs during cardiac arrest and has been implicated as a complication that can occur following cardiac surgery (Block, 1999). It induces delayed neuronal death in human and animal models, particularly in the hippocampus (Zola-Morgan et al., 1986), but also can affect the cortex (Hossmann and Sato, 1970; Koh et al., 1996; Chavez and LaManna, 2002; Murphy et al., 2008; Chen et al., 2012b; Xie et al., 2013). Inhibitory interneurons only constitute approximately 20% of cortical neurons, yet these interneurons are crucial in regulating the balance of excitation and inhibition (E/I), plasticity and functional architecture of cortical circuits (Markram et al., 2004). Among interneurons subtypes, parvalbumin (PV) neurons have been recently shown to modify sensory perception (Cardin et al., 2009; Lee et al., 2012). Moreover, accumulating evidence shows that abnormality of GABA systems, particularly in altered parvalbumin expression, is common in many brain disorders, including schizophrenia, bipolar disorder, and major depression (Torrey et al., 2005), and could putatively occur in human patients following cardiac arrest- or cardiac surgery-induced global ischemia (McKhann et al., 1997; Lim et al., 2004).

Postmortem studies have shown that hippocampal PV-neurons are more resistant to global ischemia-induced neuronal cell death. This resistance was attributed to enhanced Ca^{2+} buffering *via* parvalbumin (Nitsch et al., 1989; Freund et al., 1990; Johansen et al., 1990). However, how the structure and function of PV-neurons changes during and following a reversible ischemic event is not clear. Conventional electrophysiological approaches to directly characterize PV-neurons in this setting *via* patch clamp electrophysiology are not technically feasible due to the recording duration required and complexities involved with employing the ischemic model *in vivo*. In this study, we employed optogenetic tools (Gradinaru et al., 2010; Zhang et al., 2010) and Cre-dependent transgenic mouse lines (Madisen et al., 2010; Taniguchi et al., 2011) to investigate cortical PV-neuronal dendritic structure, intrinsic excitability, and network synaptic function during global ischemia and reperfusion. We demonstrate that PV inhibitory neurons are not spared from the damaging effects of global ischemia with respect to their structure and function.

3.2 Materials and Methods

3.2.1 Animal and Surgical Procedures

Adult male parvalbumin-Cre (PV-Cre) knockin mice (B6;129P2-Pvalb$^{tm1(cre)Arbr/J}$) (Hippenmeyer et al., 2005), Ai9 Cre reporter strain (B6;Cg-Gt(ROSA)$^{26Dortm9(CAG-tdTomato)Hze/J}$) (Madisen et al., 2010) aged 2–3 months were used. Experimental protocols were approved by the University of British Columbia Animal Care Committee and conformed to the Canadian Council on Animal Care and Use Guidelines. A 3 x 3mmcranial window was made over the somatosensory cortex. Body temperature was maintained throughout the surgical and experimental procedures at

~37°C. In all animals the cortical surface temperature was maintained at ~36.5°C by attaching a custom made stainless steel head plate connected to a temperature controlled water pump (Xie et al., 2013). Intraperitoneal injection of urethane (0.12% w/w) was used for anesthesia except for viral injection.

3.2.2 Global Ischemia Model

Five minute common carotid arterial occlusion (CCAO) was performed as in previous studies to induce a reversible global forebrain ischemia under urethane anesthesia (Murphy et al., 2008). We only considered ischemia that generated a 6 mV DC-EEG depolarization as being successful for further analysis. The PV-Cre transgenic mouse line used in this study is made within C56BL/6 background that typically lacks posterior communicating arteries, allowing bilateral CCAO to create significant forebrain ischemia (Fujii et al., 1997; Sheng et al., 1999). Reduction of blood flow (~80% of baseline level) in the somatosensory cortex during CCAO was previously confirmed by measuring red blood cell velocity in small vessels (Murphy et al., 2008) and also by assessing regional blood flow in motor and somatosensory cortices using laser speckle imaging (Xie et al., 2013) and laser Doppler flowmetry (Panahian et al., 1996). Reperfusion after 5 min of CCAO can rapidly restore flow to ~75% of baseline level within 3–5 min (Panahian et al., 1996; Xie et al., 2013).

3.2.3 Forepaw Stimulation

To stimulate the forepaw, thin acupuncture needles were inserted into the contralateral forepaw and a 1 ms, 1mA electrical pulse was delivered by a constant current stimulus isolator (A385;

World Precision Instruments) triggered by Clampex-controlled 1322A Digidata system (Molecular Devices).

3.2.4 Viral Injection

A 0.5–0.8 μl AAV1.EF1a.DIO.hChR2(H134R)-EYFP.WPRE.hGH or AAV1.CAG.FLEX.tdTomato.WPRE.bGH (Penn Vector Core) was injected by a syringe infusion pump (model UMC4; World Precision Instruments) as previously reported (Xie et al., 2010) into the forelimb somatosensory cortex (~2.3 mm lateral to the bregma, depth at 350–400 μm, speed at ~1 nl/s) of PV-Cre mice 3–4 weeks.

3.2.5 EEG Recording and Analysis

The methods have been described (Chen et al., 2012b). Briefly, a single surface electrode was placed within 1 mm of the forelimb somatosensory cortex for recording DC- EEG.EEG signals were sampled at 1 kHz. AC-EEG was filtered into 0.3–3 Hz from DC-EEG using a Chebyshev filter.

3.2.6 Optrode Stimulation, Recording, and Analysis

To obtain information from different cortical depths, a silicon optrode (A1x16–3 mm-50–413-Op16; NeuroNexus Technologies) was used for recording LFP and multi-unit activity (MUA), and also for laser-inducing ChR2 stimulation. The optrode contained 16 recording sites (413 μm2, 0.7–1.2 MO impedance), arranged linearly with 50 m spacing between each site. A 473 nm laser (IKE-473–100 OP; IkeCool) was coupled to the optrode using a fiber-optic patch cord (FC-x.x-NNC; NeuroNexus Technologies). Using coordinates obtained from an atlas of mouse cortex

(Allen Institute), the optrode probe was inserted into the forelimb somatosensory representation (posterior 0.3 mm, lateral 2.0 mm to the bregma) to a depth of 800 μm to target layers I–VI. ChR2 stimulation was performed with an optrode-integrated laser fiber (105 μm diameter). The fiber tip was positioned ~50 μm above the recording site nearest to the cortical surface. Laser power was adjusted to ~5 mW at the fiber tip and 1 ms (Thy1-ChR2) or 10 ms (PV-ChR2) laser stimulation induced consistent and stable LFP responses in all recording sites. LFP signals were digitized using a portable 16 channel data acquisition system (USB-ME16-FAI-System, Multi Channel Systems). The sixteen channel LFP signals were recorded and amplified (×1000), and all 16 channel LFP signals were sampled at 25 kHz. To quantify the PV-ChR2 stimulation-evoked LFP responses, the differences between baseline (averaged from 100 ms before the ChR2 stimulation) and downward peak (minimum LFP within 10-50 ms after the onset of ChR2 stimulation) were quantified as the putative depolarization of PV-neurons; the differences between the baseline and upward peak (maximum LFP within 10-50 ms after the onset of ChR2 stimulation) were quantified as the putative network hyperpolarization mediated by inhibitory synaptic transmission. To resolve multi-unit activity (MUA) from LFP recording, we used an open sources MATLAB-based program Wave Clus (Quiroga et al., 2004). Briefly, an off-line bandpass filtering (600-6000 hz, elliptic filter) was performed (Kahn et al., 2011). Automated amplitude thresholding (4-7 times standard deviation of background noise, negative peak only) was used to detect spikes from the filtered data. Relatively large laser stimulation artifacts were removed by setting an upper bound threshold (40 times stand deviation of background noise). Each spike was saved as 35-time point data. The spikes detected from baseline recording were averaged (reference spike) for sorting MUA (correlation coefficient to reference spike > 0.9). We

did not perform single-unit sorting because we found the optrode was not sensitive enough to resolve single unit, and also global ischemia changed the waveform. Only LFP signals from 400~600 μm depth (layer IV/V) were quantified for group data.

3.2.7 Current Sources Density Analysis

Recording from a sixteen channel optrode was used for functional analysis. For pharmacological data, current source density (CSD) analysis was averaged from at least 30 repetitions of PV-ChR2 or forepaw electrical stimulation trials. For ischemic data, CSD analysis was averaged from 10 repetitions from baseline recording (before global ischemia), and 3 repetitions following global ischemia and reperfusion for optimized temporal resolution. Baseline correction was applied using the 50 to 80 ms pre-stimulus period as baseline. CSD analysis was performed using a MATLAB based program – CSDplotter (Pettersen et al., 2006). We applied cubic spline iCSD method, where cortical parameters were set as following: standard deviation of the Gaussian filter – 0.1 mm, extracellular cortical conductivity – 0.3 S/m, top conductivity – 0.3 S/m, activity diameter – 0.5 mm. The peak amplitude of current sinks or current sources was sorted within 50 ms following PV-ChR2 or forepaw stimulation relative to the baseline recording (50 to 80 ms pre-stimulus). CSD data from 400~600 μm depth (layer IV/V) were averaged and quantified for group data.

3.2.8 Pharmacology

Ten PV-ChR2 expressed mice were used for pharmacological experiments. For experiments involving GABAA receptor antagonist - gabazine (1 μM, Sigma, n=5), or tetrodotoxin (TTX; 30

μM, Sigma, n=5) was dissolved in physiological saline solution and applied to the craniotomy (Harrison et al., 2012). Seven Thy1-ChR2 mice were used for pharmacological experiments. For experiments (n=4) involving glutamate receptor antagonists, DNQX (200 μM) and APV (500 μM) (Sigma) were dissolved in ACSF and applied to the craniotomy. Experiments (n=3) using tetrodotoxin (TTX; 3 μM, Sigma) used local microinjection within the craniotomy, and were performed under ketamine-xylazine anesthesia using a similar collimated laser delivery system (Ayling et al., 2009) with 10 ms laser pulses. The compounds were allowed to incubate for ~20 min before starting optrode stimulation and recording.

3.2.9 Transcardial Perfusion and Immunohistochemistry

Mice were transcardially perfused with PBS followed by chilled 4% paraformaldehyde (PFA) in PBS. Coronal brain sections (50 μm thickness) were cut on a vibratome (Leica VT1000S), and were incubated with mouse anti-parvalbumin antibody (1:500, Sigma) overnight, and subsequently incubated with Alexa488 or Alexa594 anti-mouse (1:1000, Molecular Probes) for 2 h. Images were acquired using confocal microscopy (Zeiss LSM510).

3.2.10 Statistical Analysis

All values were normalized to the percentage of pre-CCAO value (100%) except DC-EEG. A one-way ANOVA followed by Bonferroni's *post hoc* tests was used to compare differences in dendritic damage, LFP peaks and CSD results at each time point to pre-CCAO baselines in experimental groups. The other comparisons were analyzed with repeated measures ANOVA (RM-ANOVA). Significance was set at $P<0.05$.

3.3 Results

3.3.1 AAV Viral Transduced Selective Expression of tdTomato and ChR2-EYFP in PV-Cre Mice

Our initial work involved confirming that the ChR2 expression pattern was associated with PV inhibitory neurons. We visualized the Cre-expression pattern of PV-Cre mice by crossing them with a Rosa26 tdTomato reporter line, leading to expression patterns expected for Cre dependent AAV-vectors (Kuhlman and Huang, 2008). Immunoreactivity with PV antibody almost exclusively labels PV-Cre cells (Fig. 3.1A). PV neurons were relatively enriched in layer IV and V of the forepaw somatosensory cortex (Fig. 3.1A). To allow a selective investigation of the structure and function of PV-neurons, we injected Cre-inducible adeno-associated virus (AAV) vector containing tdTomato or ChR2-eYFP into the somatosensory cortex of PV-Cre mice (Fig. 3.1B). The virally transduced expression of tdTomato or ChR2-eYFP spanned from layer I to VI and co-localizes with PV immunostaining (Fig. 3.1B).

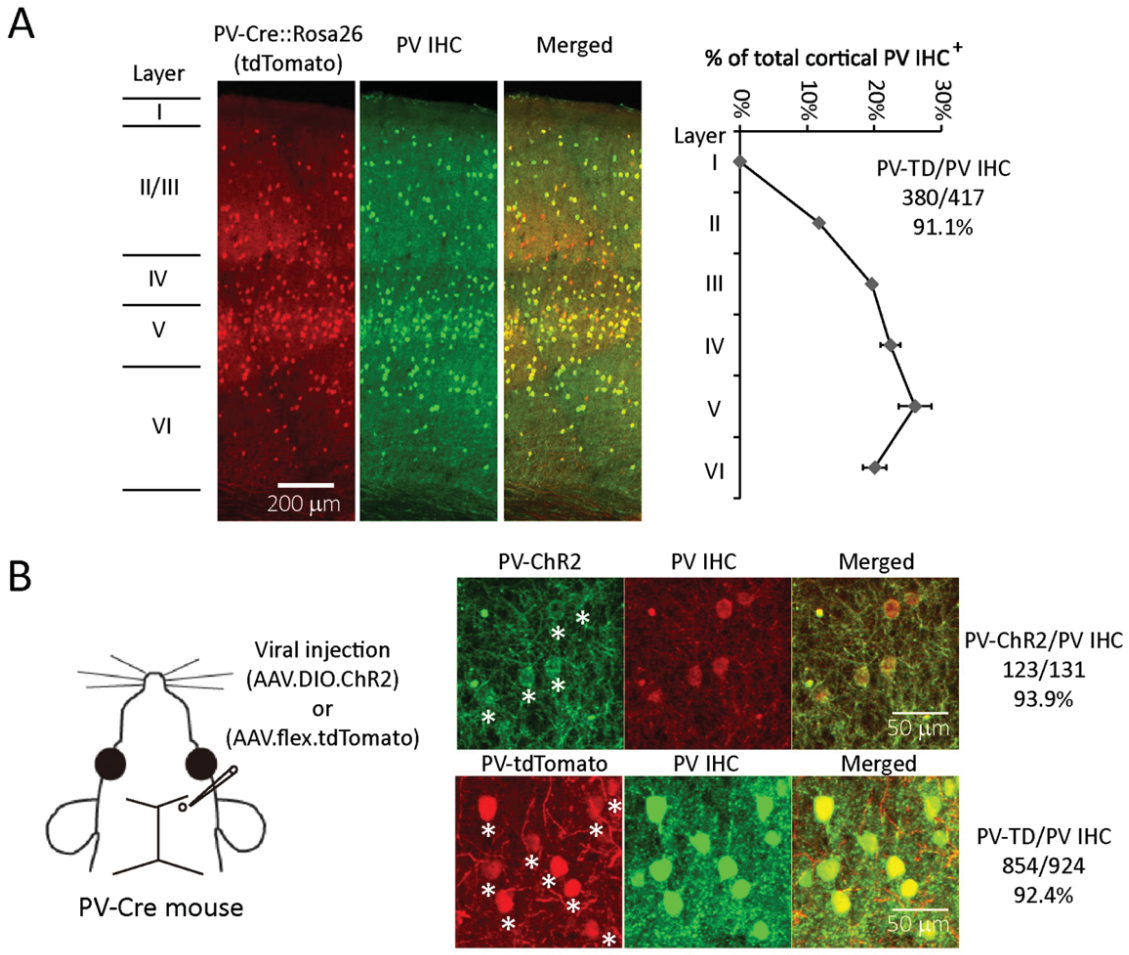

Figure 3.1 PV-Cre dependent expression within parvalbumin interneurons and experimental design with global ischemia and reperfusion model.

A. Confocal fluorescence images of coronal sections through Layer I to VI in the forepaw somatosensory cortex of PV-Cre line crossed with the ROSA-tdTomato reporter line (PV-Cre x Ai9) show overlay between PV-Cre expression and PV-antibody immunohistochemical (IHC) staining. Layer borders are indicated on the left. Ratios of PV IHC$^+$ cells distributed through layer I to VI and tdTomato expressed cells/PV IHC$^+$ cells are shown on the right (mean ± SEM, n=2). B. AAV1.DIO.ChR2-eYFP or AAV1.flex.tdTomato was injected into the somatosensory cortex (350~400 μm depth) of PV-Cre mice at ~1 nl/s using glass pipettes (tips are <25 μm in diameter) at least 3 weeks before experiments. ChR2-eYFP/tdTomato expressed cells and PV

IHC are shown. Stars indicate ChR2-EYFP and PV IHC$^+$ co-localized cells. Ratio of viral expressed cells to PV IHC$^+$ cells is shown on the right.

3.3.2 Reversible Loss of PV Neuron Dendritic Structure following Global Ischemia and Reperfusion

We investigated the impact of reversible global ischemia on the dendritic structure of PV-neuron dendrites located within the first 100 μm of somatosensory cortex (Fig. 3.1C). In contrast to layer 5 excitatory neurons (Brown et al., 2007), PV-neurons exhibited few or no clear spines on their dendrites (Fig. 3.2Aiia). Therefore, we focused on potential structural alterations apparent within the dendrites. All dendrites were imaged using ~40 to 60 μm z-stacks within layer 1 taken at ~2 min intervals. Cortical surface temperature was maintained at ~36.5 ℃ using a temperature controlled thermoregulation system (Tran et al., 2011; Xie et al., 2012). Six of ten animals exhibited >6 mV DC-EEG depolarization (Fig. 3.2B) following induction of global ischemia and this DC shift was associated with > 90% suppression of spontaneous EEG power (filtered into 0.3-3 Hz, Fig. 3.2B). Damage to dendritic structure was assessed using an automated software procedure we previously developed termed BlebQuant (Chen et al., 2011). CCAO induced dendritic damage to PV-neurons within 4 min (77.4 ± 7.6% blebbed dendrites), which correlated with the appearance of ischemic depolarization (DC-EEG). The damage consisted of regular dendritic swellings or blebs similar to reports from pyramidal neurons (Zhang et al., 2005; Andrew et al., 2007; Takano et al., 2007; Murphy et al., 2008; Mostany et al., 2010; Risher et al., 2010; Mostany and Portera-Cailliau, 2011). Reperfusion rapidly recovered the dendritic structure to near the baseline levels within 10 min (1.6 ± 0.9% blebbed dendrites) and remained stable for the following hour (0.2 ± 0.1% blebbed dendrites at 1 h). These results indicated that

the dendritic structure of PV-neurons is vulnerable to ischemic injury, but this apparent injury is reversible following reperfusion.

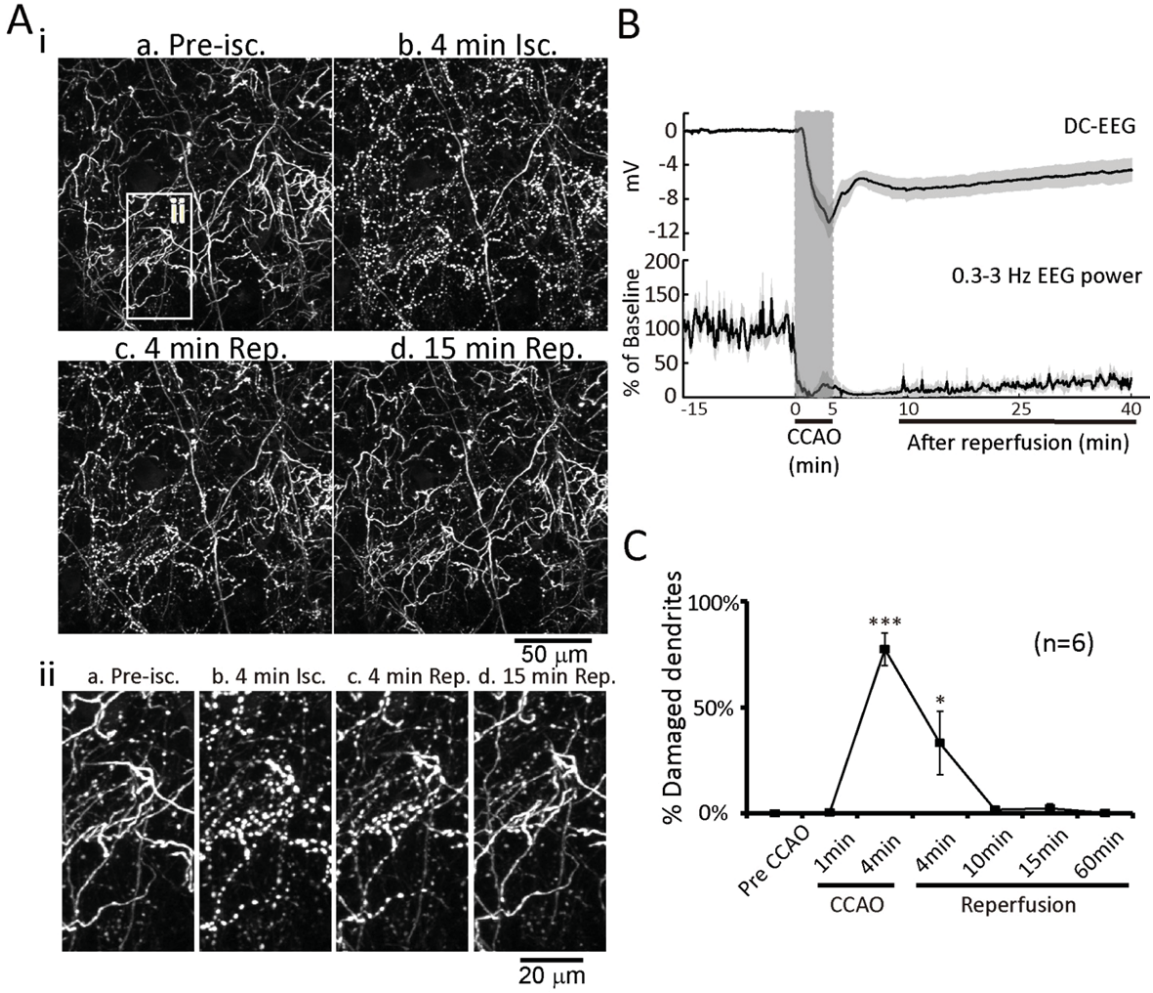

Figure 3.2 Global ischemia induces dendritic damage to parvalbumin neurons (inhibitory interneurons) and rapidly recovers following reperfusion.

A. i. 2-photon imaging (0-60 μm in depth) following 5 min global ischemia and reperfusion. The white-boxed area on the top left corresponds to a region in higher magnification illustrations below (ii). B. Changes of average direct current (DC) potential, spontaneous

electroencephalography (EEG) power (0.3-3 Hz) are shown (mean ± SEM, n=6). C. Average percentage of damaged dendrites during global ischemia and reperfusion are shown (mean ± SEM, ***p<0.001, one-way ANOVA followed by Bonferroni's post-test, compared to pre-CCAO group, n=6). CCAO, common carotid arterial occlusion; Isc, ischemia; Rep, reperfusion.

3.3.3 Pharmacological Characterization of PV-ChR2 Stimulation-Evoked Electrical Responses in the Somatosensory Cortex

In pilot studies, we were unable to reliably detect light-induced PV-ChR2 stimulation-evoked responses as EEG signals using a surface silver wire (data not shown). However, to achieve more sensitive recordings and to also provide cortical laminar information regarding PV-ChR2 stimulation-evoked responses, we employed a 16-channel optrode. The optrode permitted stimulation of ChR2-expressed PV-neurons from a laser fiber positioned ~50 μm above the cortical surface and simultaneously recording of the light-evoked LFP responses throughout the layers of the somatosensory cortex. At alternate time intervals we recorded the contralateral forepaw electrical stimulation-evoked LFP (Fig. 3.3A). Noticeably, there were larger PV-ChR2 stimulation-evoked LFP signals in layer IV/V compared to shallower layers, even with much less laser exposure at deeper layers (Fig. 3.3B).

To further confirm the localization of PV-ChR2 and forepaw stimulation-evoked responses and eliminate far-field signal contribution, we performed current source density (CSD) analysis on 16-channel LFP data. CSD analysis showed that a 10 ms 5 mW blue laser stimulation induced rapid current sinks followed by current sources in layer IV/V (Fig. 3.3C), appearing as a downward dip followed by a rapid upward rise in LFP signals (Fig. 3.3B). In theory, these were typical responses generated from photocurrent and action potential-induced current influx (sinks) followed by an inhibitory synaptic activation-mediated current outflow (sources) in the local

network (Mitzdorf, 1985). A 1 mA 1 ms forepaw electrical stimulation induced typical current sinks in layer IV that rapidly extended toward layers II/III and upper layer V (Fig. 3.4C), similar to previously reported findings in the somatosensory cortex (Mégevand et al., 2009).

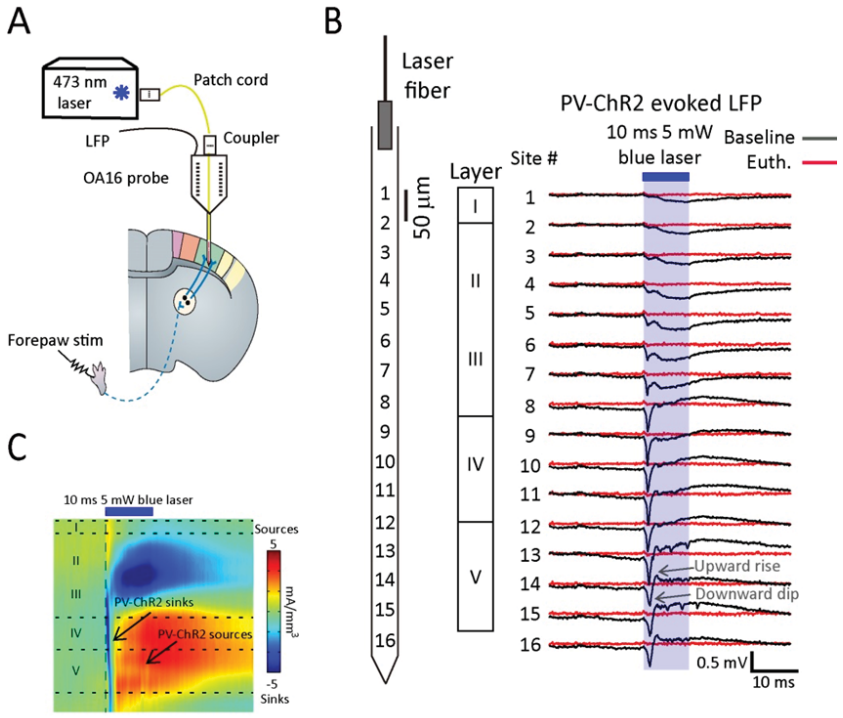

Figure 3.3 16-channel optrode laminar recording of PV-ChR2-mediated local field potential signals and current source density (CSD) analysis in the cortex.

A 16-channel optrode (OA16, NeuroNexus Technologies) with an optical fiber attached at ~50 µm above the first recording site was placed into the somatosensory cortex of AAV.DIO.ChR2-injected PV-Cre mice for local field potential recording and ChR2 stimulation. The contralateral forepaw was electrically stimulated to induce sensory cortical responses for comparison. B. On the left: a cartoon shows the distribution of each recording site of the optrode in the somatosensory cortex. On the right: 10 ms 5 mW of blue laser PV-ChR2 stimulation-evoked LFP signals corresponding to laminar layers before (black) and after euthanasia (red). C. CSD analysis is performed with Cubic spline iCSD method based on 16 channel LFP signals using a MATLAB based program – CSDplotter. LFP, local field potential; Euth, euthanasia.

Cortical surface bath application of 30 μM TTX suppressed the peak amplitude of layer IV/V PV-ChR2 stimulation-evoked current sinks to 42.3 ± 14.2% of baseline level (downward LFP to 48.5 ± 17.9% of baseline level) and abolished the current sources/upward LFP (Fig. 3.4Ai, iii, iv, C). Bathing with 1 μM GABAA receptor antagonist – gabazine abolished the peak value of the current sources/upward LFP without affecting the peak value of the current sinks/downward LFP (Fig. 3.4Aii, iii, iv, C). The action of TTX and gabazine within layer IV/V was confirmed by the blockade and amplification of forepaw stimulation-evoked current sinks/LFP signals, respectively (Fig. 3.4Bi, ii, iii, C). We suggest that the current sinks/downward LFP reflected the excitability of PV-neurons (ChR2 channel photocurrent and PV-neuron action potential), while the current sources/upward LFP reflected a GABAergic inhibitory synaptic network activity upon PV-neurons stimulation.

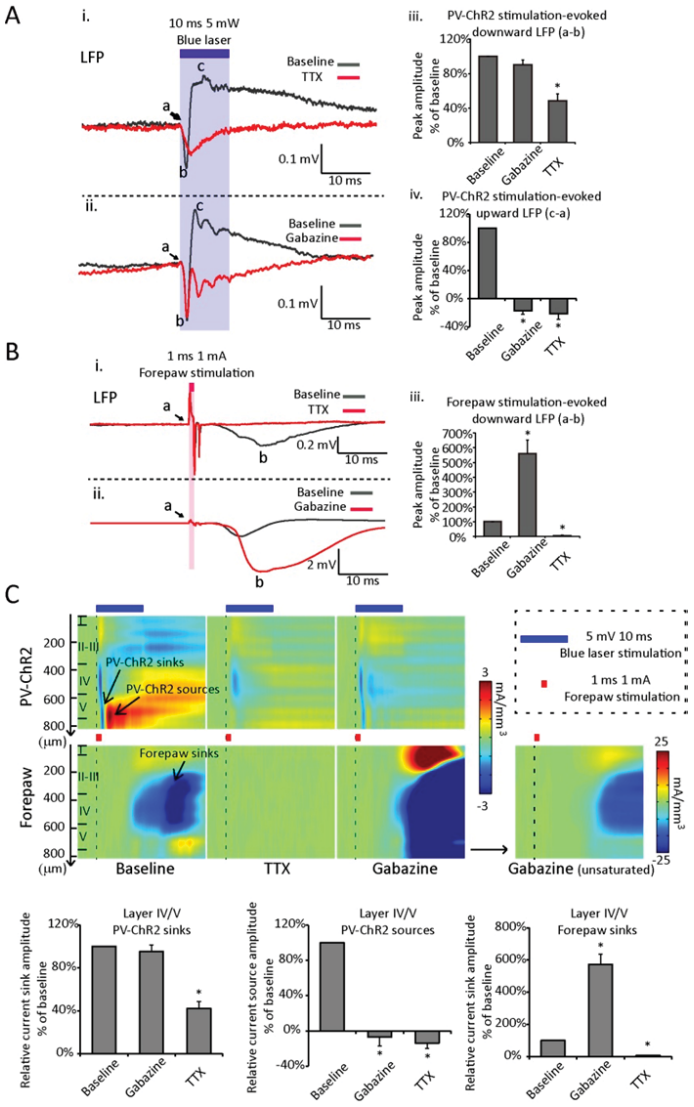

Figure 3.4 Pharmacological definition of PV-ChR2 stimulation-evoked local field potential signals.

A. Cortical application of 30 μM tetrodotoxin partially suppresses the peak value of 10 ms 5 mW light-evoked PV-ChR2 downward LFP signals (i, iii, peak value is calculated as the difference between the downward peak (b) and baseline (a)) and abolishes the light-evoked upward LFP signals (i, iv, c-a, c – upward peak, a – baseline value) in layer IV/V. Cortical application of 1

μM gabazine depresses the PV-ChR2 stimulation-evoked upward LFP signals (ii, iv), while it does not significantly change the peak value of the downward LFP signals (ii, iii) in layer IV/V. B. The same application of TTX or gabazine abolishes (i, iii) or amplifies (ii, iii) the peak value of 1 ms 1-1.5 mA forepaw stimulation-evoked LFP signals (b-a) at the same recording site respectively, confirming the drug action deep input layers. C. Current source density analysis of the PV-ChR2 stimulation-evoked and the forepaw stimulation-evoked responses through layer I to V confirms the conclusion from LFP measurements without potential far-field contamination. TTX partially suppresses the PV-ChR2 stimulation-evoked current sinks and abolishes the PV-ChR2 stimulation-evoked current sources in layer IV/V; gabazine abolishes the PV-ChR2 stimulation-evoked current sources in layer IV/V. All numbers are normalized to the value before drug application, mean ± SEM, *$p<0.001$, RM-ANOVA, n=5 for each drug. All traces in A, B, C are averaged from 20-30 repetitions. Some sweeps with occasional seizure-like depolarization in gabazine experiment were removed from the analysis. LFP, local field potential; TTX, tetrodotoxin.

3.3.4 ChR2-Based Functional Assessment of PV-Neurons in the Cortex following a 5 min Transient Global Ischemia and Reperfusion

Pharmacologically defined excitability (current sinks/downward LFP) and GABAergic synaptic network activity upon PV-ChR2 stimulation (current sources/upward LFP) were used to characterize the function of PV-neurons in layer IV/V following a 5 min global ischemia and reperfusion in the forelimb somatosensory cortex in mice. We considered an animal that has >6 mV DC-EEG shift following the onset of global ischemia as successful global ischemia (Fig. 3.5A, n=5). 0.3-3 Hz AC-EEG power exhibited faster suppression during global ischemia and delayed recovery compared to DC-EEG shift following reperfusion (Fig. 3.5A), which was consistent with our previous reports (Murphy et al., 2008; Chen et al., 2012b; Xie et al., 2013) and structural experiments (Fig. 3.2B). We recorded 10 ms 5 mW blue laser stimulated PV-ChR2-evoked LFP responses as well as 1 ms 1~1.5 mA electrical stimulation of contralateral forepaw-evoked LFP responses throughout cortical layers (0 – 800 μm) before, during a 5 min global ischemia and following reperfusion (Fig. 1C) and then performed CSD analysis (Fig.

3.5B, D). Multi-unit activity (MUA) was extracted from raw LFP signals, where spiking activity was counted over a 150 ms period following the onset of electrical forepaw stimulation and over a 70 ms period following the onset of blue laser stimulation (Fig. 3.5Ci, ii, iii). We considered the short-latency PV-ChR2 stimulation evoked MUA as mostly PV-neuron single unit activity, given the stimulation of the inhibitory neurons should have suppressed spontaneous MUA. This proposal is supported by a silent period following the laser stimulation where few spikes were observed (Fig. 3.5Cii, baseline). Peak values of current sinks (downward LFP) and current sources (upward LFP) from the pre-stimulation values were measured. 5 min global ischemia greatly suppressed all forms of activity in layer IV/V evoked by PV-ChR2 stimulation or forepaw stimulation. Activity gradually recovered within ~ 1 h following reperfusion (Fig. 3.5E), suggesting the function of PV inhibitory interneurons was not spared from the effect of ischemia, but can be partially restored by introducing reperfusion.

We then compared the PV-ChR2 stimulation-evoked current sources, sinks, and MUA to further determine the relationship between the changes of putative excitability of PV-neurons (current sinks, time-locked MUA), and GABAergic synaptic network activity upon PV-neuron stimulation (current sources, upward LFP). 1 min after the onset of global ischemia, the PV-ChR2 stimulation-evoked current sources were suppressed more rapidly than the current sinks (24.2 ± 10.7% *vs.* 84.9 ± 13.4% of baseline, $p<0.01$). Global ischemia further depressed both the current sources and sinks (putative GABAergic synaptic network activity and PV-neurons excitability measure respectively) to less than 10% of baseline level at 4 min. ~3 min after the induction of reperfusion, the excitability of PV-neurons (current sinks) started to recover, whereas the inhibitory synaptic transmission mediated network activity (current sources)

exhibited prolonged suppression (84.9 ± 13.4% of baseline *vs.* 2.1 ± 4.3%, $p<0.001$). The mismatch between the recovery of current sinks and sources was present during the first hour after reperfusion (Fig. 3.5F). Interestingly, the stimulation time-locked MUA of PV-neurons showed a slower suppression and faster recovery compared to the current sources during global ischemia and immediate following reperfusion. This suggested a period that PV-neurons can still generate action potentials, yet cannot fully synaptically signal surrounding neurons to generate the GABAergic synaptic network activity. Similar to PV-ChR2 simulation-evoked current sources, the forepaw stimulation-evoked current sinks and MUA were depressed rapidly following the induction of global ischemia and recovered more slowly and incompletely following reperfusion (Fig. 3.5G), consistent with our previous work with LFP analysis (Chen et al., 2012b). Noticeably, the forepaw stimulation-evoked MUA in layer IV/V depressed more rapidly during global ischemia, and recovered more slowly within 9 min following reperfusion, compared to the current sinks (Fig. 3.5G). It indicated a period that the cells in layer IV/V had current influx, but were less likely to generate action potentials following sensory stimulation. There were no differences between the suppression and recovery of PV-ChR2 stimulation-evoked GABAergic synaptic activity and the forepaw stimulation-evoked responses within the first 0.5 h following reperfusion ($p>0.05$, Fig. 3.5G). The differences between PV-ChR2 stimulation-evoked current sources and forepaw stimulation-evoked current sinks at 55 min following reperfusion (Fig. 3.5G) may suggest a mismatch of layer IV/V network activity that are dependent on GABAergic synaptic transmission (Fig. 3.4C) and glutamatergic synaptic transmission (Chen et al., 2012b).

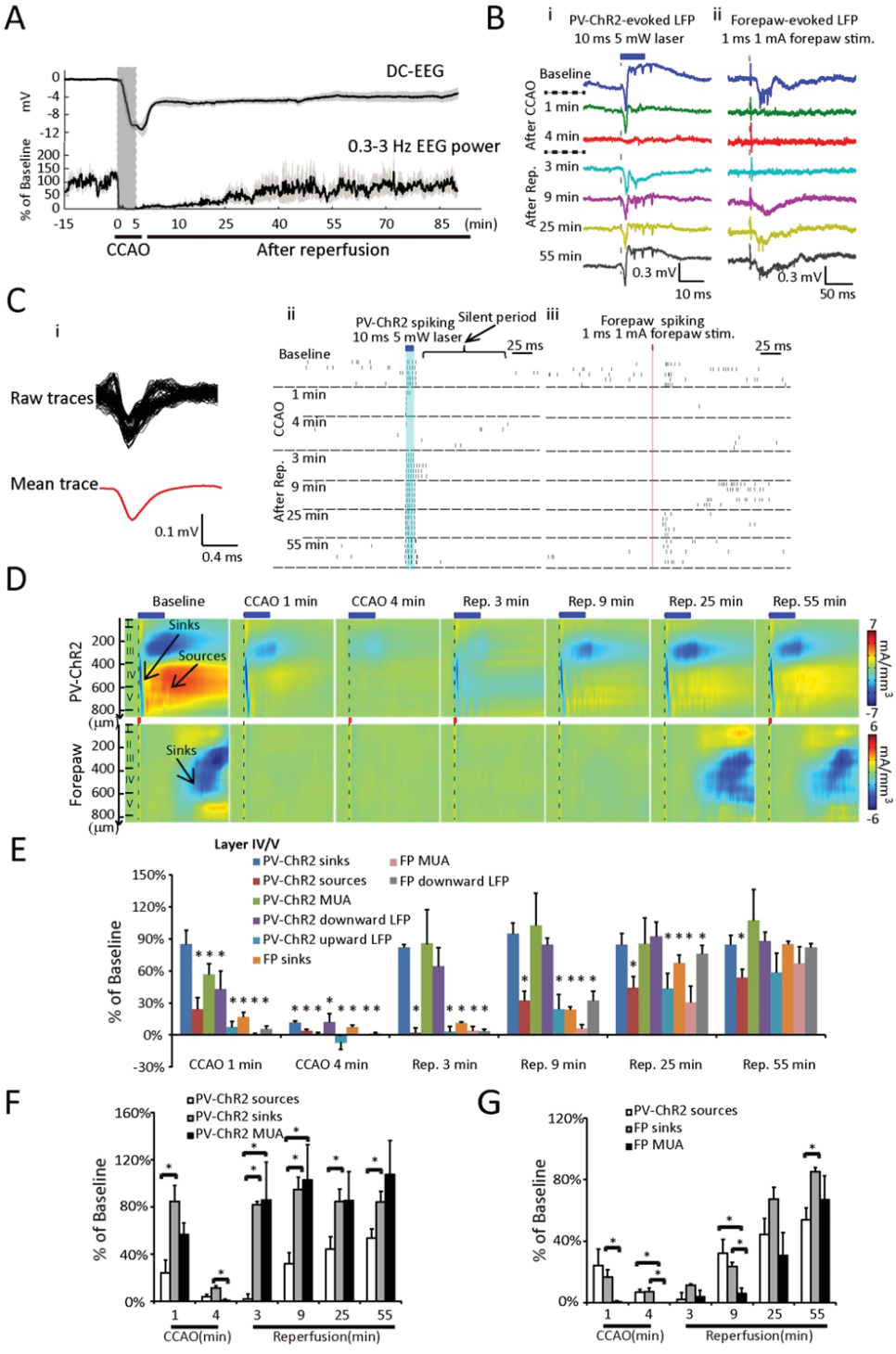
A
DC-EEG
0.3-3 Hz EEG power
mV
% of Baseline
CCAO
After reperfusion
(min)
B
i PV-ChR2-evoked LFP
10 ms 5 mW laser
ii Forepaw-evoked LFP
1 ms 1 mA forepaw stim.
Baseline
After CCAO
After Rep.
0.3 mV
10 ms
50 ms
C
i
Raw traces
Mean trace
0.1 mV
0.4 ms
ii
PV-ChR2 spiking
10 ms 5 mW laser
Silent period
iii
Forepaw spiking
1 ms 1 mA forepaw stim.
25 ms
CCAO
After Rep.
D
Baseline
CCAO 1 min
CCAO 4 min
Rep. 3 min
Rep. 9 min
Rep. 25 min
Rep. 55 min
PV-ChR2
Forepaw
Sinks
Sources
mA/mm3
E
Layer IV/V
PV-ChR2 sinks
PV-ChR2 sources
PV-ChR2 MUA
PV-ChR2 downward LFP
PV-ChR2 upward LFP
FP sinks
FP MUA
FP downward LFP
% of Baseline
F
PV-ChR2 sources
PV-ChR2 sinks
PV-ChR2 MUA
CCAO(min)
Reperfusion(min)
G
PV-ChR2 sources
FP sinks
FP MUA
CCAO(min)
Reperfusion(min)

Figure 3.5 Reperfusion recovers layer IV/V PV-neurons excitability rapidly, but recovers GABAergic synaptic network activity more slowly and incompletely from a 5 min global ischemia-induced suppression.

A. Changes of average DC potential, spontaneous EEG power (0.3-3 Hz) are shown (mean ± SEM, n=5). B. i. 10 ms 5 mW PV-ChR2 stimulation-evoked LFP responses; ii. 1ms 1 mA forepaw electrical stimulation-evoked LFP responses in layer IV/V before and after global ischemia and reperfusion. Traces represent single LFP signals at various indicated time points. C. i. Averaging spike waveform for multi-unit spike sorting; ii, iii. Rasterplots show the PV-ChR2 stimulation-evoked spiking activities and the forepaw stimulation-evoked spiking activities. 5 trials are shown at each time point. D. Current source density analysis shows the PV-ChR2 stimulation and the forepaw stimulation-evoked current sinks and sources through layer I to V at various indicated time points. E. Changes of all the forms of the PV-ChR2 stimulation and the forepaw stimulation-evoked responses in layer IV/V at various indicated time points corresponding to the 5 min global ischemia and reperfusion, compared to the baseline level. All numbers are normalized to the value before global ischemia (100%), mean ± SEM, n=5. *p<0.05, RM-ANOVA. F. Group comparison of PV-ChR2 simulation-evoked current sinks, current sources and time-locked spiking number (MUA) in layer IV/V at various time points are shown. All numbers are normalized to the value before global ischemia (100%), mean ± SEM, n=5, *p<0.05, RM-ANOVA. G. Group comparison of PV-ChR2 simulation-evoked current sources, forepaw stimulation-evoked current sinks and forepaw stimulation-evoked spiking number (MUA) in layer IV/V. All numbers are normalized to the value before global ischemia (100%), mean ± SEM, n=5, *p<0.05, RM-ANOVA. Stim, stimulation.

3.4 Discussion

In the present study, we have selectively investigated the structure and network function of PV neurons in mouse forelimb somatosensory cortex during acute global ischemia and reperfusion using optogenetic tools, *in vivo* imaging, and optrode recording. Despite having structurally intact dendrites and excitable membranes, GABAergic synaptic transmission dependent network activity was not functionally recovered within the first hour after reperfusion.

3.4.1 Inhibitory Neurons Are Not Spared from Dendritic Damage during Global Ischemia

Previous studies in both humans and rodents suggest that global ischemia induced neuronal loss is enriched in the hippocampal CA1 region, and can result in impaired learning and memory (Zola-Morgan et al., 1986; Block, 1999). However, it has been shown that the cortex can also be impaired by short periods of global ischemia despite lacking widespread neuronal death; and this could contribute to cognitive deficits (McKhann et al., 1997; Lim et al., 2004). We have previously shown that a transient global ischemia can induce a reversible damage of the apical dendritic structure of layer V excitatory neurons during ischemic depolarization (Murphy et al., 2008). Our current findings suggest that PV-neurons are as vulnerable as pyramidal neurons to the acute insult of ischemia on dendritic structure. This vulnerability is apparent despite previous reports indicating enhanced resistance of PV-neurons to ischemia-induced neuronal death, that has been attributed to their enhanced Ca^{2+} buffering *via* parvalbumin (Nitsch et al., 1989; Freund et al., 1990; Johansen et al., 1990; Tortosa and Ferrer, 1993). Conceivably, this enhanced Ca^{2+} buffering is insufficient against the initial ischemic depolarization-triggered massive Ca^{2+} elevation that can be independent of direct NMDA-receptor-mediated Ca^{2+} influx (Jarvis et al., 2001; Anderson et al., 2005; Thompson et al., 2006; Murphy et al., 2008). It is also possible that some changes to PV-neuron structure may be indirectly caused by ischemic depolarization induced-compression due to swollen components of adjacent cells (Andrew et al., 2007; Risher et al., 2012).

3.4.2 Dissecting the Cortical Laminar Electrical Signals upon PV-ChR2 Stimulation

Compared to the conventional techniques used to measure excitability and synaptic function of select neurons, such as patch clamp electrophysiology (Pang et al., 2002; Runyan et al., 2010), optogenetic-based measurements have the advantage of potentially being less invasive and able to sample potentially more locations. However, we acknowledge our approach using extracellular electrophysiological recording of optogenetic stimulation-evoked responses may not be a specific measurement restricted to light-activated neurons, as other synaptically active cells are within the network. In support of the method, we pharmacologically show that the PV-ChR2 stimulation induces rapid current sinks followed by current sources in layer IV/V that were dependent on PV-neuron depolarization and GABAergic inhibitory synaptic transmission-mediated network activity, respectively. It is unclear why the PV-ChR2 simulation-evoked current sinks and sources were localized in relatively deep layers, despite these layers receiving much less illumination from the laser localized above the cortical surface. This might be due to a relatively higher density of PV-neurons in layer IV/V (Fig. 3.1A) (Ren et al., 1992; Pfeffer et al., 2013). It is also possible that the anesthesia suppresses neuronal activity in superficial layers (Petersen et al., 2003; Constantinople and Bruno, 2011; Chen et al., 2012a).

3.4.3 Mechanisms of Prolonged Loss of GABAergic Synaptic Network Activity following Reperfusion

In our study, the reduction of PV-neuron excitability during and immediately following ischemic depolarization is likely related to a loss of membrane potential and depolarization block of PV-neurons. The observed persistent suppression of GABAergic network activity (evoked by PV-

ChR2 stimulation) following reperfusion is consistent with previous reports from rat hippocampal brain slices (Zhan et al., 2006), and may in part be mediated by a depression of presynaptic release caused by adenosine receptor activation (Pang et al., 2002; Ilie et al., 2006; Chen et al., 2012b). Alternatively, ischemia-induced internalization or down-regulation of post-synaptic GABAergic receptors (Alicke and Schwartz, 1995; Qü et al., 1998) is a postsynaptic mechanism for loss of inhibitory synaptic activity. Moreover, reversal of GABA transporter following ischemia (Allen et al., 2004) could deplete the sources of presynaptic exocytosis and saturate the post-synaptic receptors to suppress generation of phasic GABA activity.

3.4.4 Implications of Prolonged Deficits in PV-Neuron Stimulation-Dependent GABAergic Synaptic Transmission following Reperfusion on Cognition and Functional Recovery

Previous evidence has shown that focal stroke can cause sustained alterations in the E/I balance in peri-infarct cortex (Buchkremer-Ratzmann and Witte, 1997; Clarkson et al., 2010, 2011; Carmichael, 2012). Restoring the E/I balance by blocking tonic GABA currents (Clarkson et al., 2010) or stimulating AMPA-type glutamate receptors (Clarkson et al., 2011) promotes functional recovery after focal stroke. Despite the fact that inhibitory neuron-mediated phasic GABA current is not the predominant inhibitory conductance source in the cortex (tonic currents can be greater) (Carmichael, 2012), it could still be critical for stroke recovery since it can regulate brain states (Cardin et al., 2009) and sensory processing that leads to perception (Lee et al., 2012; Wilson et al., 2012; Pfeffer et al., 2013). There is no direct *in vivo* evidence about whether global ischemia and reperfusion could result in E/I imbalance. Previous work using brain slice

electrophysiology has shown that 4 min of *in vitro* ischemia and reperfusion, which mimics *in vivo* global ischemia and reperfusion model, permanently impaired the excitability and GABAergic synaptic transmission of cortical inhibitory neurons. Interestingly, this manipulation made principal neurons more excitable during reperfusion (Wang, 2003). Our *in vivo* results have shown that the structure and excitability of both cortical pyramidal neurons and PV inhibitory neurons recovered concurrently with the repolarization of the recorded EEG during reperfusion after stroke (Murphy et al., 2008; Chen et al., 2012b; Xie et al., 2013), whereas PV-neurons stimulation dependent GABAergic synaptic network activity exhibited a prolonged suppression at least over the first hour that were assessed. Our work assessing sensory responses suggests excitatory circuits also experience a persistent suppression, but were less impaired than the GABAergic synaptic network activity upon PV-ChR2 stimulation 1 h after reperfusion. We propose that the incomplete recovery of GABAergic synaptic transmission could contribute to E/I imbalance and lead to the deficits of sensory and motor processing in the cortex (Lesnick et al., 1984; Chen et al., 2012b; Xie et al., 2013). While we mention changes in E/I balance, it is also important to remember that these changes are likely to occur in the background of profoundly suppressed activity that occurs in the days to weeks after stroke (Krakauer et al., 2012). These mismatches may contribute to cognitive dysfunction following a transient global ischemia (Nunn and Hodges, 1994; McKhann et al., 1997; Lim et al., 2004). Optogenetic-based chronic recordings in combination with behavioral assessments are needed to further explore these hypotheses in the future.

In this study, we have developed a novel methodology to assess the structure and network function of a particular inhibitory neuron population *in vivo*, following a transient ischemic

episode. This method can be applied to chronically study changes within inhibitory neuronal networks during other brain diseases with a chronic imaging window (Holtmaat et al., 2009; Drew et al., 2010; Yang et al., 2010), or optrode implantation (Gradinaru et al., 2010; Zhang et al., 2010). With the development of multi-color optogenetic techniques (Tye and Deisseroth, 2012; Lin et al., 2013; Klapoetke et al., 2014), it would be possible to monitor the function of different neuronal subtypes in the same mouse following stroke. Moreover, our approach can also be used to test potential stimulation paradigms that target inhibitory neuron networks as potential treatments for stroke patients (Hummel and Cohen, 2006; Kravitz et al., 2010; Cheng et al., 2014).

Chapter 4: Resistance of Optogenetically Evoked Motor Function to Global Ischemia and Reperfusion in Mouse *in vivo*

4.1 Introduction

Stroke is characterized as a disturbance of blood flow to the brain, resulting in neuronal death and impairment of sensory, motor and cognitive function (Murphy and Corbett, 2009). During recovery, neurons exhibit either short-term or long-term plasticity to re-establish the lost functions (Carmichael, 2012). We adapted a model of global ischemia that permits timely and precise bilateral occlusion of the common carotid arteries (CCAO) and reperfusion. This model is relevant to brain insults due to cardiac arrest or other transient period of ischemia to study its impact on motor function. Previously, we found that reperfusion led to a recovery of dendritic structure from 7-9 min transient global ischemia, and a gradual but partial recovery of sensory response in the cortex after ~1 hour (Murphy et al., 2008; Murphy and Corbett, 2009). Changes in motor function following stroke have been assessed exclusively in focal ischemia models using intracortical microstimulation (ICMS) (Nudo, 2006) or behaviour test (Ruscher et al., 2011) . However, rapid plasticity has been largely unstudied since a single ICMS map may require up to an hour to perform and the invasive nature of ICMS limits the repeatability of mapping (Tennant et al., 2011). Recently developed automated motor mapping techniques based on light activation of Channelrhodopsin-2 (ChR2) permit non-invasive investigation of both motor output and map integrity with high temporal resolution following stroke (Ayling et al., 2009). Pairing this method with measurements of cortical EEG evoked by direct ChR2 stimulation (ChR2-EEG) and peripheral sensory stimulation of the same limb (forepaw-EEG) where the motor output was

assessed, we compared motor function, cortical neuronal excitability, and sensory function within the same mouse following global ischemia and reperfusion. This study provides new insights into the recovery of motor and sensory processing following global ischemia.

4.2 Materials and Methods

4.2.1 Animal, Surgical Procedures and Regulation of Cortical Temperature

Adult male *Thy1*-ChR2-yellow fluorescent protein (YFP) transgenic mice (B6.Cg-Tg(Thy1-COP4/EYFP)18Gfng/J) (Arenkiel et al., 2007) aged 2~3 months were used. Experimental protocols were approved by the University of British Columbia animal care committee and conformed to the Canadian Council on Animal Care and Use guidelines. A 4 × 4 mm cranial window was made over the somatosensory and motor cortex leaving the dura intact. Body temperature was maintained throughout surgical and imaging procedures at 37 ± 0.5 °C. In all animals, the cortical surface temperature was maintained at ~36.5 °C by attaching a custom-made stainless steel head plate connected to a water pump (Xie et al., 2012).

4.2.2 Global Ischemia Model

Bilateral occlusion of the common carotid arteries (CCAO) was performed as in previous studies to induce global forebrain ischemia under ketamine/xylazine anesthesia.

4.2.3 Light-Based Motor Mapping and ChR2 Stimulation

Light-based motor mapping (LBM) methodology has been described previously (Ayling et al., 2009). In the present study, we used a scanning stage (ASI MS-2000, Applied Scientific Instrumentation Inc., OR, USA) controlled by custom Igor Pro software (Wavemetrics, OR,

USA) to direct a 473 nm laser beam (CrystaLaser, NV, USA; focused to 100 μm diameter, 10 ms pulses) to an array of cortical sites (12 × 14, with 300 μm spacing between sites). EMG responses were collected at 5 kHz, and band-pass filtered (0.5-500 Hz), fully rectified, and integrated over 0.1 s from stimulus offset to generate values arrayed in maps. Each value represents the mean of 2 repetitions. We first performed motor mapping (n=5) using 120 mW/mm^2 laser power before CCAO for a baseline map, and then started to generate maps from 5-10 min after the induction of CCAO with an ~12 min interval between each map. In a second group of mice (n=5), we first generated a motor map using 120 mW/mm^2 laser power and then delivered repeated 5 ms 635 mW/mm^2 stimuli with a 10 s interstimulus interval to the center of the map.

4.2.4 Laser Speckle Contrast Imaging

The procedures for laser speckle imaging was performed as described previously (Murphy et al., 2008). Briefly, the cortical surface was illuminated by a 784 nm, 32 mW StockerYale SNF-XXX-785S-35 laser (NH, USA) with an Edmund Optics anamorphic beam expander T47274 (NJ, USA), and images were collected at 1 Hz with a Dalsa M60 Pantera camera (ON, Canada).

4.2.5 EEG and EMG Recording

We employed the same system for EEG (Chen et al., 2012b) recording and forelimb EMG (Ayling et al., 2009). A single electrode was placed close to the forelimb somatosensory cortex (Fig.4.1 insert – b electrode) for recording DC-EEG signal, which was high pass filtered (0.1 Hz, Bessel filter, 8 pole) to exclude the slow DC shift for bipolar EEG studies. EEG signals were

sampled at 1000 Hz. EMG signals were sampled at 1000 Hz for single point ChR2 stimulation and at 5000 Hz for motor mapping.

4.2.6 Statistical Analyses

Forepaw-EEG and ChR2-EEG amplitudes were the minimum value in a 40 s period after stimulation. For speckle imaging analysis, we randomly selected three arterioles that were within the motor map representation to quantify blood flow velocity changes by examining changes in speckle contrast signal before and after the induction of CCAO and reperfusion. Results were expressed as percentages of pre-CCAO occlusion speckle contrast after subtracting post-euthanasia values (as 0% blood flow). In the analysis, we assume that the velocity of blood flow is proportional to the inverse of square of the speckle contrast as shown previously (Cheng and Duong, 2007) and scaled over a range corresponding to maximal and minimal flow for each animal. All values except DC-EEG were normalized to percentage of pre-CCAO. A one-way ANOVA followed by Bonferroni's post-tests was used to compare differences in blood flow, EMG and EEG values at each time point to pre-CCAO baselines in experimental groups. Differences between ChR2-EEG, ChR2-EMG and forepaw-EEG were analyzed with Student's t test. Statistically significance was set at $p<0.05$.

4.3 Results

4.3.1 Monitoring the Reduction and Recovery of Cortical Blood Flow during Global Ischemia and Reperfusion

The reduction and recovery of blood flow in the cortex during 5 min global ischemia and reperfusion was confirmed with laser speckle contrast imaging. Within the somatosensory cortex confirmed significant decreases in arterial blood flow (18.9 ± 5.3% of the baseline value, $p<0.01$) at 1 min after the on-set of CCAO and maintained below 20% of the baseline value before the induction of reperfusion (n=4, Fig 4.1 Ci). Within 2 min of reperfusion, arteriole blood flow in the motor representation rapidly recovered to 79.0 ± 26.5% of the baseline value ($p>0.05$) and maintained at ~75% of the baseline value after the first minutes (Fig 4.1).

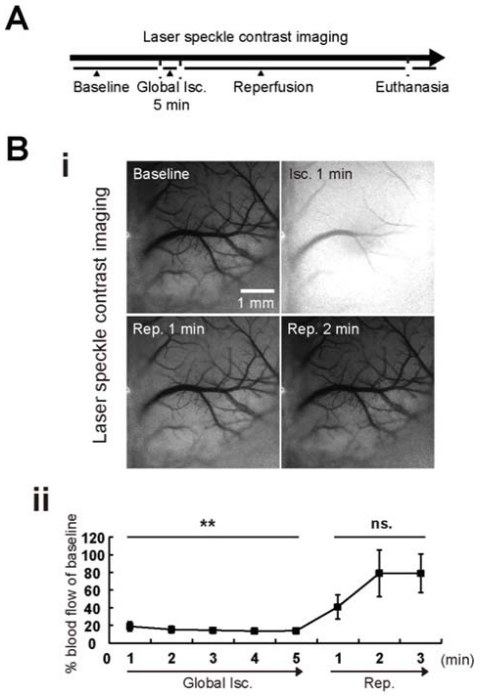

Figure 4.1 Five min CCAO suppresses the blood flow in the motor cortex, with rapid recovery following reperfusion reviewed by laser speckle contrast imaging.

A.) Experimental design. laser speckle contrast imaging was performed during baseline, 5 min CCAO and reperfusion. B.) Laser speckle contrast imaging confirms >80% decrease in blood flow in the forelimb motor representation during CCAO which recovers to >80% of pre-CCAO value within 2 min after reperfusion. i. Representative laser speckle contrast images at pre-CCAO, 1 min after ischemia, 1 and 2 min after reperfusion. ii. Quantitative summary of blood flow in the motor representation following CCAO and reperfusion. (n=4, **p<0.01, compared with pre-CCAO value, one-way ANOVA). All data are shown as mean ± SEM.

4.3.2 ChR2-Based Functional Assessment of Cortical Motor/Sensory Processing following a 5 min Transient Global Ischemia and Reperfusion

Here, we apply optogenetics to evaluate changes in motor representations while simultaneously generating EEG maps of cortical neuronal excitability during and after a 5 min period of

transient global ischemia (Fig 4.2A). In a second group of mice, these changes were assessed with greater temporal resolution by repeated stimulating a single point at the center of forelimb motor cortex while also collecting forepaw-evoked EEG, ChR2-EEG, and spontaneous EEG signals (Fig 4.2B).

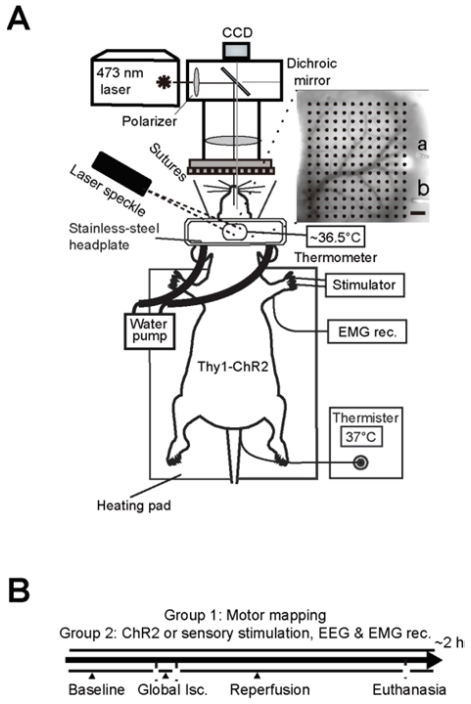

Figure 4.2 An overview of experimental set-up and design.

A.) Anesthetized, head-fixed mice are placed on a scanning stage and an array of cortical points (insert) is stimulated by a 473 nm collimated laser beam directed through a video microscope objective. Motor output is detected by EMG electrodes in forelimb muscles. Surface temperature (a–temperature probe) and cortical EEG signal (b-electrode) are collected. Scale bar is 500 μm. B.) Experimental design. 2 groups of mice are used to conduct either motor mapping or motor output (repetitive center stimulation in the motor map) assessment during baseline, 5 min CCAO and reperfusion.

We performed repeated optogenetic mapping before, during and after CCAO, with EMG map and EEG maps collected every ~15 min following CCAO and reperfusion. The motor map was diminished to 6.6 ± 2.6% of the baseline value ($p<0.001$) in the first mapping session, 5-20 min after the onset of a 5 min CCAO, recovered partially by the second map (21-35 min post stroke, 32.6 ± 8.4%, $p<0.01$) and reached 80.7 ± 17.0% of baseline ($p>0.05$) by the third map 36-50 min after CCAO onset (Fig 4.3Di). The sum of integration of ChR2-EEG signal measured from the center of the motor map (3 × 3 pixels) was suppressed to 21.8 ± 8.4% of the baseline value ($p<0.001$) 5-20 min after occlusion, partially recovered to 63.6 ± 4.3% ($p<0.01$) after 21-35 min and further recovered to 61.6 ± 6.6% ($p<0.01$) 36-50 min after CCAO and reperfusion (Fig 4.3Dii). We found that ChR2-evoked EEG map recovered faster than the ChR2 stimulation generated motor map, indicating that excitability of cortical layer 5 neurons recovered sooner than motor output.

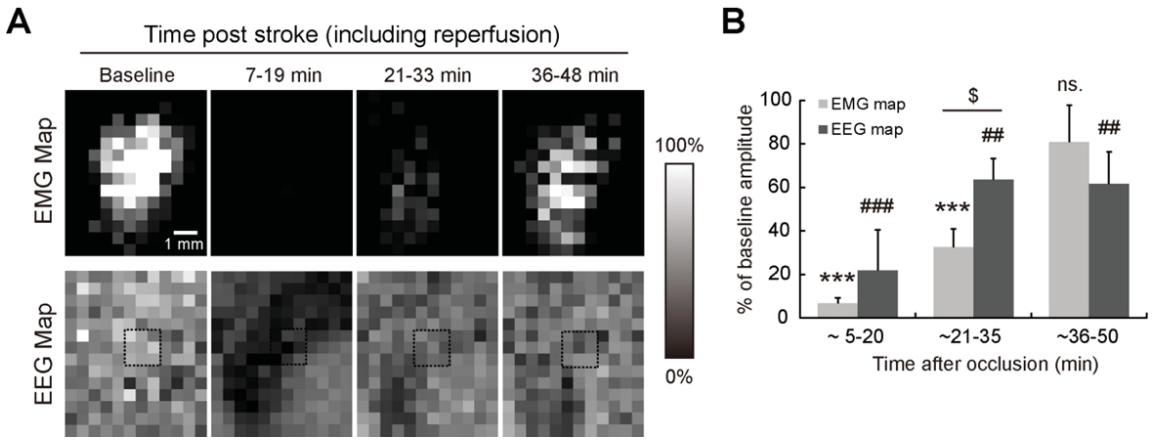

Figure 4.3 5 min CCAO diminishes the amplitude of the EMG and EEG maps evoked by cortical ChR2 stimulation, with rapid recovery following reperfusion.

A.) 5 min CCAO depresses both EEG and EMG maps (integration of signals) evoked by the cortical ChR2 stimulation. Following reperfusion recovers both maps within 1 h. Representative EMG maps (i) and EEG maps (ii) evoked by the cortical ChR2 stimulation following 5 min CCAO and reperfusion. Only the center of motor map (3X3 pixels indicated by black dash line) is used to calculate the ChR2 evoked EEG signal. B.) Quantitative summaries of EMG maps and EEG maps following CCAO and reperfusion (n=5, ***$p<0.001$, $^{\#\#}p<0.01$, $^{\#\#\#}p<0.001$, compared with the pre-CCAO values, one-way ANOVA; $^{\$}p<0.05$, EMG map *vs.* EEG map, Student's t-test). All data are shown as mean ± SEM.

We next compared recovery of motor processing and sensory processing within animals. We first performed optogenetic mapping, then in a separate group of animals to increase temporal resolution of sensory and motor responses laser-stimulation was restricted to the center of the motor map (while measuring EMG from the contralateral forelimb). In single point stimulation animals, we also electrically stimulated the contralateral forelimb and measured the resulting cortical EEG response. Cortical motor and peripheral sensory stimulation were interleaved and repeated every 10 s before, during and after CCAO (n=5, Fig 4.4A). Global ischemia induced ischemic depolarization and suppression of spontaneous 0.3-3 Hz EEG power. Reperfusion rapidly, but partially recovered the ischemia-induced DC-shift, and slowly recovered spontaneous 0.3-3 Hz EEG power (Fig 4.4B). A >10 mV DC shift was observed in all 5 animals, consistent with our above results which used both DC-EEG and IOS imaging to determine ischemic spreading depression in the same model. Changes in the peak amplitude of ChR2 and forepaw-evoked EEG (the minimum value in a 40 ms period after stimulation) were correlated with changes in DC-EEG and 0.3-3 Hz EEG power following CCAO and reperfusion respectively (Fig 4.4B). Within 1 min after occlusion, the forepaw-evoked response was blocked while ChR2-EEG and ChR2-EMG were preserved. Responses evoked by ChR2 and forepaw stimulation were suppressed relative to baseline measures at 5 min after onset of occlusion (ChR2-EEG: 5.9 ± 2.2%; ChR2-EMG: 3.88 ± 1.24%; forepaw-EEG: 7.6 ± 2.3%). ChR2- EMG

recovered faster than the forepaw-EEG (66.2 ± 20.2% *vs.* 15.1 ± 5.9% at 25 min after reperfusion, $p<0.05$). Although motor output recovered more rapidly than peripherally-evoked EEG responses, it was still slower than the recovery of ChR2-EEG (ChR2-EEG: 86.1 ± 32.5% *vs.* ChR2-EMG: 3.9 ± 1.3%, $p<0.05$, or *vs.* forepaw-EEG: 6.5 ± 1.5%, $p<0.05$ at 5 min after reperfusion) (Fig 4.4C). We also observed gradual declines in ChR2-EEG after it recovered to the peak value (96.3 ± 18.8%) at 10 min following reperfusion, which may be due to delayed damage induced by the ischemic insult. However, the ChR2-evoked EMG responses recovered further (97.8 ± 30.5% at 55 min, 123.4 ± 27.8% at 85 min after CCAO and reperfusion) despite the partial suppression of excitability of the neurons which were mediating the EMG responses.

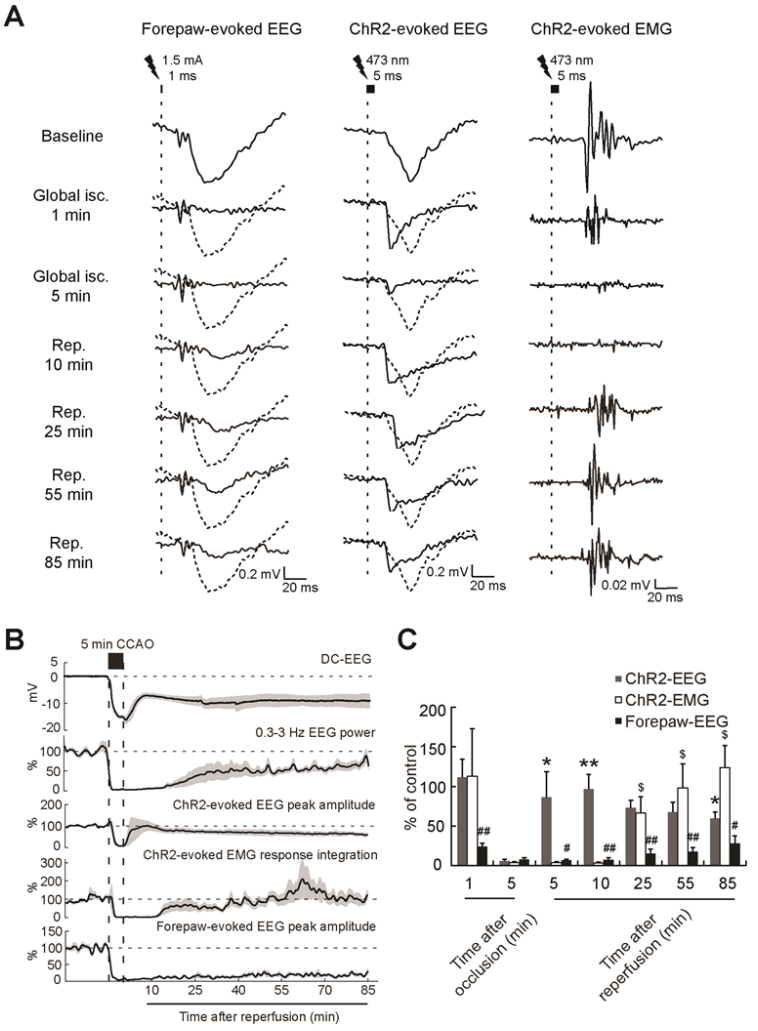

Figure 4.4 Single point ChR2 cortical stimulation and EEG and EMG recording reveal rapid response recovery following reperfusion despite persistent deficits in forepaw stimulation-evoked cortical EEG responses.

ChR2 and sensory stimulation are interleaved and repeated every 10 s. A.) Representative traces of forepaw stimulation evoked EEG (left column), ChR2 stimulation evoked EEG (middle column), and ChR2 stimulation evoked EMG (right column). B.) Changes of DC-EEG (n=5), 0.3 to 3 Hz EEG power (n=5), ChR2 evoked peak amplitude (n=5), ChR2 evoked EMG responses integration (n=5) and forepaw-evoked peak amplitude (n=5) are shown from top to bottom.

Except for DC-EEG, the other statistical data were based on relative values, which were normalized to pre-CCAO value as 100%. The shaded band indicates SEM. C.) Statistical analysis of ChR2 mediated EEG (ChR2-EEG) and EMG (ChR2-EMG) responses, and forepaw stimulation mediated EEG responses (forepaw-EEG) following 5 min CCAO and reperfusion at select time points. (*$p<0.05$, **$p<0.01$, ChR2-EEG *vs.* ChR2-EMG; $^{\$}p<0.05$, ChR2-EMG *vs.* forepaw-EEG; $^{\#}p<0.05$, ChR2-EEG *vs.* forepaw-EEG, Student's t-test). All data are shown as mean ± SEM.

4.4 Discussion

We investigated changes in sensorimotor processing following a transient global ischemia by assessing EMG and EEG responses to cortical optogenetic stimulation and forepaw electrical stimulation. Optogenetics have allowed us to study acute effects of global ischemia that may be relevant to transient ischemic attacks. We discovered that motor output was suppressed during global ischemia and gradually recovered following reperfusion, though recovery of motor output was relatively slower than that of ChR2-EEG responses. We identified a period of time when the cortex was excitable (by ChR2-EEG) but motor output (by ChR2-EMG) was blocked, which corroborates earlier studies comparing sensory processing with cortical neuronal excitability (Chen et al., 2012b). The changes in ChR2-EEG waveform following ischemia may be the result of an incomplete recovery of synaptic transmission since the waveform reflects both direct depolarization of ChR2 excited neurons and a secondary synaptic transmission-induced response (Chen et al., 2012b; Lim et al., 2013). Interestingly, after reperfusion, motor output was nearly fully recovered, consistent with previous reports of cortically evoked responses detected in the brain stem following a transient middle cerebral artery occlusion in rats (Bolay and Dalkara, 1998). However, the delayed and incomplete recovery of the sensory processing suggests that rehabilitative manipulations may need to take the relative vulnerability of sensory and motor systems into consideration following transient ischemic attacks. Given that transient stroke can

induce persistent deficits in presynaptic transmitter release (Bolay et al., 2002), the most probable mechanism that results in the difference is that ChR2 is predominately expressed in layer 5B pyramidal neurons, which can project to the spinal cord, whereas sensory processing involves polysynaptic transmission within the cortex (Carvell and Simons, 1987), which is more likely to be suppressed by global ischemia, consistent with previous findings (Hossmann et al., 1987). Given recent results showing mild sensory stimulation could be protective following ischemia (Lay et al., 2011), it is possible that the sensory and ChR2 stimulation paradigm could alter damage. However, the short single pulses employed in either ChR2 or forepaw stimulation is unlikely to produce a significant hemodynamic response which is proposed to rescue brain function during the acute phase of focal ischemia (Lay et al., 2011).

Here, we show that optogenetics can be employed to study rapid plasticity of neuronal excitability and motor function following global ischemia with high temporal and spatial resolution. In future, with chronic preparations and non-invasive motion sensors (Ayling et al., 2009), we could extend the current study to longitudinal investigation. Potentially, this method may benefit the assessment of both acute and long-term therapeutics for stroke and their potential actions on sensory versus motor processing.

Chapter 5: Resolution of High-Frequency Mesoscale Intracortical Maps Using the Genetically-Encoded Glutamate Sensor – iGluSnFR

5.1 Introduction

One of the goals in neurophysiology is to acquire *in vivo* real-time measures of ongoing neuronal activity (Knöpfel et al., 2006; Akemann et al., 2010; Huber et al., 2012; Tian et al., 2012; Chen et al., 2013b; Stroh et al., 2013; Madisen et al., 2015). When making such measurements, one needs to be aware of potential limitations in monitoring approaches. Currently, the standard for electrophysiological assessment is the measurement of transmembrane voltage using an intracellular electrode, or extracellular potentials using electrodes. However, microelectrode-based methods are limited due to the small number of cells that can be simultaneously recorded. Voltage sensitive dyes (VSDs) provide cellular and regional measures of neuronal excitation and inhibition (Grinvald and Hildesheim, 2004; Ferezou et al., 2007; Akemann et al., 2010), but are not direct measures of synaptic activity. Calcium indicators provide exquisite sensitivity due to relatively large changes of indicator fluorescence associated with physiological Ca^{2+} transients (Grynkiewicz et al., 1985; Tian et al., 2009). Although calcium indicator signals can be large, they can non-linearly relate to calcium concentration (Rose et al., 2014), which in turn has a complex relationship to membrane voltage (Berger et al., 2007). Furthermore, (genetically encoded) Ca^{2+}-indicator signals have relatively slow kinetics, limiting their use in multi-cell imaging applications to detection of spike-related signals at low frequencies. In addition, Ca^{2+} imaging is most appropriate for monitoring suprathreshold events (Chen et al., 2013b). Despite the limiting kinetics of calcium modalities, the current generation of intracellular calcium sensors

are more than sufficient for mapping neuronal activity with low time resolution on the order of seconds (Tian et al., 2009; Chen et al., 2013b; Vanni and Murphy, 2014), but may not directly follow higher frequency circuit dynamics.

Recently, organic dyes or genetically encoded sensors for neurotransmitters, including the major excitatory neurotransmitter glutamate, have been developed (Hires et al., 2008; Okubo et al., 2010; Marvin et al., 2013). Here, we use a genetically encoded glutamate sensor, iGluSnFR (Marvin et al., 2013), *in vivo* to assess cortical activity and intracortical functional connectivity. iGluSnFR is targeted to neurons and detects extracellular glutamate concentration with ~1 ms rise and 40 ms decay times when tested using glutamate uncaging *in vitro* (Marvin et al., 2013). This rise time is much faster than the ~ 10 ms timescale of sensory response rise time measured *in vivo* using organic VSDs (Ferezou et al., 2007; Sachidhanandam et al., 2013), indicating that iGluSnFR assessment of sensory processing is not limited by slow kinetics.

A functional marker of glutamate concentration amenable to mesoscopic imaging has several advantages including detection of an endogenous neurotransmitter with clear functional significance. Indeed, the utility of a glutamate reporter for the characterization of normal and pathologic brain states is obvious due to glutamate's role in synaptic transmission, plasticity and learning, as well as in illnesses such as stroke or in psychopathology. We report the *in vivo* characterization of iGluSnFR using both AAV injected and transgenic mice. Specifically, in both anesthetized and awake states, we use both spontaneous and sensory-evoked activity to characterize the sensitivity, specificity, and kinetics of this new rapid sensor, in comparison to existing sensors.

5.2 Materials and Methods

All procedures were approved by the University of British Columbia Animal Care Committee and conformed to the Canadian Council on Animal Care and Use guidelines. Mice were housed in clear plastic cages in groups of two to five under a 12 h light, 12 h dark cycle with ad libitum food and water.

5.2.1 Animals

Adult (2-4 month) C57BL/6J mice from Charles River were acquired for viral-injection experiments and voltage sensitive dye (VSD) imaging experiments using widefield epi-fluorescence imaging (Fig. 5.1). Transgenic mice were imaged at adulthood (2-4 month). In all experiments, only male mice were used. In all experiments, only male mice were used.

We generated "EMX-CaMKII-iGluSnFR" transgenic mice by crossing homozygous B6.129S2-Emx1$^{tm1(cre)Krj}$/J strain (Jax no. 005628) and B6.Cg-Tg(CamK2a-tTA)1Mmay/DboJ strain (Jax no.007004) with hemizygous B6; 129S-Igs7$^{tm85(teto-iGluSnFR)Hze}$/J strain (the Allen Institute for Brain Science, Ai85). This crossing is expected to produce expression of iGluSnFR within all excitatory neurons across all layers of the cortex, but not in GABAergic neurons (Gorski et al., 2002; Huang and Zeng, 2013; Madisen et al., 2015).

We generated "EMX-CaMKII-GCaMP6s" transgenic mice by crossing homozygous B6.129S2-Emx1$^{tm1(cre)Krj}$/J strain (Jax no. 005628) and B6.Cg-Tg(CamK2a-tTA)1Mmay/DboJ strain (Jax no.007004) with hemizygous B6;Cg-Igs7$^{tm94.1(tetO-GCaMp6s)Hze}$/J strain (Jax no.024104, Ai94) (Madisen et al., 2015). As previously described (Zariwala et al., 2012; Vanni and Murphy,

2014), we generated "EMX-GCaMP3" by crossing homozygous B6.129S2-Emx1$^{tm1(cre)Krj}$/J strain (Jax no. 005628) with hemizygous B6;129S-Gt(ROSA)$^{26Sortm38(CAG-GCaMP3)Hze}$/J strain (Jax no.014538, Ai38). Animals with the desired combination of transgenes were selected on the basis of genotyping data (Table 5.1).

Table 5.1 A list of genotyping information for the transgenic mice used in the study.

	Forward	Reverse	Product size	Jax no.
CaMKII-tTA	CAACCCGTAAACTCGCCCAGAAG	GGCCGAATAAGAAGGCTGGCTCT	492 bp	007004
EMX-Cre	GCGGTCTGGCAGTAAAAACTATC	GTGAAACAGCATTGCTGTCACTT	330 bp	005628
GCaMP6s (Ai94)	CAGCTCGCCTACCACTACCAGCA	TTGAAGAAGATGGTGCGCTCCTG	509 bp	024104
iGluSnFR (Ai85)	ACTCCAACGCCATTGTTGAAGCA	GTTTCTTCGCTTTCGCACGTTCA	450 bp	In process
GCaMP3 (Ai38)	CTTCAAGATCCGCCACAACATCG	TTGAAGAAGATGGTGCGCTCCTG	546 bp	014538

5.2.2 Viral Injection

Viral delivery of iGluSnFR utilized 1 μl of AAV1.hSyn.iGluSnFR.WPRE.SV40 (Penn Vector Core) injected by a syringe infusion pump (model UMC4; World Precision Instruments) as previously reported (Xie et al., 2014). C57BL/6J mice were injected (depth: ~350 μm; infusion speed: ~1 nl/s 3–4 weeks before implantation of the cranial window and imaging. Injections were performed at 3 sites: 1) motor cortex (1 mm anterior and 2 mm lateral to bregma); 2) somatosensory cortex (1.5 mm posterior and 2.5 mm lateral to bregma); and 3) visual cortex (3.5 mm posterior and 2 mm lateral to bregma) (Fig. 5.2A). Isoflurane (1.5%) in oxygen was used for anesthesia.

5.2.3 Surgical Procedures for Implanting Chronic Transcranial Window

To implant chronic windows (Fig. 5.1B), animals were anesthetized with isoflurane (1.5% in pure O_2) and the body temperature was maintained at 37°C using a feedback-regulated heating-pad and monitored by a rectal thermometer. Mice received an intramuscular injection of 40 μl of dexamethasone (2 mg/ml) and a 0.5 ml subcutaneous injection of a saline solution containing burprenorphine (2 μg/ml) atropine (3 μg/ml), and glucose (20 mM) and were placed in a stereotaxic frame. After locally anesthetizing the scalp with lidocaine (0.1 ml, 0.2%), the skin covering the skull was removed and replaced by transparent dental (Parkell, Edgewood, NY, USA; product: C&B Metabond) cement and a glass coverslip (see Fig. 5.1B) (Silasi et al., 2013; Vanni and Murphy, 2014). A 4-40 metal stud was attached to the skull for future head fixation during recordings. At the end of the procedure, the animal received a second subcutaneous injection of saline (0.5 ml) with 20 mM of glucose and recovered in a warmed cage for 30 min. For subsequent chronic recordings, animals were anesthetized with isoflurane (~1.5%) to produce a constant level of cortical activity, and the head was stabilized by attaching the bolt to a pole mounted on a base-plate. The body temperature was maintained, and hydration was ensured by subcutaneous injection of saline (0.3 ml) with 20mM of glucose at 2 h intervals. In most cases, longitudinal imaging with the chronic window could last > 2 months (Fig. 5.3E).

5.2.4 Craniotomy and Voltage Sensitive Dye Imaging

VSD imaging was performed in acute experiments as we previously reported (Mohajerani et al., 2010, 2013) using RH 1692 dye (Optical Imaging, New York, NY) (Shoham et al., 1999). Ten-week old mice were anesthetized with isoflurane (1.5%) for induction and during craniotomy

surgery. Mice were placed on a metal plate that could be mounted onto the stage of the upright macroscope, and the skull was fastened to a steel plate. A 7 × 6 mm unilateral craniotomy (bregma 2.5 to −4.5 mm, lateral 0 to 6 mm) or bilateral craniotomy (bregma 2.5 to −4.5 mm, lateral 0 to 3 mm in both sides) was made, and the underlying dura was removed. Throughout surgery and imaging, body temperature was maintained at 37 °C using a heating pad with a thermistor for feedback. RH-1692 voltage sensitive dye was dissolved in 4-(2-hydroxyethyl)-1-piperazineethanesulfonic acid (HEPES)-buffered saline solution (1 mg/ml) and applied to the exposed cortex for 90 min, which stained all neocortical layers. The brain was covered with 1.5% agarose made in HEPES-buffered saline and sealed with a glass coverslip. VSD was excited with light delivered by a red LED (Luxeon K2, 627-nm center) through a 630 ± 15 nm excitation filter. Ambient light resulting from VSD excitation (630 nm) was ~10 W/m^2. Imaging was performed under light anesthesia (isoflurane, 0.75 ~ 1%). VSD epi-fluorescence was imaged through a 688 +/-15 nm bandpass filter (Semrock).

5.2.5 Sensory Stimulation and Imaging

Images of the cortical surface were projected through a pair of back-to-back photographic lenses (50 mm, 1.4 f:135mm,2.8 f or 50mm,1.4 f:30mm, 2 f) onto a 1M60Pantera CCD camera (Dalsa). iGluSnFR and GCaMP were excited with light from a blue-light-emitting diode (Luxeon, 473 nm) delivered through a bandpass filter (Chroma, 467–499 nm). Ambient light resulting from iGluSnFR and GCaMPs excitation (473 nm) was ~10 - 20 W/m^2. iGluSnFR and GCaMP fluorescence emission was filtered using a 510–550 nm bandpass filter (Chroma). We collected 12-bit images at 150 Hz using XCAP imaging software (see Fig. 5.1A). When collecting

somatosensory-evoked cortical activity, we used piezoelectric bending actuators touching the skin of single limb or individual or multiple whiskers, which moved at most 90 μm in an anterior-to-posterior direction (a 2.6° angle of deflection). Visual stimulation was produced by a 1 ms pulse of light from a 435 nm LED placed at a consistent height and distance from the right eye. Averages of responses to sensory stimulation were calculated from 20 trials of stimulation with an inter-stimulus interval of 10 s. Awake mice were placed on a flat running wheel with the head stabilized by attaching the fixation bolt to a pole mounted on a base-plate (Fig. 5.2Fa); and were habituated for 2-3 sessions before imaging. A camera (30 Hz) was used to monitor behavior, confirming that the animals were awake and showed no signs of distress.

5.2.6 Analysis for Wide Field Imaging

All green fluorescent indicators have excitation spectra that overlap with the absorption spectrum of hemoglobin (Hillman, 2015); whereas red-shifted VSD signals are not significantly contaminated by heart beat pulses and hemodynamic responses (Shoham et al., 1999; Petersen et al., 2003). To remove the contribution of global hemodynamic and potential illumination fluctuations from iGluSnFR and GCaMP imaging, raw data were corrected with signal regression (Aguirre et al., 1998; Fox et al., 2009) for each pixel with the following:

$$S_i(t) = g(t) * A_i + x_i(t)$$

Where $g(t)$ is a regressor, A_i is the regression coefficient, and x_i is the signal within the i^{th} pixel after regression. Here, global signal regression (GSR) was used. Time traces of all pixels defined as brain were averaged to create a global brain signal, $g_{GSR}(t)$ and regressed from every pixel labeled as brain, where

$$g_{GSR}(t) = \frac{1}{N}\sum_{j=1}^{N} S_j(t)$$

N is the number of all brain pixels in the field of view (128x128 pixels, 66.7 μm per pixel).

To calculate the iGluSnFR and GCaMP responses evoked by sensory stimulation, images collected from the 20 trials were averaged and the normalized difference to the average baseline (~50 ms) recorded before stimulation was calculated ($\Delta F/F_0$; region of interest - ROI=667 μm * 667 μm). GSR was applied for each trial to remove global fluctuations produced by blood volume changes and hemodynamic responses.

The peak of sensory-evoked responses was defined as the largest $\Delta F/F_0$ value averaged from a 10 x 10 pixels region of interest placed within V1 within 200 ms (iGluSnFR and VSD) or 1000 ms (GCaMP3 & GCaMP6s) following sensory stimulation. Peak amplitude measurements that were less than 3 times the standard deviation of baseline fluctuations (~50 ms) were classified as a failed response (peak $\Delta F/F_0 = 0$) and were excluded from time to peak and decay $\tau_{1/2}$ analysis. The decay $\tau_{1/2}$ was calculated as the time to half the peak amplitude. Signal-to-noise ratio (SNR) was quantified as peak $\Delta F/F_0$ response over the standard deviation during baseline and calculated on averaged responses (20 sweeps per animal).

Spontaneous activity of each ROI in the recording sequence was calculated by dividing each frame by the mean fluorescence of the entire time series (F_0). The result of iGluSnFR, GCaMP, and VSD signals was then temporally band-pass filtered to the indicated frequency bands using the Chebyshev in Matlab (R2014b, MathWorks), and then GSR was applied. To create the seed

pixel correlation map, cross-correlation coefficient r values between the temporal profiles of a single selected pixel and all the other pixels of the ROI were calculated (White et al., 2011; Mohajerani et al., 2013). For every map presented, spatial smoothing (σ = 67 - 134 μm) was applied to improve contrast. Ongoing brain activity during active whisking or other significant movements (recorded by behavior camera) were excluded from spontaneous activity in awake animals. The total duration of spontaneous activity was maintained constant for all animals (20,000 frames recorded at 150 Hz) when generating correlation maps.

5.2.7 Two Photon (2p) Imaging and Data Analysis

2P imaging was performed as previously reported (Xie et al., 2012, 2014). Briefly, a small craniotomy (3 × 3 mm) was made over the visual cortex. 2P excitation was performed with a Mai Tai Ti-sapphire laser and tuned to 920 nm to excite iGluSnFR (Marvin et al., 2013). All experiments were performed using a 20× objective (Olympus, NA = 0.95) immersed in HEPES-buffered saline solution. Time series images were acquired at frame rates of ~20 Hz and at 100-150 μm depth from the surface of cortex. A median filter (radius, 1 pixel) was applied to reduce photon and photomultiplier tube noise. $\Delta F/F_0$ value was calculated to describe the responses upon 1 ms light flash stimulation. The stimulus light source was isolated from the detectors and we did not detect imaging artifacts from light stimulation. Spontaneous activity was processed the same way as it was for the wide field imaging.

5.2.8 Pharmacology

A small craniotomy (3 × 3 mm) was made over the visual cortex (n = 4). Threo-beta-benzyloxyaspartate (TBOA,Tocris Bioscience), a glutamate transporter blocker, was dissolved

into DMSO to 50 mM as stock solution, and then diluted with HEPES-buffered saline solution to 500 μM for direct cortical incubation. The compound was allowed to incubate for > 20 min before starting imaging of spontaneous and visual stimulation-evoked activity.

5.2.9 Transcardial Perfusion and Brain Slice Imaging

Mice were transcardially perfused with PBS followed by chilled 4% paraformaldehyde (PFA) in PBS. Coronal brain sections (100 μm thickness) were cut on a vibratome (Leica VT1000S). Images were acquired with a Zeiss Axiovert 200M fluorescence microscope using ZEN 2012 software.

5.3 Results

5.3.1 Cortical Mapping of Sensory-Evoked Responses by Virally Transduced iGluSnFR through a Chronic Window

We first employed viral expression of iGluSnFR to characterize the *in vivo* kinetics of the iGluSnFR sensor using cortical responses to sensory stimulation. AAV1.hSyn.iGluSnFR was injected into the motor cortex, somatosensory cortex and visual cortex (Fig. 5.2A) to exclusively express iGluSnFR in cortical neurons (Aschauer et al., 2013). The probe is expected to measure extracellular glutamate in the vicinity of infected neurons, but is not targeted to a particular sub-cellular compartment. At least 3 weeks following AAV injection, we observed a wide spatial expression of iGluSnFR covering almost the entire cortical hemisphere visible within the chronic window, including the somatosensory, motor, visual and some of the associative cortices (Fig. 5.2B). As expected, there was higher expression near the injection sites (layer 1-3, Fig. 5.2C).

The distribution of viral iGluSnFR expression in deep layers (layer 4-6) was not as uniform as in superficial layers (Fig. 5.2C).

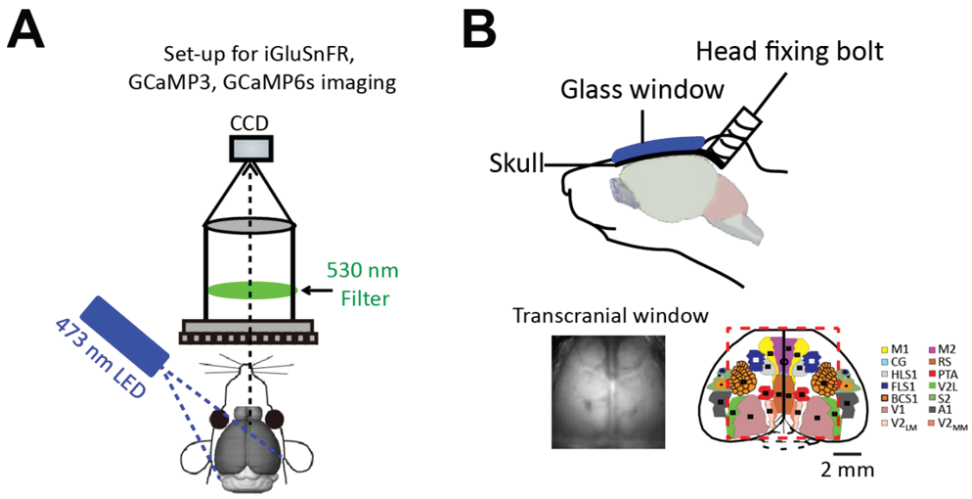

Figure 5.1 Set-up and surgical preparation for wide field imaging with genetically encoded sensors.

A. A CCD camera was used to image cortical iGluSnFR signals (λ = 530 nm) excited by blue LED (λ = 473 nm). B. A chronic window was implanted on the top of mouse skull after removing skin. The chronic window is relatively transparent, covering ~ 8 mm x 8 mm field of view on the cortex, including the motor, somatosensory, visual, and association cortices. M1, primary motor; CG, anterior segment of cingulate cortex; HLS1, hindlimb area of the primary somatosensory cortex; FLS1, forelimb area of the primary somatosensory cortex; BCS1: primary barrel sensory cortex; V1, primary visual cortex; $V2_{LM}$, lateromedial visual cortex; M2, secondary motor cortex; RS, retrosplenial cortex; PTA, parietal association area; V2L, lateral secondary visual cortex; S2, secondary somatosensory cortex; A1, auditory cortex; $V2_{MM}$: mediomedial secondary visual cortex.

We imaged different modalities of sensory stimulation-evoked glutamate signals under 1.5% isoflurane anesthesia. We found iGluSnFR was sensitive enough to detect responses to relatively weak stimuli – a single 1ms piezo deflection of the whisker pad or tap to the plantar surface of forelimb or hindlimb (Fig. 5.2D, E), which is insufficient to elicit GCaMP3 signals (data not

shown). We also imaged cortical glutamate levels following visual stimulation (1 ms light flash) in anesthetized and awake animals. Under both conditions, iGluSnFR signals can be clearly observed in the visual cortex (Fig. 5.2D, F). Interestingly, 1 ms visual stimulation induced consistent secondary responses at ~200-400 ms in awake animals, which was not clearly observed in 1.5% isoflurane anesthetized animals (Fig. 5.2Eb, Fc).

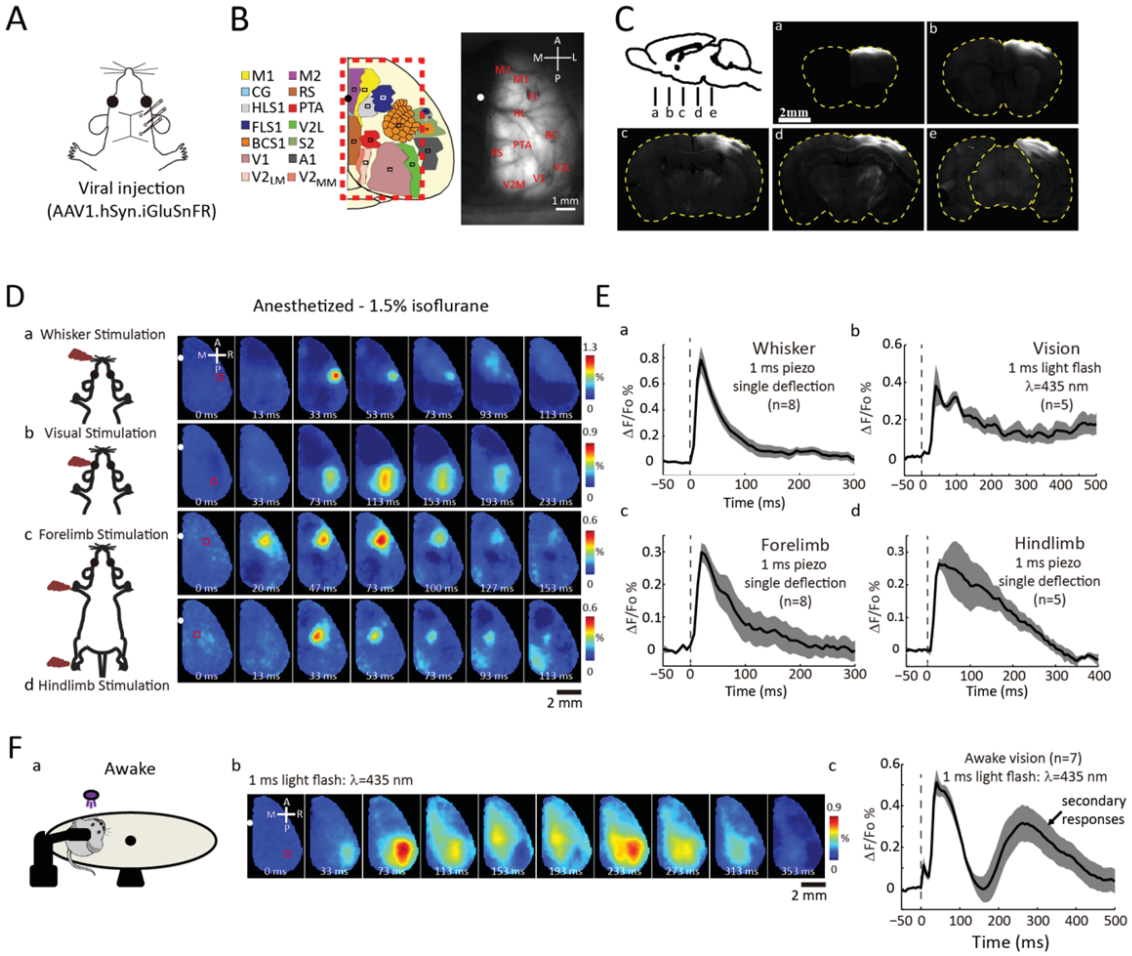

Figure 5.2 Virally transduced iGluSnFR robustly reports sensory-evoked responses in the cortex.

AAV1.hSyn.iGluSnFR was injected into the forelimb, barrel and visual cortex ~ 4 weeks before implanting chronic window. B. Expression of virally transduced iGluSnFR in half of the hemisphere, across the motor, somatosensory and visual cortex. C. Brain slice sections show that the virally-transduced iGluSnFR is expressed in the superficial layers of the cortex. D. Multiple sensory-evoked cortical responses in virally transduced iGluSnFR mouse show sensitive, specific and rapid event-related kinetics under 1.5% isoflurane anesthesia. Representative montage shows the iGluSnFR responses in the cortex following sensory stimulation and is averaged from 20 trials. E. Time-course plots of sensory-evoked responses (a, b, c, and d are whisker, visual, forelimb, and hindlimb stimulation, respectively; mean ± SEM) measured from the respective primary sensory region (ROI: 667 x 667 μm, n – number of animals). F. 1 ms Flash light visual stimulation induces an initial rapid response followed by a clearly separated, delayed secondary response in the awake mouse. a. Scheme illustrating the experimental set-up of visual stimulation in the awake mouse. b. Representative montage of cortical iGluSnFR responses following visual stimulation (mean of 20 trials). c. Plot of light flash-evoked visual responses shown as mean ± SEM from 667 x 667 μm boxes placed within V1 (red box shown in b) (n – number of animals).

5.3.2 Regional Mapping of Sensory Stimulation-Evoked Responses by Transgenic iGluSnFR through a Chronic Window

To achieve a more uniform expression of iGluSnFR and reduce methodological limitations related to viral injection (e.g., traumatic injury, inflammation, etc.), we acquired transgenic mice (Ai85) from the Allen Institute for Brain Science (Madisen et al., 2015). The expression, kinetics, and *in vivo* function of these genetically encoded iGluSnFR animals was not previously functionally characterized. Using a tTA-based transcriptional amplification approach targeted to the TIGRE insertion locus, iGluSnFR was intersectionally and doubly regulated by both Cre and tTA to drive robust expression with improved precision to a targeted cell population (Huang and Zeng, 2013; Madisen et al., 2015). Crossing Emx1-Cre with CaMKII-tTA and TIGRE-iGluSnFR (Fig. 5.3Ai) resulted in robust and uniformly expressed iGluSnFR within the chronic cortical window (Fig. 5.3Aii). Brain sections of the positive transgenic mice confirmed robust expression in the cortex and hippocampus (Fig. 5.3B) (Madisen et al., 2015). It was difficult to resolve

subcellular expression of iGluSnFR in the cortex due to the dense expression of membrane protein (Fig. 5.3B) (Marvin et al., 2013; Madisen et al., 2015). iGluSnFR expression using our approach is designed to be doubly regulated by Emx-Cre and CaMKII-tTA to express selectively in the excitatory neurons of the cortex (Mayford et al., 1996; Gorski et al., 2002) and consistent with other recently developed lines using the same approach (Madisen et al., 2015).

We performed sensory mapping of the Emx-CaMKII-iGluSnFR mouse under 1.5% isoflurane anesthesia. Stimulation was performed as in the virally-infected mice using stimuli produced by single piezo deflections on the whisker pad, forelimb and hindlimb plantar surface, as well as a 1 ms light flash for visual stimulation. Consistent with imaging from virally transduced iGluSnFR, we were able to detect responses in the cortex with high temporal and spatial resolution to even weak sensory stimuli in transgenic mice expressing iGluSnFR (Fig. 5.3C, D). Again, visual stimulation evoked large iGluSnFR signals in the visual cortex (Fig. 5.3C, D), and awake animals exhibited a secondary delayed response at ~200-400 ms (Fig. 5.3E). A similar secondary response has been shown in the barrel cortex with whisker stimulation (Sachidhanandam et al., 2013) and in the visual cortex with light flash stimulation in awake mice (Funayama et al., 2015), which are both associated with sensory perception. Moreover, as with virally delivered iGluSnFR, transgenically expressed iGluSnFR demonstrated stable sensory evoked responses over time thereby permitting longitudinal imaging (Fig. 5.3Eb).

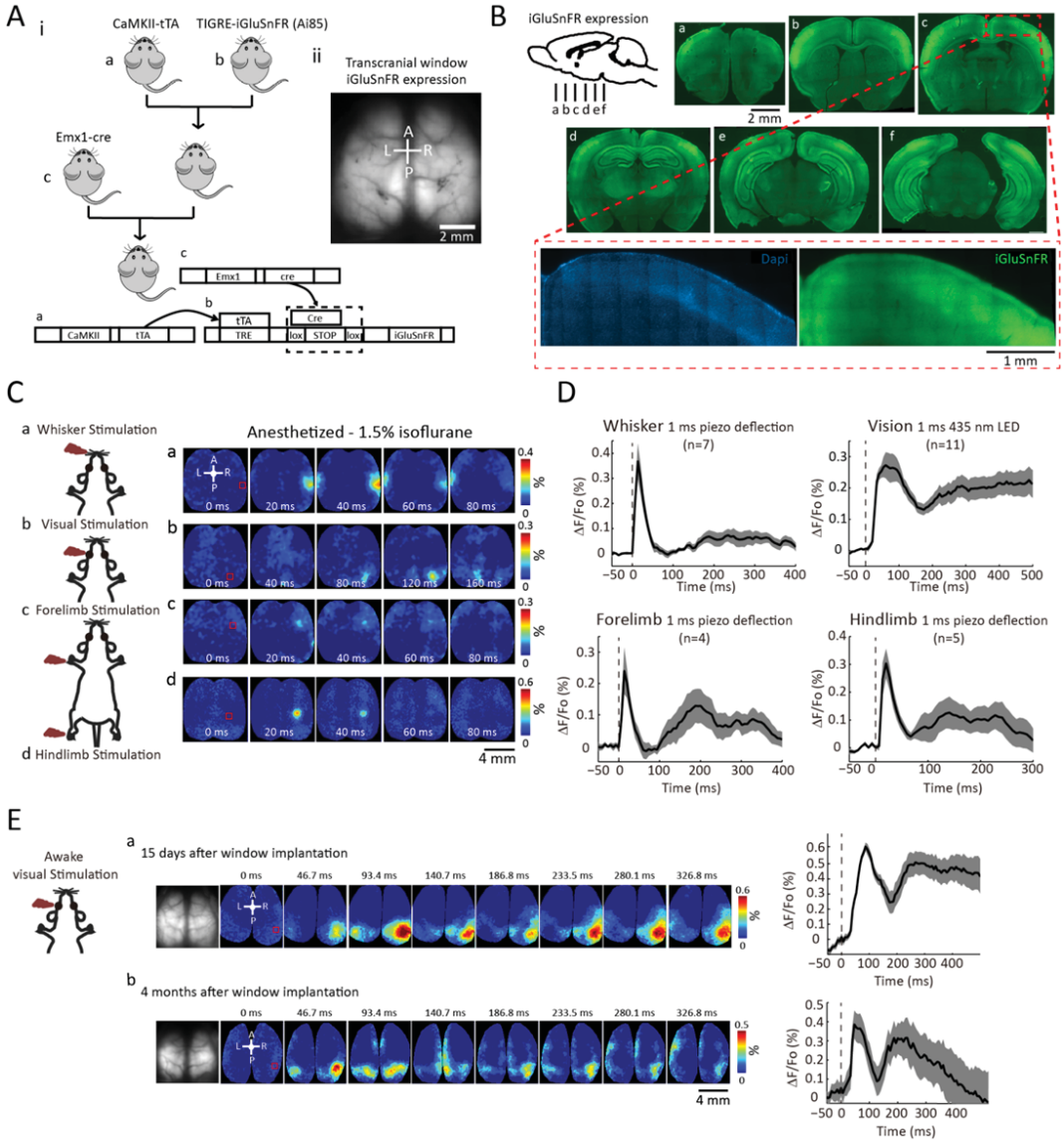

Figure 5.3 Ai85 transgenic iGluSnFR mouse reveals the sensitive, specific and rapid kinetics of iGluSnFR by detecting sensory stimulation-evoked regional responses in the cortex.

Specific expression of iGluSnFR in cortical excitatory neurons is achieved by crossing Emx-Cre mouse line and cre-dependent iGluSnFR to the CaMKII gene locus; ii. Emx-CaMKII-iGluSnFR mouse exhibits uniform cortical expression of iGluSnFR at mesoscopic level. Image shows the wide field green fluorescence from the cortex. B. Coronal brain sections show dense expression of iGluSnFR in cortex and hippocampus in Emx-CaMKII-iGluSnFR mouse. Coronal sections (a-f) correspond to locations indicated in schematic diagram. C. Brief sensory stimulation evokes large and fast cortical responses of iGluSnFR signals in Emx-CaMKII-iGluSnFR mouse. Representative montage of 20 trials averaged iGluSnFR responses following sensory stimulation. D. Plots of sensory-evoked responses are mean ± SEM from 667 x 667 μm boxes placed within the corresponding primary sensory cortices denoted by the red boxes in C (n – number of animals). E. One ms flash light visual stimulation induces an initial fast response followed by a clearly separated secondary response in awake Emx-CaMKII-iGluSnFR mouse. a. and b. Representative montage of iGluSnFR responses following visual stimulation in the same animal 4 months apart. Representative montage of 20 trials averaged iGluSnFR responses following visual stimulation. Plot of visual responses shown as mean ± SEM from 667 x 667 μm boxes placed within V1 (red boxes in a & b, n = 20 trials).

5.3.3 Intra-Cortical Long-Range Connections Are Observed in EMX-CaMKII-iGluSnFR Mice

Resting-state spontaneous activity provides samples of brain activity and requisite functional connectivity without requiring the testing subjects to engage in tasks, and therefore has utility in physiological and pathological brain states (van den Heuvel and Hulshoff Pol, 2010; Zhang and Raichle, 2010). Cortical resting-state activity assessed by voltage signals (Mohajerani et al., 2013), Ca^{2+} signals (Vanni and Murphy, 2014) and intrinsic signals (White et al., 2011) have been recently applied to determine regional functional connectivity and also aberrant functional connectivity caused by brain diseases in rodents (Bero et al., 2012; Bauer et al., 2014). To our knowledge, this type of wide-field characterization of spontaneous activity by glutamatergic signaling – presumably reflecting synaptic activity – has not been previously reported.

Imaging spontaneous iGluSnFR signals in the cortices of mice under 1.5% isoflurane revealed robust signals of spontaneous activity (Fig. 5.4Aa). Processing the signals with GSR significantly reduced the artifacts related to breathing as well as heart beat-induced blood volume –related signals (Fig. 5.4Ab). Activity-dependent autofluorescence is not expected to make a large contribution to the measured fluorescence signals because of the higher absolute fluorescence associated with iGluSnFR (Díez-García et al., 2007; Vanni and Murphy, 2014). We tested whether the mirrored bilateral activity identified with voltage and Ca^{2+} imaging (Mohajerani et al., 2010; Vanni and Murphy, 2014) was reflected in glutamatergic signals as detected by iGluSnFR. Fig. 5.4Aa shows synchronized iGluSnFR signals in the left and right hindlimb somatosensory cortex (red and blue trace), which were not synchronized with iGluSnFR signals in the (left/right) visual cortex (green trace, Fig. 5.4Aa). Correlation maps of iGluSnFR signals in various frequency bands further confirmed the inter-hemisphere functional connectivity, as well as local connectivity (Fig. 5.4B). Placing the seed pixel in the center of sensory cortices, we generated maps using iGluSnFR (Fig. 5.4C) that resembled those with VSD signals and Ca^{2+} signals (Mohajerani et al., 2013; Vanni and Murphy, 2014), which are thought to be reflective of anatomical long-range connections within the cortex, but could also be attributed to regions sharing a common drive (Mohajerani et al., 2013; Hunnicutt et al., 2014; Oh et al., 2014; Zingg et al., 2014).

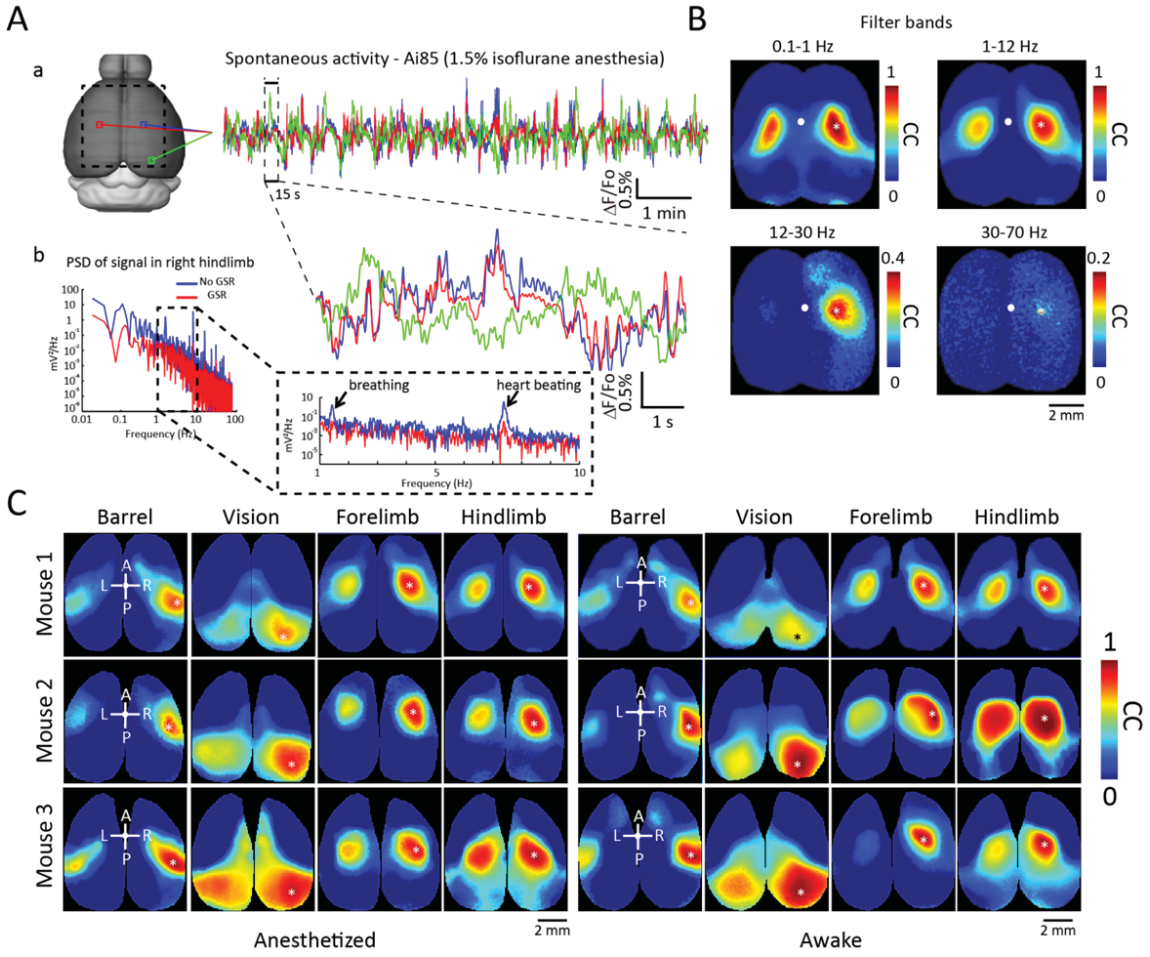

Figure 5.4 Inter-hemispheric connections are revealed by iGluSnFR spontaneous activity.

Spontaneous iGluSnFR activity from 333 x 333 μm boxes placed in the left (red) and right hindlimb cortex (blue) as well as the right visual cortex (green) from an isoflurane-anesthetized (1.5%) Emx-CaMKII-iGluSnFR (Ai85) mouse. Raw iGluSnFR imaging was recorded at 150 Hz; and the signals were corrected with global signal regression (GSR) and bandpass filtered to 0.1 – 12 Hz. b. Power spectral density (PSD) analysis indicates that iGluSnFR signals contain signal power likely contributed to by breathing and heart beating-induced hemodynamic responses (arrows). GSR removes most of the heart beat-related signals without significantly affecting the other signals. B. Seed-pixel based correlation maps of iGluSnFR signals show inter-hemispheric connections of left and right hindlimb cortex within 0.1 – 30 Hz frequency range in 1.5% isoflurane anesthetized Emx-CaMKII-iGluSnFR mouse. "*" indicates seed locations. C. Seed-pixel based correlation maps of 0.1 – 12 Hz iGluSnFR activity illustrate the inter-hemisphere

connections for different sensory modalities; and also reveal long-range intra-hemisphere connections (e.g., barrel cortex – motor cortex, visual cortex –cingulate cortex) in 3 animals under 1.5% isoflurane anesthesia and quiet wakefulness. "*" indicates seed locations. The maps are similar under anesthesia and quiet wakefulness in the same animal.

5.3.4 Blocking Glutamate Transporter Amplifies Sensory Stimulation Evoked and Spontaneous iGluSnFR Signals

Blocking excitatory amino acid transporter 1 and 2 (EAAT1 and EAAT2) with TBOA (Shimamoto et al., 1998), increases both the amplitude and the decay time constant of the spontaneous iGluSnFR events in the inner plexiform layer bipolar cells (Marvin et al., 2013). To confirm that wide field iGluSnFR signals can also be manipulated by blocking glutamate re-uptake in mouse cortex *in vivo*, 500 μM TBOA was applied to the craniotomy over the visual cortex (Fig. 5.5A), and was allowed to incubate for > 20 min before imaging spontaneous and visual stimulation-evoked activity. We previously demonstrated the cortical incubation enables drug diffusion into as deep as layer 5 (Xie et al., 2014). It should be mentioned that the open skull craniotomy (Fig. 5.5A) is relatively more invasive than the intact skull window (Fig. 5.1B). Blocking glutamate re-uptake significantly increased the amplitude of iGluSnFR signals in response to 1 ms visual stimulation (first peak amplitude: baseline *vs.* TBOA: 0.77 ± 0.12% *vs.* 1.17 ± 0.22%, $p < 0.05$, mean ± SEM, n=4, Fig. 5B,C) and during spontaneous activity in the visual cortex (Fig. 5.5Db). In addition, the standard deviation map during a period of 133 s spontaneous activity exhibited an ~2-fold increase within the craniotomy where TBOA had access to tissue (Fig. 5.5Da). These results demonstrate that blocking glutamate re-uptake amplifies sensory stimulation-evoked and spontaneous iGluSnFR signals in wide field imaging, which is consistent with results from cellular imaging in retina (Marvin et al., 2013).

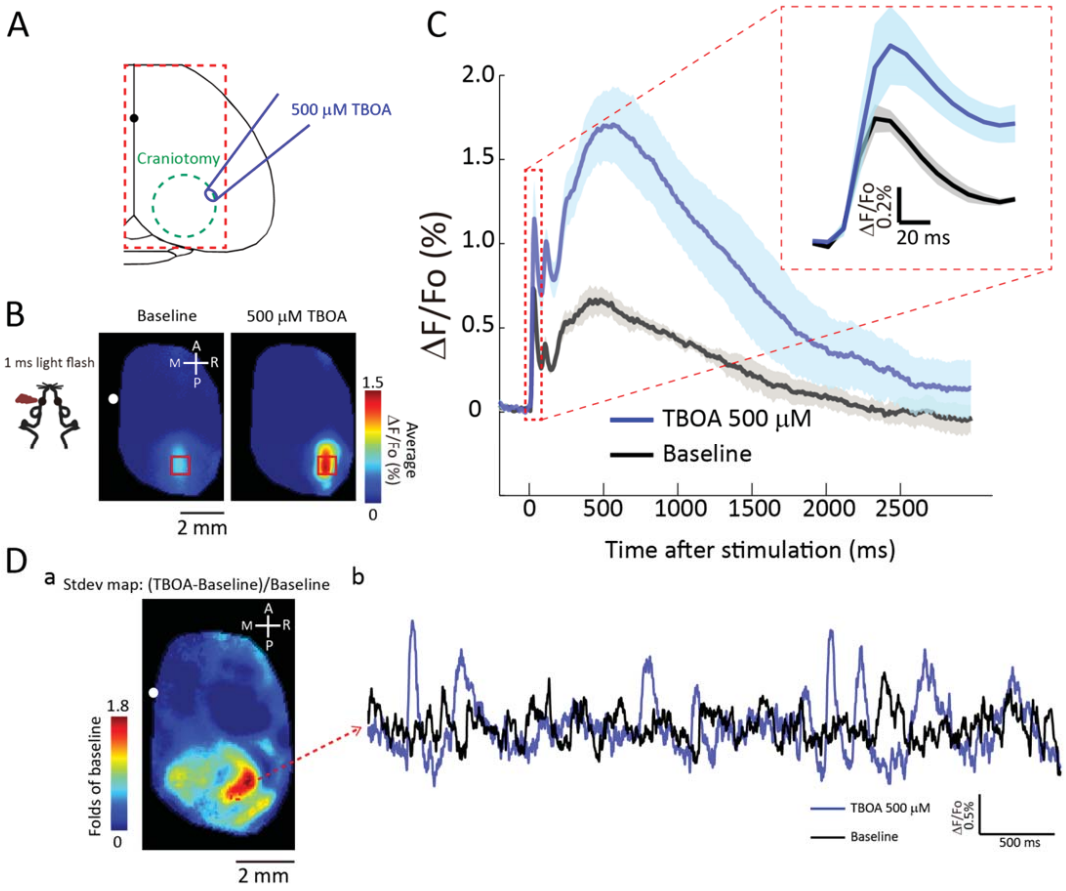

Figure 5.5 Glutamate transporter blocker - TBOA amplifies 1 ms flash light visual stimulation-evoked responses and spontaneous activity in Ai85 iGluSnFR transgenic mice.

A. An open skull craniotomy (~ 3 x 3 mm) was made over the visual cortex. 500 µM TBOA in HEPES-buffered saline was incubated over the exposed cortex after baseline recording. B. Representative image showing iGluSnFR responses to visual stimulation with 1 ms flash light visual stimulation in an isoflurane-anesthetized (1%) Emx-CaMKII-iGluSnFR mouse (left), which is amplified in the presence of 500 µM TBOA (right). Images show visual responses averaged from stimulation onset to 2 s in one mouse in the presence or absence of TBOA (40 trials). C. Plot of visual responses shown as mean ± SEM from 667 x 667 µm region of interest placed within the V1 (show in red in B, n = 4 mice). Insert shows higher magnification of visual responses within the first 140 ms from the onset of light flash. D. a. Representative image demonstrating that 500 µM TBOA increases the standard deviation of spontaneous activity within the craniotomy compared to baseline recording. Standard deviation (stdev) map of

iGluSnFR spontaneous activity after 500 μM TBOA application was calculated over the 133 s recording, and was normalized to fold increase over baseline. b. Raw traces show iGluSnFR spontaneous activity with or without 500 μM TBOA application.

5.3.5 Two-Photon *in vivo* Imaging Reveals the Dense Expression of iGluSnFR and Confirms Visual Stimulation-Evoked Responses in Emx-CaMKII-iGluSnFR Mice

Two-photon (2P) *in vivo* imaging was applied to explore the cellular distribution of iGluSnFR expression and the cellular compartments where the spontaneous and evoked-activity occur in the visual cortex of Emx-CaMKII-iGluSnFR mice. Consistent with brain sections histology (Fig. 5.3B), 2P imaging revealed a dense expression of iGluSnFR spanning a depth of at least 300 μm depth in visual cortex (Fig. 5.6A). Consistent with wide field imaging results, we observed a general increase in fluorescence intensity (> 1% $\Delta F/F_0$) from neuropil in superficial layers (imaged at a depth of 100-150 μm) of visual cortex following 1 ms light flash visual stimulation in 1% isoflurane anesthetized Emx-CaMKII-iGluSnFR mice (Fig. 5.6B). In addition, 2P imaging also revealed spontaneous iGluSnFR signals (Fig. 5.6C). Despite challenges with respect to resolving the cellular origin of the iGluSnFR signals, 2P imaging resulted in improved signal, in part due to lessened blood volume artifacts, compared to wide field.

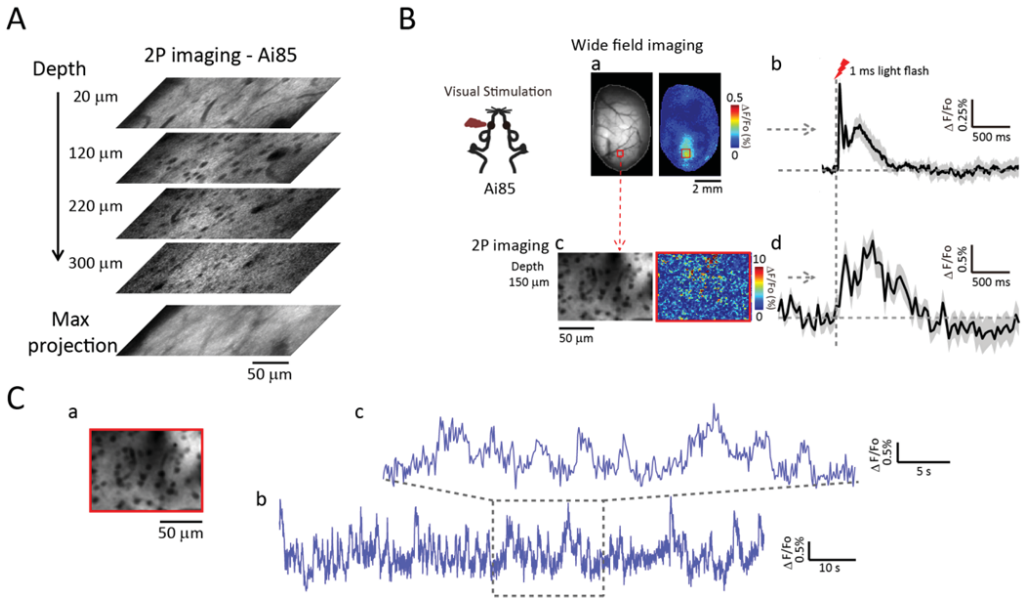

Figure 5.6 Two-photon imaging of sensory-evoked and spontaneous iGluSnFR signals in the visual cortex of Ai85 iGluSnFR transgenic mice.

A. Two-photon imaging reveals dense expression of iGluSnFR in the visual cortex of Emx-CaMKII-iGluSnFR transgenic mice. Images show the depth-series of iGluSnFR expression from brain surface to -300 µm depth and the maximal intensity projection of iGluSnFR expression from the first 300 µm (3 µm interval for Z-scanning). B. 1 ms light flash visual stimulation evokes a similar profile of iGluSnFR responses in the visual cortex of 1% isoflurane-anesthetized mouse in wide field and two photon imaging. a. Representative wide field imaging shows iGluSnFR responses in the visual cortex (left, brain image; right, averaged map of iGluSnFR responses within the first second from the stimulation onset). b. Plots of visual responses are shown as mean ± SEM from 667 x 667 µm box placed within the V1 (red box in a-right; 20 trials). c. Representative two-photon imaging shows iGluSnFR responses in the visual cortex (red box in a-left) at a depth of -150 µm (left, structural image; right, averaged map of iGluSnFR responses within the first second from stimulation onset). d. Plots of visual responses are shown as mean ± SEM from the entire imaging field (red box in c-right, 20 trials). C. A representative trace of iGluSnFR spontaneous signals (blue) is shown a. Region of interest for extracting spontaneous iGluSnFR signals. b. Raw trace of iGluSnFR signals. c. Higher magnification of iGluSnFR signals from the box in b. 2P: two-photon.

5.3.6 iGluSnFR Signal Has Faster Kinetics for Regional Imaging of Spontaneous and Sensory-Evoked Responses than GCaMP3 and GCaMP6s

A key to obtaining real-time measures of ongoing neuronal activity and processing using imaging techniques is to employ the sensors with high sensitivity and fast kinetics. We next compared the response amplitude and kinetics of iGluSnFR signals with GCaMP3 signals and VSD signals. Though GCaMP3 signals have smaller amplitude than the fastest Ca^{2+} sensor – GCaMP6f (by $\Delta F/F0$ under physiological conditions), they share similar rise-time (τ_{peak}: GCaMP3 137 ± 4 ms *vs.* GCaMP6f 80 ± 35 ms, 10 action potentials) and decay time ($\tau_{1/2}$: GCaMP3 597 ± 8 ms *vs.* GCaMP6f 400 ± 41 ms, 10 action potentials) (Chen et al., 2013b). For comparison, 10 action potential associated iGluSnFR signals showed faster kinetics with 15 ± 11 ms rise $\tau_{1/2}$ and 92 ± 11 ms decay $\tau_{1/2}$ (Marvin et al., 2013).

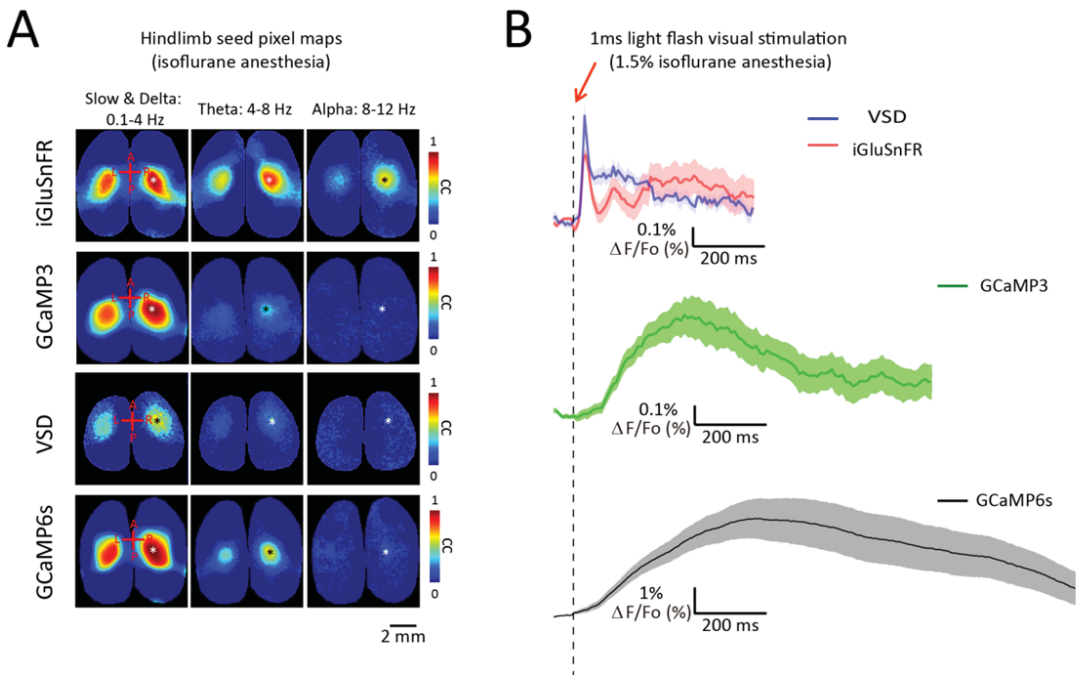

Figure 5.7 iGluSnFR is a fast regional activity reporter compared to other recombinant neuronal activity sensors.

A. Comparison of seed-pixel correlation maps seeded within the hindlimb somatosensory cortex among various neuronal activity sensors within delta, theta and alpha frequency band indicates that iGluSnFR preserves the most high frequency components for generating maps showing inter-hemispheric connections. All maps were generated from 20,000 frame sequences recorded at 150 Hz and were processed with global signal regression. "*" indicates seed locations. B. A plot of the visual stimulation-evoked responses measured from visual cortex and showing rapid kinetics of iGluSnFR signals that are comparable to VSD signals and are faster than GCaMP3 and GCaMP6s. Representative traces are shown as mean ± SEM of signals within V1 from the indicated sensors in individual animals (20 trials).

We filtered the imaging data into delta (0.1-4 Hz), theta (4-8 Hz) and alpha bands (8-12 Hz) (Drongelen, 2007) to compare functional connectivity maps developed from seeds (Mohajerani et al., 2013) in the right hindlimb cortex. We applied the same image processing protocols to all sensors. It is worth nothing that iGluSnFR signals have superior sensitivity and kinetics for inter-

hemisphere functional connectivity in the alpha band, whereas other sensors failed to resolve this (Fig. 5.7A). Moreover, the functional connectivity maps of iGluSnFR signals were also more robust within theta bands, compared to other sensors (Fig. 5.7A). To compare the kinetics of sensory-evoked responses between various sensors, a 1 ms light flash with same intensity was applied. The SNR of 20 averaged trials was comparable across iGluSnFR, VSD and GCaMP3 (Table 5.2). The kinetics (time to peak and decay $\tau_{1/2}$) of iGluSnFR signals were 4-8 times faster than GCaMP3 and GCaMP6s signals, and were close to the kinetics of the VSD signal with similar time to peak value and ~2 fold increased decay $\tau_{1/2}$ value (Table 5.2, Fig. 5.7B).

Table 5.2 Amplitude, signal to noise ratio, time to peak, decay time for 1 ms light flash visual stimulation-evoked responses in anesthetized EMX-CaMKII-iGluSnFR, EMX-GaMKII-GCaMP6s and EMX-GCaMP3 mice, as well as RH1692 VSD imaged mice.

	ΔF/F(%)	Time to peak (ms)	Decay $\tau_{1/2}$ (ms)*	SNR
Ai85 - iGluSnFR (n=11)	0.37 ± 0.03	67.55 ± 6.54	56.04 ± 11.26	44.69 ± 6.11
RH1692 - VSD (n=4)	0.47 ± 0.07	51.93 ± 1.68	26.80 ± 6.12	37.01 ± 8.77
Ai38 - GCaMP3 (n=12)	0.42 ± 0.05	406.38 ± 52.03	207.42 ± 19.78	47.55 ± 3.89
Ai94 - GCaMP6s (n=4)	2.72 ± 0.38	504.18 ± 107.63	495.80 ± 100.24	154.58 ± 15.78

* The decay time reflects the time to 50% of peak amplitude, which for Ai85 and RH1692 occurred over the fast initial component of the response (see Figure 5.7B).

5.4 Discussion

We report the *in vivo*, wide field imaging of a genetically encoded glutamate indicator, iGluSnFR (Marvin et al., 2013) in awake and anesthetized mice. We employed longitudinal mesoscopic imaging of iGluSnFR expressed in the dorsal cerebral cortex using an intact skull

chronic window preparation (Guo et al., 2014a; Silasi and Murphy, 2014; Vanni and Murphy, 2014). iGluSnFR reports extracellular glutamate concentration that we interpret as a surrogate of glutamatergic synaptic activity. Using both viral delivery and transgenic approaches to express iGluSnFR in cortical neurons, our data indicates that iGluSnFR signals exhibit rapid kinetic properties and high SNR for reporting sensory-evoked cortical responses and spontaneous activity, which were both amplified by blocking glutamate transporter. By comparing evoked cortical responses across iGluSnFR, GCaMP3, GCaMP6s, and VSD signals, we found that iGluSnFR provides superior temporal kinetics than available state-of-the-art genetically encoded sensors for regional imaging of event-related activity. Although current GCaMPs including GCaMP6f/s have a greater signal ($\Delta F/F_0$), GCaMP3 which we have tested most extensively has similar reported decay kinetics to GCaMP6f (Chen et al., 2013b). Moreover, functional connectivity assessed by seed-pixel correlation maps generated from spontaneous iGluSnFR signals was consistent with maps described from GCaMP or VSD signals. Our results indicate that mesoscopic cortical imaging of iGluSnFR will enable longitudinal studies of synaptic activity and cortical circuits during plasticity paradigms, or in pathological brain states with higher temporal resolution.

5.4.1 Interpretation of iGluSnFR Signals

The signal from iGluSnFR likely reflects both the dynamics of glutamate release and clearance (Haustein et al., 2014). When changes are observed in regional iGluSnFR signals (or even at the cellular level), it is difficult to separate the contribution of release and re-uptake. Potentially, the rapid rise-time of the signals is more dependent on glutamate release, and the decay period

reflects unbinding, diffusion, and glutamate clearance by re-uptake. Consistent with this, cellular imaging results have also shown that the blockade of reuptake lengthens iGluSnFR decay responses by approximately one order of magnitude (Marvin et al., 2013; Haustein et al., 2014). We observed amplified visual stimulation-evoked regional iGluSnFR signals following reduction in glutamate re-uptake with 500 μM TBOA. However, TBOA did not lengthen the decay time (Fig. 5.5B), suggesting a nuanced interpretation of the factors determining regional iGluSnFR signal kinetics *in vivo*. It is possible that re-uptake is not a rate limiting factor for the kinetics of visual responses from a glutamate perspective.

Using 2P imaging, we investigated the nature of wide field iGluSnFR signals during spontaneous activity and following sensory stimulation (Fig. 5.6). This approach confirms a predominantly neuropil origin of iGluSnFR signals throughout the superficial cortical layers. Unfortunately, dense iGluSnFR expression in cortical excitatory neurons prevented identification of cellular iGluSnFR signals in Emx-CaMKII-iGluSnFR mice. The fluorescence is present in membrane compartments making it difficult to resolve individual processes or somata. However, membrane localization is critical for monitoring extracellular glutamate. Membrane fluorescence contrasts with the relatively larger volumes that soluble probes such as GCaMPs occupy making discrete somata relatively easy to resolve. When sparsely expressed, individual dendrites can be visualized using iGluSnFR imaging (Marvin et al., 2013), however, the probe is not selectively targeted and is expected to be present in both axonal and dendritic compartments (Marvin et al., 2013; Haustein et al., 2014). Future *in vivo* study utilizing sparse expression strategies will improve our understanding of local iGluSnFR signals.

5.4.2 Comparison with Other Genetically Encoded Sensors for Mesoscopic Imaging

Signal strength and kinetic properties of activity sensors are crucial for informative studies of event-related responses and cortical dynamics *in vivo*. We characterize these responses here using sensory-evoked responses and spontaneous brain activity. Various genetically encoded sensors have been developed (Akemann et al., 2010; Chen et al., 2013b; Huang and Zeng, 2013), but their usage in imaging at the mesoscopic level have not been carefully examined and compared. When tested *in vitro*, these recombinant glutamate sensors can have millisecond activation rates and <100 millisecond decay kinetics. In addition to its specificity for glutamate signaling (Marvin et al., 2013), we found that iGluSnFR had the best kinetic properties for monitoring regional activity, compared to other state-of-the-art genetically encoded sensors, such as GCaMPs (Chen et al., 2013b; Vanni and Murphy, 2014; Madisen et al., 2015). It could be attributed to the fast clearance of extracellular glutamate, as well as the faster on- and off-rate of iGluSnFR compared to Ca^{2+} signaling and the kinetics of GCaMPs. Given that iGluSnFR reflects rapid excitatory neurotransmitter-related transmission it may be suitable to the study of synaptic excitation/inhibition balance during wakefulness (Haider et al., 2013). While visual responses to single flash stimuli offer the ability to extend imaging to awake animals (non-contact and less invasive), single brief stimuli directed to the whisker or limbs are likely best for evaluating the speed of processing.

5.4.3 iGluSnFR Can Reveal Frequency-Dependent Mesoscopic Bilateral Functional Connectivity

The seed-pixel correlation maps of iGluSnFR over 0.1 to 12 Hz were generally similar to what we found with GCaMP3 and VSD imaging using either 0.1 to 1 Hz or 0.5 to 6 Hz frequency spontaneous activity, respectively (Mohajerani et al., 2013; Vanni and Murphy, 2014). These spontaneous activity maps reflect structural connections within the cortex (Mohajerani et al., 2013; Oh et al., 2014), or areas receiving common upstream drive. Due to its rapid kinetics, we suggest that the regional activity of spontaneous iGluSnFR signals will be able to report bilateral homotopic functional connectivity that are associated with higher frequency events in particular in up to 12-30 Hz (Harris and Mrsic-Flogel, 2013; Mohajerani et al., 2013). Interestingly, while iGluSnFR may be able to assess functional connectivity in higher frequency bands of activity, initial analysis suggests that long-distance functional connectivity can be well-represented in ~ 1 Hz activity. However, close inspection of maps reveals that mirrored homotopic maps may be less-prevalent at 12-30 Hz indicating a frequency dependence to laterality (van Kerkoerle et al., 2014). The mesoscopic imaging of fast cortical iGluSnFR signals may assist monitoring information flow among cortical regions during behavior tasks (Matyas et al., 2010; Chen et al., 2013a; Guo et al., 2014b; Li et al., 2015). Consistent with this proposal, we readily observe both a primary and late secondary visual response (peaks at 200-250 ms) using iGluSnFR *in vivo* that may be related to intracortical reverberation of activity (Sachidhanandam et al., 2013; Funayama et al., 2015) in awake states.

5.4.4 Signal Processing Considerations

All the single wavelength green fluorescent protein-based sensors, including GCaMPs and iGluSnFR, suffer from breathing, heart beat-induced, and hemodynamic artifacts (Hillman, 2015). Dual wavelength voltage-dependent Forster resonance energy transfer (FRET) sensors – VSFP- Butterfly 1.2 or ratiometric Yellow Cameleon have the advantage to parse these other signals by applying signal equalization (Horikawa et al., 2010; Akemann et al., 2012), principal component analysis (PCA) (Carandini et al., 2015), or other ratiometric methods (Minderer et al., 2012; Chen et al., 2013a). In our case GSR (Aguirre et al., 1998; Fox et al., 2009) was applied to reduce global artifacts that may result from changes in blood volume and hemodynamic responses for GCaMP and iGluSnFR signals. However, we acknowledge that application of GSR could introduce artificial anti-correlation into the resting-state functional connectivity (Fox et al., 2009; Murphy et al., 2009), as well as removal of real global neuronal activity (Schölvinck et al., 2010). Therefore, interpretation of GSR-regressed data can require caution when slow signals and in particular when reductions in signal are evaluated (not the case for present work). On the other hand, ratiometric optical signals of FRET-based glutamate sensors (Hires et al., 2008) may provide a convenient means to reduce movement and hemodynamic noise, but they have to be adapted to match the sensitivity of iGluSnFR (Marvin et al., 2013). Background signals due to flavoprotein autofluorescence, as previously proposed (Díez-García et al., 2007; Husson et al., 2007), and blood volume artifacts are unlikely to have contaminated iGluSnFR data significantly given that these artifacts are relatively slow and have been shown to minimally impact less sensitive and slower GCaMP3 signals (Vanni and Murphy, 2014). Control experiments (Vanni and Murphy, 2014) performed in wild type non-fluorescent mice and activity-insensitive green

fluorescent protein (GFP) mice (Feng et al., 2000) demonstrate that flavoprotein autofluorescence responses are much slower than iGluSnFR signals and only contribute to less than 3% of the green fluorescent responses in Emx-GCaMP3 mice. Signal fluctuations resulting from the absorption of the blue excitation light and green emission fluorescence by local hemoglobin concentration (estimated from GFP mice) was less pronounced compared to GCaMP3 signal (SD: 8% relative to Emx-GCaMP3 spontaneous activity) (Vanni and Murphy, 2014). Given that iGluSnFR signals are of comparable magnitude to GCaMP3 (but have faster kinetics), we expect these artifacts to contribute an even smaller percentage of variance to iGluSnFR signals.

In conclusion, longitudinal mesoscopic imaging of extracellular glutamate signals provides a new tool to monitor synaptic activity, with faster kinetics and neurotransmitter specificity, compared to other genetically-encoded sensors such as GECIs. iGluSnFR has utility in normal physiology, as well as neurologic and psychiatric pathologies that are associated with glutamatergic abnormalities.

Chapter 6: General discussion

6.1 Optogenetics as a Tool to Assess Brain Excitability and Function following Ischemia

In current study, we have adapted optogenetic tools to assess neuronal excitability and network activity in the cortex during an event of transient global ischemia in mice. We found that a transient global ischemia can lead to prolonged deficits of motor-sensory processing, which may be associated with prolonged suppression of synaptic function, despite immediate recovery of neuronal excitability and structural integrity.

6.1.1 Strengths and Limitations for Using Optogenetic Stimulation to Assess Selective Neuronal Excitability following Ischemia

Using optogenetic tools, we describe the dynamics of neuronal excitability and synaptic activity in cortical excitatory and inhibitory neuronal populations following a transient global ischemia in mice. Compared to conventional stimulation tools used in assessing brain excitability in humans (e.g., tDCS, TMS, etc.) or in rodents (e.g., electrical stimulation), optogenetic stimulation-based assessment owns the strength of population selectivity (Gradinaru et al., 2010). To achieve the selective stimulation for assessing excitability in different neuronal populations, we selectively expressed optogenetic activator in Cre transgenic mice. For example, we expressed ChR2 in PV-Cre transgenic mouse, delivered by AAV injection. While viral injection is associated with damage to cortex (Cetin et al., 2006), we selected this approach as transgenic expression was low when crossing loxp-ChR2 transgenic mouse and ChR2 transgenic mice (Madisen et al., 2012) and responded to light stimulation much smaller. For future studies, one might consider other

transgenic mice to avoid viral delivery, such as the VGAT-ChR2 transgenic mice. They express ChR2 in all inhibitory neurons (Zhao et al., 2011; Guo et al., 2014a; Anenberg et al., 2015). Although it lacks subpopulation specificity as we found the evoked electrical responses (data not shown) generally agreed with that observed from similar stimulation from the PV-ChR2 mouse. We anticipate that the VGAT-ChR2 would be a valid transgenic line for monitoring inhibitory neuron excitability.

Concurrently, we optogenetically stimulated excitatory neuronal populations, specifically using the Thy1-ChR2 transgenic line to selectively stimulate excitatory neurons in the cortex. In this line, ChR2 is mainly expressed in cortical layer 5B neurons, which are primarily large pyramidal neurons (Arenkiel et al., 2007; Lim et al., 2014). These neurons are thick tufted, with extensive projections in layer 2/3, and are intrinsically-bursting (firing bursts of action potentials in response to depolarizing current injections) (Hattox and Nelson, 2007). Expression of ChR2 in cortical excitatory neurons also can be achieved by crossing loxp-ChR2 transgenic mice with CaMKII-Cre transgenic mice or viral expression of Cre-dependent ChR2 in CaMKII-Cre transgenic mice (Gorski et al., 2002; Cardin et al., 2009).Therefore, as with the aforementioned inhibitory approach, optogenetics can be utilized to selectively direct neuronal activity with population specificity.

Another advantage of using optogenetics for brain stimulation is its little invasiveness, especially when the stimulation is applied over the cortex (Chen et al., 2012b). This is crucial for stroke studies given that the invasiveness of investigation tools, for example, intracellular or extracellular electrophysiological recordings, can confound findings. In current study, we

initially applied a surface EEG electrode to collect the electrical responses from ChR2 stimulation, which was conducted by shining a laser light through the craniotomy, thereby minimizing damage to the brain. Future experiment can adapt an intact skull preparation for chronic EEG recording and optogenetic stimulation (Silasi et al., 2013) to further reduce invasiveness. Not only was our approach less invasive, it provided high spatial and temporal fidelity (Ayling et al., 2009; Harrison et al., 2012; Anenberg et al., 2014). This allows cortical mapping of rapid changes of regional excitability after stroke at high resolution, and also allows combination with other imaging and electrophysiological tools (Lim et al., 2012, 2014; Anenberg et al., 2014). Further still, using optogenetic tools to both independently stimulate and monitor neuronal activity would be another way to achieve the goal of reducing the invasiveness and maximizing fidelity when assessing cortical excitability (Guo et al., 2009; Mancuso et al., 2011; Lim et al., 2013). This is currently limited by the challenge of improving the sensitivity of optogenetic sensors, while simultaneously developing sensors and activators with non-overlapping light spectra (Akerboom et al., 2013).

Nevertheless, there are disadvantages that are associated with using optogenetics to study models of ischemia. First, despite the aforementioned cell-specificity, high spatial and time resolution (Miesenböck, 2011), the physiological relevance of optogenetic stimulation-evoked responses is actively debated (Fenno et al., 2011; Grosenick et al., 2015). In our studies, the pattern of optogenetic stimulation was not biologically determined, and therefore their physiological relevance is unclear. In future, a stimulation pattern that is consistent with neuronal intrinsic firing pattern would not be subject to this limitation. Second, despite cell and spatial specificity, optogenetic stimulation evokes network of responses involving polysynaptic interactions, and

therefore the recorded responses require decoding. In presented investigations, we chose to pharmacologically define the signatures of electrical responses arising from the optogenetic stimulation of excitatory and inhibitory neuronal populations to facilitate deciphering these network responses (see the discussion in Chapter 2 and 3). Indeed, such approaches are crucial to understanding the nature of optogenetic stimulation-evoked signals (Tye and Deisseroth, 2012). Last but not least, optogenetic stimulation relies on the expression and channel properties of optogenetic activators (Lin et al., 2009). Brain diseases, such as ischemia, alter the expression and channel properties by direct protein degradation and changing pH (Siesjö et al., 1990). Therefore, the ischemia-induced changes of optogenetic stimulation-evoked responses (Chen et al., 2012b; Lim et al., 2014; Xie et al., 2014) might be also partially attributed to the changes of ChR2 expression or its channel properties.

6.1.2 Considerations about the Specificity of Neuronal Population Targeting ChR2

In our previous and current studies, we have used the transgenic mice that express ChR2 under the control of the Thy1 promoter to assess the cortical excitability (Chapter 2), in addition to mapping intact motor cortex (Ayling et al., 2009; Harrison et al., 2012) as well as following ischemia (Harrison et al., 2013; Xie et al., 2013; Anenberg et al., 2014). Thy1 is an immunoglobulin superfamily member that is expressed by projection neurons in many parts of the nervous system, as well as by several non-neuronal cell types, including thymocytes (hence its name) (Morris, 1985; Gordon et al., 1987). Genetic ablation of a particular intron selectively abolishes expression in non-neural cells, therefore using the thy1 promoter allows specific expression of ChR2 in projection neurons (Vidal et al., 1990; Feng et al., 2000; Arenkiel et al.,

2007). Though the expression of ChR2 using the Thy1 promoter is predominately in cortical layer 5B pyramidal neurons (excitatory neurons), this is also sparsely expression in neurons within the upper cortical layers (Feng et al., 2000; Arenkiel et al., 2007; Chen et al., 2012b; Lim et al., 2014). Most inhibitory neurons are not projection neurons, with the exception of somatostatin neurons, however, it is still unknown whether any ChR2 is expressed in inhibitory neurons in Thy1-ChR2 transgenic mice (Arenkiel et al., 2007; Lim et al., 2014). Using the CaMKII promoter for targeting Cre-recombinase can improve the specificity of transgene in excitatory neurons (Gorski et al., 2002).

To express ChR2 in PV neurons, we used the power of Cre recombinase (Xie et al., 2014). In our hands, the expression efficacy is above 90% (PV-ChR2/PV immunostaining positive) with either transgenic crossing or viral injection (Xie et al., 2014). Unfortunately, Cre strains can express Cre recombinase in non-target cells and tissues (Heffner et al., 2012), and this is true of the PV-Cre transgenic utilized in our investigations (Kobayashi and Hensch, 2013; Pfeffer et al., 2013). The off-target expression of Cre-recombinase and ChR2 can potentially confound experimental interpretation and reproducibility (Bonder and McCarthy, 2014; Stuber et al., 2015), and therefore caution is warranted when using the Cre-lox system. To control gene targeting more rigorously, one could consider using Cre recombinase together with another inducible binary system, for example tetracycline-dependent transcription (Berens and Hillen, 2004). In this system, the expression of bacterial tetracycline-regulated transactivator (tTA) is driven by a gene promoter that then activates the expression of a reporter gene under the control of the tetracycline-responsive element, tetO, only in the absence of tetracycline or doxycycline. For example, the EMX-CaMKII-GCaMP and EMX-CaMKII-iGluSnFR mice used in our study (see

Chapter 5) have restricted expression only in cortical excitatory neurons, as the Cre expression is driven by EMX promoter (drives the expression in the cortical neurons and glias (Gorski et al., 2002)), and the tTA expression is driven by CaMKII promoter (drives the expression in the excitatory neurons (Mayford et al., 1996)).

6.1.3 Considerations about Optical Neural Interfaces

In our study, we have adapted an optical neural interface that is using laser to stimulate ChR2 and surface EEG or a multichannel optrode to record electrophysiological signals in the mouse cortex (Chapter 2 and 3). Integrating ChR2 stimulation and surface EEG recording enables relatively non-invasive assessment of neuronal excitability, but EEG signals are insensitive to subtle changes, difficult to interpret, and also cannot resolve spiking activity (Teplan, 2002). The multichannel optrode is well suited for LFP and multiunit recording. The light source for ChR2 activation was placed 50 μm above the surface of the cortex and the electrophysiological recording sites spanned multiple layers of the cortex with 50 μm separating each recording site. However, as reported by other groups, we also observed an optoelectronic artifact introduced by light stimulation (Han et al., 2009; Cardin et al., 2010). Fortunately, our experiments do not require continuous light input. Future studies can adapt chronic multisite optrodes to longitudinally assess neuronal excitability in mice following transient global ischemia (Yizhar et al., 2011). Other electrical readouts that can be coupled with optogenetic stimulation including silicon probes, stereotrodes and tetrode microdrives, and multielectrode arrays (Warden et al., 2014). Still, the remaining challenge for better performance of these electrical readouts is reducing the optoelectronic artifact seen in LFP signals, in which illumination of the metal

recording electrode can produce a significant slow-voltage change (Han et al., 2009; Cardin et al., 2010). This problem may be partially resolved by appropriate configuration of light delivery and recording electrode, by choosing a less susceptible electrode coating, or electrode material itself (Cardin et al., 2010; LeChasseur et al., 2011).

Another method to probe circuitry activity with optogenetic stimulation is to integrate optogenetic stimulation and brain imaging techniques (e.g., optogenetic sensors, organic indicators, or fMRI, etc.) (Guo et al., 2009; Lee et al., 2010; Lim et al., 2012, 2014; Akerboom et al., 2013). Among the tools, fMRI has low temporal and spatial resolution for mapping the mouse brain (Lee et al., 2010; Desai et al., 2011). To more precisely monitor network activity, our lab has previously shown that ChR2 stimulation can be coupled with mesoscopic VSD imaging for direct excitability mapping and connectivity mapping in the cortex under normal physiology (Lim et al., 2012), or following focal stroke (Lim et al., 2014). Unfortunately, these experiments were terminal so that the changes cannot be compared within the same animal before and after stroke. Integration of optogenetic stimulation and optogenetic sensing with independently addressable spectral channels for stimulation and imaging (Guo et al., 2009; Akerboom et al., 2013) would provide opportunities for longitudinal optogenetic cortical mapping, which remains a goal in the field.

6.1.4 Optogenetic Stimulation and Imaging for the Diagnosis or the Treatment of Diseases

My work has shown a relatively non-invasive method by using optogenetic activators and electrophysiological recording to monitor the changes of neuronal excitability and synaptic

transmission in a mouse model of stroke. In the clinical setting, the combination of TMS with EEG or fMRI enables clinicians and researchers to directly monitor local and network cortical plasticity in humans, and characterize their changes during brain diseases, such as stroke (Pascual-Leone et al., 2011). However, TMS lacks neuron population specificity. More importantly, the mechanistic underpinning of TMS is still unclear; as such the safety profile and potential for harm is unclear. Indeed, optogenetic stimulation with higher temporal and spatial resolution can unravel circuitry mechanisms behind psychiatric symptoms or brain diseases (Tye and Deisseroth, 2012; Lim et al., 2014), which allows a more sophisticated understanding of disease etiology. For example, our lab has shown that the ischemia penumbra exhibited heterogeneous recovery of excitability and network connectivity following a focal stroke, suggesting that regional understanding of cortical recovery after stroke may lead to improved interventions (Lim et al., 2014).

In current studies, we have also adapted newly generated transgenic mice expressing optogenetic sensors (e.g., GCaMPs, iGluSnFR, etc.) (Madisen et al., 2015) to perform mesoscopic cortical imaging. These sensors allow longitudinal and noninvasive characterization of cortical activity, which when applied to questions such as transient global ischemia would permit repeated mapping of sensory-evoked cortical responses or spontaneous cortical activity over time.

In the clinical setting, tools for observing brain activity and connectivity are still largely restricted to non-invasive technology, and therefore human characterizations are limited to tools with limited temporal and/or spatial resolution, such as EEG, contrast fMRI dependent on blood oxygen level and diffusional MRI for inferring the path of axonal tracts. Translational studies in

animals can provide mechanistic insights. Indeed, mesoscopic imaging of cortical activity has been providing valuable information for studying brain disease. For instance, we have previously shown deficits in sensory mapping following a focal stroke using VSD imaging in mice (Brown et al., 2009; Mohajerani et al., 2011). Another longitudinal mesoscopic cortical mapping study using IOS (monitors blood oxygenation) revealed a disrupted functional connectivity when mice were subjected to a focal stroke (Bauer et al., 2014). A bidirectional relationship between cortical functional connectivity and amyloid-β deposition in mouse brain was demonstrated using IOS imaging (Bero et al., 2012).

With the work presented in this dissertation, we have provided characterizations of transgenic mice expressing optogenetic sensors (GCaMPs, iGluSnFR, etc.) that are suited to longitudinal mesoscopic imaging. Our characterization includes the kinetic properties of these sensors, and suggests that iGluSnFR might have the highest temporal resolution for monitoring cortical activity among all the currently available optogenetic sensors. We speculate that this is likely attributable to the fast on and off rate of glutamate binding (Marvin et al., 2013). These tools not only improve the quality of signal compared to IOS imaging, but also allow the longitudinal recording of defined neuronal activity. In the future, iGluSnFR can be used to monitor the dynamics of glutamate (the major neurotransmitter contributing to excitotoxicity during brain injury) concentration, following stroke and during recovery.

6.1.5 Future Improvement of Optogenetic Stimulation for Assessing Neuron Excitability

Optogenetic approaches for brain stimulation can be further refined with improved optogenetic activators. Indeed, there has been progressive development of optogenetic activators during the

past decade (Gradinaru et al., 2010; Fenno et al., 2011; Berndt et al., 2014). Currently, the most widely used variant of optogenetic activators is ChR2 (H134R) (Boyden et al., 2005; Zhang et al., 2007b), which has millisecond-precision control and was used in our study to activate pyramidal neurons and PV neurons (Arenkiel et al., 2007; Cardin et al., 2009). The fast decay ChR2 variant – ChETA or ChIEF could be more suitable to activate fast spiking PV neurons at their intrinsic firing frequency (Lin, 2011). Other efforts have also been made to enhance the function of ChR2 through the fusion of multiple genes to create hybrid proteins. For example, adding a PDZ-binding domain to ChR2 can cause it to cluster at post-synaptic dendrites (Gradinaru et al., 2007). Fusions of ChR2 with a myosin-binding domain can target ChR2 expression to the somatodendritic compartment of neurons (Lewis et al., 2009), whereas ChR2 can be localized to the axon initial segment by creating a fusion of ChR2 and the ankyrinG-binding loop of voltage-gated sodium channels (Grubb and Burrone, 2010). These techniques may allow more accurate light stimulation to the defined compartment in neurons; however the usage of many of them has not been validated *in vivo*. Moreover, efforts have also been made to push the optimum excitation/absorbance light spectrum of optogenetic activators to the red spectrum (e.g., C1V1, Chrimson, ReaChR etc.) (Zhang et al., 2007b; Lin et al., 2013; Klapoetke et al., 2014), since red light has better tissue penetration, and can be readily integrated with the usage of current GFP-based optogenetic sensors for readouts, such as GCaMPs or iGluSnFR. Future development may further improve the properties of light-activatable opsins or the targeting of their expression in specific cell compartments.

6.2 Implications for Further Understanding the Pathophysiology of Transient Global Ischemia

6.2.1 A 5 min Transient Global Ischemia Induces Prolonged Functional Deficits

In current study, the most important finding is: even a very brief period of transient global ischemia (as short as ~5 min) can result in prolonged functional deficits in synaptic activity in the cortex. This is coincident with prolonged sensory and motor dysfunction, despite a rapid recovery of neuronal excitability and structural integrity. Our *in vivo* and high resolution data (summary figure: Figure 6.1) have replicated and integrated previous pieces of evidence that have separately shown in neuronal culture, brain slice recordings or anesthetized animals with other experimental approaches (Hossmann, 1971; Hossmann et al., 1987; Xu and Pulsinelli, 1994; Abdel-Hamid and Tymianski, 1997; Pang et al., 2002; Zhang et al., 2006, 2008; Ruan et al., 2009)

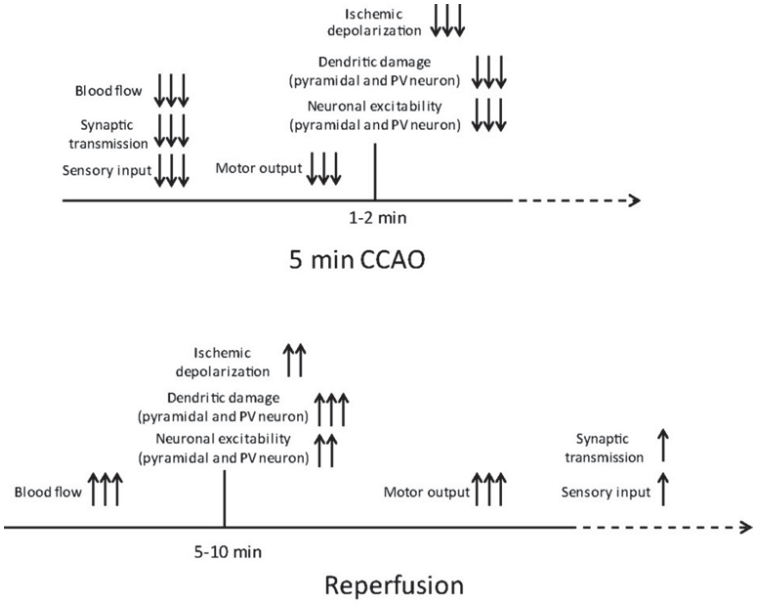

Figure 6.1 Summary figure: changes of blood flow, cell membrane potential, synaptic transmission, neuronal excitability, and motor and sensory processing following a 5 min global ischemia and reperfusion in mice.

Our results suggest that the synaptic deficits in both excitatory and inhibitory networks may lead to the deficits of sensory-motor processing following stroke, despite the rapid recovery of dendritic structure and neuronal excitability (Figure 6.1). Synaptic deficits during ischemia might be due to depolarization block or a structural damage during ischemia (Dirnagl et al., 1999; Andrew et al., 2007). The prolonged synaptic deficits following reperfusion can be attributed to deficits in presynaptic release, receptor internalization, or excitotoxicity-induced neuronal death (Bolay et al., 2002; Pang et al., 2002; Liu et al., 2006, 2007; Lai et al., 2014). Simultaneous assessment of motor and sensory function, together with optogenetic assessment of cortical neuronal excitability and overall membrane potentials (EEG signals) in the cortex, provides novel insights regarding the temporal relationship between each parameter. For example, we were able to demonstrate that neuronal excitability and structure are suppressed and damaged by ischemia with the onset of ischemic depolarization, and both are recovered with the normalization of ischemic depolarization. We found that the synaptic activity and sensory-motor function recovers much slower and incompletely (Figure 6.1). Therefore, we emphasize that functional recovery (Clarkson et al., 2010, 2011; Carmichael, 2012), particularly the recovery of synaptic function (Johansson, 2000; Clarkson et al., 2010, 2011; Overman et al., 2012), is an important therapeutic target for transient global ischemia or focal ischemia (Anenberg et al., 2014), in addition to neuroprotection (Aarts et al., 2002; Lai et al., 2014) and neuron replacement (stem cell treatment) (Bang et al., 2005; Locatelli et al., 2009).

6.2.2 Considerations about Our Transient Global Ischemia

We utilized the stroke model of transient global ischemia, in which the common carotid arteries are occluded for 5 min after perfusion resumes. Compared to other animal models of ischemia, the transient global ischemia model has the advantage of being experimentally amenable for coupling with continuous imaging, electrical recording, and motor mapping with precise control of induction and reperfusion. More importantly, it has clinical relevance and models ischemic changes that can occur during cardiac arrest or cardiac surgery (Ginsberg and Busto, 1989; Kawai et al., 1992). Our laser speckle contrast imaging results, along with results using other blood flow monitoring (e.g., Laser Doppler, 2P imaging of the speed of red blood cell), have shown that the induction of CCAO in C57/B6 mouse background leads to an 80 to 90% reduction of blood flow in the cortex (Yonekura et al., 2004; Murphy et al., 2008; Xie et al., 2013). The level of remaining blood flow during global ischemia is similar to that in the penumbra following a focal ischemia (Dunn et al., 2001; Bandera et al., 2006); therefore it may also model the clinically important penumbra, where neuronal excitability is suppressed, but is still recoverable with the restoration of blood flow (Lo, 2008). In addition, our transient global ischemia model may also reflect pathology associated with transient ischemic attack, which is a highly prevalent form of ischemia in human patients, for which there are limited validated animal models (Albers et al., 2002). Conversely, because the global ischemia model indiscriminatingly diminishes blood flow in the entire brain and induces spatial and cell-type selective vulnerability (Fujii et al., 1997; Sheng et al., 1999), application to these findings to clinical conditions should be considered with cautions as mechanistic interpretation of the underlying circuitry deficits can be complicated.

6.2.3 Implications for Stroke Treatment and Rehabilitation

Our results (Murphy et al., 2008; Chen et al., 2012b; Xie et al., 2013, 2014), together with others' (Risher et al., 2010, 2011; Dreier, 2011), suggest ischemic depolarization is one of the major causes of dendritic damage and the loss of neuronal excitability. Mitigating spreading depolarization can reduce the dendritic damage during ischemia or cortical spreading depolarization (Risher et al., 2010, 2011; Steffensen et al., 2015). Since the currently available reagents (e.g., dibucaine) for preventing spreading depolarization cannot be applied systematically (Risher et al., 2011; Steffensen et al., 2015), it is possible to locally apply it to the brain to reduce structural damage.

Inhibition of synaptic transmission during ischemia or following reperfusion might be attributed to the dendritic damage, the loss of the neuronal excitability, the energy failure-induced deficits in presynaptic release, presynaptic reuptake, or postsynaptic deficits (Dirnagl et al., 1999; Rossi et al., 2000). A recent study showed that the extrasynaptic $GABA_A$ receptor mediated-tonic inhibition might also play a role in the suppression of neuronal excitability and synaptic activity in the penumbra days after ischemia, which can further lead to the impairment of functional recovery (Clarkson et al., 2010). Mitigating dendritic damage by blocking ischemic depolarization may reduce the ischemia-induced suppression in synaptic activity (Dreier, 2011). Early studies have also tested the effects of reducing excitotoxic neurotransmitter release from glutamate transporter during ischemia (Rossi et al., 2000). However, glutamate transporter inhibitor, such as TBOA, shows no neuroprotective effects, and can even exacerbate ischemic neuronal death (Colleoni et al., 2008).

In the acute phase, ischemic insults promote rapid internalization of glutamate receptor subunit 2 containing AMPA receptors from synaptic sites *via* clathrin-dependent endocytosis (Liu et al., 2006). Meanwhile, cerebral ischemia also causes persistent presynaptic deficits, which leads to the impairment of neurotransmitter release (Bolay et al., 2002). Using brain slice recording, researchers found transient ischemia depresses the fast excitatory synaptic transmission in large aspiny neurons, which is due to the activation of presynaptic adenosine A1 receptor (Pang et al., 2002). In the chronic phase, transient cerebral ischemia induces rapid down-regulation of $GABA_A$ receptors in hippocampal neurons (Li et al., 1993; Alicke and Schwartz, 1995). In contrast, $GABA_A$ receptor is upregulated in the penumbra following focal ischemia (Neumann-Haefelin et al., 1999). This upregulation might contribute to the upregulation of extrasynaptic GABA receptor for generating tonic inhibition, which may further impair the recovery of motor function following focal ischemia (Clarkson et al., 2010). Indeed, restoring the brain function following ischemia is not only a simple task to normalize the altered function of excitatory or inhibitory synapses, but also needs to balance between the excitation and inhibition (Clarkson et al., 2010; Carmichael, 2012).

My work also suggests that transient global ischemia suppressed sensory processing more severely than motor processing, despite the fact that blood flow was reduced to a similar level within both the sensory and motor cortices. There are a few possible explanations. First, there are direct neuronal projections from the motor cortex layer 5B neurons (where ChR2 expresses) to the spinal cord (Yamawaki et al., 2014), whereas sensory inputs from spinal cord to the sensory cortex are polysynaptic (Carvell and Simons, 1987), which is more vulnerable to the ischemia-induced synaptic dysfunction. Second, global ischemia induces selective damage to different

brain structures, causing more severe impairment in the hippocampus, but also affects the thalamus and cortex (Koh et al., 1996). Therefore, the subcortical regions that are involved in sensory processing (e.g., the thalamocortical projections) can be more affected by transient global ischemia (Shoykhet et al., 2012; Wu et al., 2012). Overall, our results suggest a differential sensitivity of sensory and motor systems to the effects of global ischemia and reperfusion that may have implications for rehabilitation. However, we only grossly measured the input strength of sensory and the output strength of motor processing. Future studies are needed to investigate how transient global ischemia impairs the detailed motor and sensory function, such as digital movements and sensory perception.

6.3 Mesoscopic Imaging with Optogenetic Sensors and Its Application

6.3.1 Mesoscopic Imaging with Optogenetic Sensors

In the current study, we have validated the usage of genetically encoded sensors (e.g., GCaMPs and iGluSnFR) to perform mesoscopic imaging, and characterized their signal properties during spontaneous activity and sensory stimulation-evoked responses in the cortex. Mesoscopic imaging stands in between microscopic imaging and macroscopic imaging. It monitors regional interaction (Markounikau et al., 2010), for example, the interaction between the motor and sensory cortex (Lim et al., 2013; Mohajerani et al., 2013; Vanni and Murphy, 2014), and can be combined with cellular imaging (Issa et al., 2014; Vanni and Murphy, 2014) or optogenetic stimulation (Lim et al., 2012, 2014). Some previous tools for mesoscopic imaging in mouse cortex have been limited by slow temporal resolution and low spatial resolution (e.g., IOS imaging), or by requiring invasive surgical procedures that do not allow recovery and chronic

imaging (e.g., VSD imaging). Our demonstration of mesoscopic imaging using GCaMPs and iGluSnFR enables high resolution and longitudinal mapping of cortical activity that can be readily applied to study the alteration of brain responses and network connectivity during brain plasticity or brain diseases. The pros and cons of using mesoscopic imaging with currently available genetically encoded sensors have been extensively discussed in Chapter 5 (see the discussion in Chapter 5).

6.3.2 Application of Mesoscopic Cortical Imaging for Mapping the Cortex under Normal Physiology or Pathology

Our lab has previously shown that mesoscopic imaging can be applied to map connectivity within the mouse cortex under anesthesia or quiet wakefulness using seed-pixel correlation maps (Mohajerani et al., 2010, 2013) of resting-state activity or direct optogenetic stimulation-based mapping (Lim et al., 2013). Further studies revealed that the resting-state connectivity maps are reflected in underlying monosynaptic axonal projections (Mohajerani et al., 2013). Using VSD imaging, we revealed that the seed-pixel connectivity maps generated from resting-state infraslow activity bands (< 0.1 Hz) recapitulate our previously observed high frequency activity motifs (Chan et al., 2015), which provides strong support for using the neuronal correlated – resting-state fMRI BOLD signals for mapping the human brain (Biswal et al., 1995; Fox and Greicius, 2010). Furthermore, our mesoscopic imaging of GCaMP3 and iGluSnFR confirmed that the resting-state correlation maps were preserved across various sensors that report different aspects of neuronal activity (Vanni and Murphy, 2014).

Previous studies using imaging techniques to investigate regional connectivity during behavior tasks or sensory processing (e.g., the interaction between the sensory and motor cortex) often involved complicated genetic labeling for projections (Huber et al., 2012; Chen et al., 2013a), but still fail to image regions simultaneously. Mesoscopic imaging enables imaging of regions simultaneously (Matyas et al., 2010), despite lacking cellular resolution. Along with the development of cell population specific expression (Madisen et al., 2010; Huang and Zeng, 2013), it is possible to collect wide-field signals while still knowing the signal origins from specifically identified cell populations (Cui et al., 2014; Gunaydin et al., 2014). For instance, we have used transgenic mice expressing GCaMPs under the control of tTA with CaMKII promoter and Cre with EMX promoter; thereby the imaging signals are constrained by the restriction of the expression to cortical excitatory neurons (Madisen et al., 2015). Moreover, combination cranial window preparation (8 × 8 mm) (Silasi et al., 2013) and genetically encoded sensors enables both non-invasive head-fixed imaging and longitudinal imaging for mapping the cortex during behavior learning or sensory processing.

Mesoscopic imaging has been used in characterizing the alterations of sensory maps following brain diseases, such as stroke (Brown et al., 2007, 2009; Zhang and Murphy, 2007). Most of the results showed deficits in sensory-stimulation evoked activity following brain injury, which provides a measurement for evaluating the damage during brain diseases and the recovery following rehabilitation or therapeutic treatment. Using mesoscopic imaging of resting-state spontaneous activity over the mouse cortex, recent studies have unraveled interesting facts regarding the alterations of network connectivity following brain diseases, such as stroke (Bauer et al., 2014; Lim et al., 2014), spreading depolarization (Li et al., 2012) and Alzheimer's disease

(Bero et al., 2012). These results indicate that even a small focal brain damage could result in a global network changes in addition to the local impact within the damaged region, called diaschisis (Carrera and Tononi, 2014; Silasi and Murphy, 2014). Network analysis in the transgenic modeling Alzheimer's disease revealed a bidirectional relationship between functional connectivity and amyloid-β deposition in mouse cortex (Bero et al., 2012), which confirmed clinical results in human patients (Vlassenko et al., 2010). Therefore, as proposed for the usage of network analysis in human brain, the network analysis on resting-state activity or ChR2 mapping in the cortex using animal models may provide a mesoscopic view for the investigation and therapeutic evaluation of brain diseases, including the identification of novel biomarkers.

Bibliography

Aarts M, Liu Y, Liu L, Besshoh S, Arundine M, Gurd JW, Wang Y-T, Salter MW, Tymianski M (2002) Treatment of ischemic brain damage by perturbing NMDA receptor- PSD-95 protein interactions. Science 298:846–850.

Abdel-Hamid KM, Tymianski M (1997) Mechanisms and effects of intracellular calcium buffering on neuronal survival in organotypic hippocampal cultures exposed to anoxia/aglycemia or to excitotoxins. J Neurosci 17:3538–3553.

Adamantidis AR, Zhang F, Aravanis AM, Deisseroth K, de Lecea L (2007) Neural substrates of awakening probed with optogenetic control of hypocretin neurons. Nature 450:420–424.

Aguirre GK, Zarahn E, D'Esposito M (1998) The inferential impact of global signal covariates in functional neuroimaging analyses. Neuroimage 8:302–306.

Akemann W, Mutoh H, Perron A, Park YK, Iwamoto Y, Knöpfel T (2012) Imaging neural circuit dynamics with a voltage-sensitive fluorescent protein. J Neurophysiol 108:2323–2337.

Akemann W, Mutoh H, Perron A, Rossier J, Knöpfel T (2010) Imaging brain electric signals with genetically targeted voltage-sensitive fluorescent proteins. Nat Methods 7:643–649.

Akerboom J et al. (2013) Genetically encoded calcium indicators for multi-color neural activity imaging and combination with optogenetics. Front Mol Neurosci 6:2.

Akerboom J, Rivera JDV, Rodríguez Guilbe MM, Malavé ECA, Hernandez HH, Tian L, Hires SA, Marvin JS, Looger LL, Schreiter ER (2009) Crystal structures of the GCaMP calcium sensor reveal the mechanism of fluorescence signal change and aid rational design. J Biol Chem 284:6455–6464.

Albers GW, Caplan LR, Easton JD, Fayad PB, Mohr JP, Saver JL, Sherman DG (2002) Transient ischemic attack--proposal for a new definition. N Engl J Med 347:1713–1716.

Alicke B, Schwartz RD (1995) Rapid down-regulation of GABA(A) receptors in the gerbil hippocampus following transient cerebral ischemia. J Neurochem:2808–2811.

Allan SM, Rothwell NJ (2001) Cytokines and acute neurodegeneration. Nat Rev Neurosci 2:734–744.

Allen NJ, Rossi DJ, Attwell D (2004) Sequential release of GABA by exocytosis and reversed uptake leads to neuronal swelling in simulated ischemia of hippocampal slices. J Neurosci 24:3837–3849.

Anderson TR, Jarvis CR, Biedermann AJ, Molnar C, Andrew RD (2005) Blocking the anoxic depolarization protects without functional compromise following simulated stroke in cortical brain slices. J Neurophysiol 93:963–979.

Andrew RD, Labron MW, Boehnke SE, Carnduff L, Kirov S a (2007) Physiological evidence

that pyramidal neurons lack functional water channels. Cereb Cortex 17:787–802.

Anenberg E, Arstikaitis P, Niitsu Y, Harrison TC, Boyd JD, Hilton BJ, Tetzlaff W, Murphy TH (2014) Ministrokes in channelrhodopsin-2 transgenic mice reveal widespread deficits in motor output despite maintenance of cortical neuronal excitability. J Neurosci 34:1094–1104.

Anenberg E, Chan AW, Xie Y, LeDue JM, Murphy TH (2015) Optogenetic stimulation of GABA neurons can decrease local neuronal activity while increasing cortical blood flow. J Cereb Blood Flow Metab.

Anikeeva P, Andalman AS, Witten I, Warden M, Goshen I, Grosenick L, Gunaydin LA, Frank LM, Deisseroth K (2011) Optetrode: a multichannel readout for optogenetic control in freely moving mice. Nat Neurosci 15:163–170.

Antal A, Polania R, Schmidt-Samoa C, Dechent P, Paulus W (2011) Transcranial direct current stimulation over the primary motor cortex during fMRI. Neuroimage 55:590–596.

Aravanis AM, Wang L-P, Zhang F, Meltzer LA, Mogri MZ, Schneider MB, Deisseroth K (2007) An optical neural interface: in vivo control of rodent motor cortex with integrated fiberoptic and optogenetic technology. J Neural Eng 4:S143–S156.

Arenkiel BR, Peca J, Davison IG, Feliciano C, Deisseroth K, Augustine GJ, Ehlers MD, Feng G (2007) In Vivo Light-Induced Activation of Neural Circuitry in Transgenic Mice Expressing Channelrhodopsin-2. Neuron 54:205–218.

Aschauer DF, Kreuz S, Rumpel S (2013) Analysis of transduction efficiency, tropism and axonal transport of AAV serotypes 1, 2, 5, 6, 8 and 9 in the mouse brain. PLoS One 8:e76310.

Astrup J (1982) Energy-requiring cell functions in the ischemic brain: their critical supply and possible inhibition in protective therapy. J Neurosurg 56:482–497.

Astrup J, Siesjö BK, Symon L (1981) Thresholds in cerebral ischemia-the ischemic penumbra. Stroke 12:723–725.

Astrup J, Symon L, Branston NM, Lassen NA (1977) Cortical evoked potential and extracellular K+ and H+ at critical levels of brain ischemia. Stroke 8:51–57.

Attwell D, Laughlin SB (2001) An energy budget for signaling in the grey matter of the brain. J Cereb Blood Flow Metab 21:1133–1145.

Ayling OGS, Harrison TC, Boyd JD, Goroshkov A, Murphy TH (2009) Automated light-based mapping of motor cortex by photoactivation of channelrhodopsin-2 transgenic mice. Nat Methods 6:219–224.

Ba AM, Guiou M, Pouratian N, Muthialu A, Rex DE, Cannestra AF, Chen JWY, Toga AW (2002) Multiwavelength optical intrinsic signal imaging of cortical spreading depression. J Neurophysiol 88:2726–2735.

Bandera E, Botteri M, Minelli C, Sutton A, Abrams KR, Latronico N (2006) Cerebral blood flow threshold of ischemic penumbra and infarct core in acute ischemic stroke a systematic

review. Stroke 37:1334–1339.

Bang OY, Lee JS, Lee PH, Lee G (2005) Autologous mesenchymal stem cell transplantation in stroke patients. Ann Neurol 57:874–882.

Barth AMI, Mody I (2011) Changes in hippocampal neuronal activity during and after unilateral selective hippocampal ischemia in vivo. J Neurosci 31:851–860.

Bauer AQ, Kraft AW, Wright PW, Snyder AZ, Lee J-M, Culver JP (2014) Optical imaging of disrupted functional connectivity following ischemic stroke in mice. Neuroimage 99:388–401.

Bazan NG (1976) Free arachidonic acid and other lipids in the nervous system during early ischemia and after electroshock. In: Function and metabolism of phospholipids in the central and peripheral nervous systems, pp 317–335. Springer.

Bazan NG, Squinto SP, Braquet P, Panetta T, Marcheselli VL (1991) Platelet-activating factor and polyunsaturated fatty acids in cerebral ischemia or convulsions: Intracellular PAF-binding sites and activation of a fos/jun/AP-1 transcriptional signaling system. Lipids 26:1236–1242.

Beamer NB, Coull BM, Clark WM, Hazel JS, Silberger JR (1995) Interleukin-6 and interleukin-1 receptor antagonist in acute stroke. Ann Neurol 37:800–805.

Berens C, Hillen W (2004) Gene regulation by tetracyclines. Genet Eng (N Y) 26:255–277.

Berger M, Speckmann EJ, Pape HC, Gorji A (2008) Spreading depression enhances human neocortical excitability in vitro. Cephalalgia 28:558–562.

Berger T, Borgdorff A, Crochet S, Neubauer FB, Lefort S, Fauvet B, Ferezou I, Carleton A, Lüscher H-R, Petersen CCH (2007) Combined voltage and calcium epifluorescence imaging in vitro and in vivo reveals subthreshold and suprathreshold dynamics of mouse barrel cortex. J Neurophysiol 97:3751–3762.

Berndt A, Lee SY, Ramakrishnan C, Deisseroth K (2014) Structure-guided transformation of channelrhodopsin into a light-activated chloride channel. Science 344:420–424.

Bero AW, Bauer AQ, Stewart FR, White BR, Cirrito JR, Raichle ME, Culver JP, Holtzman DM (2012) Bidirectional relationship between functional connectivity and amyloid-β deposition in mouse brain. J Neurosci 32:4334–4340.

Bhogal SK, Teasell RW, Foley NC, Speechley MR (2015) Community reintegration after stroke.

Biswal B, Yetkin FZ, Haughton VM, Hyde JS (1995) Functional Connectivity in the Motor Cortex of Resting. Brain 34:537–541.

Block F (1999) Global ischemia and behavioural deficits. Prog Neurobiol 58:279–295.

Bokil H, Andrews P, Kulkarni JE, Mehta S, Mitra PP (2010) Chronux: A platform for analyzing neural signals. J Neurosci Methods 192:146–151.

Bolay H, Dalkara T (1998) Mechanisms of motor dysfunction after transient MCA occlusion:

persistent transmission failure in cortical synapses is a major determinant. Stroke 29:1988–1993; discussion 1994.

Bolay H, Gürsoy-Özdemir Y, Sara Y, Onur R, Can A, Dalkara T (2002) Persistent defect in transmitter release and synapsin phosphorylation in cerebral cortex after transient moderate ischemic injury. Stroke 33:1369–1375.

Bonder DE, McCarthy KD (2014) Astrocytic Gq-GPCR-Linked IP3R-Dependent Ca2+ Signaling Does Not Mediate Neurovascular Coupling in Mouse Visual Cortex In Vivo. J Neurosci 34:13139–13150.

Bota M, Swanson LW (2007) The neuron classification problem. Brain Res Rev 56:79–88.

Boyden ES, Zhang F, Bamberg E, Nagel G, Deisseroth K (2005) Millisecond-timescale, genetically targeted optical control of neural activity. Nat Neurosci 8:1263–1268.

Brown CE, Aminoltejari K, Erb H, Winship IR, Murphy TH (2009) In vivo voltage-sensitive dye imaging in adult mice reveals that somatosensory maps lost to stroke are replaced over weeks by new structural and functional circuits with prolonged modes of activation within both the peri-infarct zone and distant sites. J Neurosci 29:1719–1734.

Brown CE, Li P, Boyd JD, Delaney KR, Murphy TH (2007) Extensive turnover of dendritic spines and vascular remodeling in cortical tissues recovering from stroke. J Neurosci 27:4101–4109.

Brunoni AR, Nitsche MA, Bolognini N, Bikson M, Wagner T, Merabet L, Edwards DJ, Valero-Cabre A, Rotenberg A, Pascual-Leone A (2012) Clinical research with transcranial direct current stimulation (tDCS): challenges and future directions. Brain Stimul 5:175–195.

Buchkremer-Ratzmann I, Witte OW (1997) Extended brain disinhibition following small photothrombotic lesions in rat frontal cortex. Neuroreport 8:519–522.

Bütefisch CM, Netz J, Weßling M, Seitz RJ, Hömberg V (2003) Remote changes in cortical excitability after stroke. Brain 126:470–481.

Callaway EM (2005) A molecular and genetic arsenal for systems neuroscience. Trends Neurosci 28:196–201.

Capdeville C, Pruneau D, Allix M, Plotkine M, Boulu RG (1985) Model of global forebrain ischemia in the unanesthetized rat. J Pharmacol 17:553–560.

Carandini M, Shimaoka D, Rossi F, Sato TK, Benucci A, Knöpfel T (2015) Imaging the Awake Visual Cortex with a Genetically Encoded Voltage Indicator. J Neurosci 35:53–63.

Cardin J a, Carlén M, Meletis K, Knoblich U, Zhang F, Deisseroth K, Tsai L-H, Moore CI (2009) Driving fast-spiking cells induces gamma rhythm and controls sensory responses. Nature 459:663–667.

Cardin J a, Carlén M, Meletis K, Knoblich U, Zhang F, Deisseroth K, Tsai L-H, Moore CI (2010) Targeted optogenetic stimulation and recording of neurons in vivo using cell-type-specific expression of Channelrhodopsin-2. Nat Protoc 5:247–254.

Carmichael ST (2012) Brain excitability in stroke: the yin and yang of stroke progression. Arch Neurol 69:161–167.

Carrera E, Tononi G (2014) Diaschisis: past, present, future. Brain.

Carvell GE, Simons DJ (1987) Thalamic and corticocortical connections of the second somatic sensory area of the mouse. J Comp Neurol 265:409–427.

Catterall W a (1984) The molecular basis of neuronal excitability. Science 223:653–661.

Celio MR (1990) Calbindin D-28k and parvalbumin in the rat nervous system. Neuroscience 35:375–475.

Cetin A, Komai S, Eliava M, Seeburg PH, Osten P (2006) Stereotaxic gene delivery in the rodent brain. Nat Protoc 1:3166–3173.

Chan AW, Mohajerani MH, Ledue JM, Wang YT, Murphy TH (2015) Mesoscale infraslow spontaneous membrane potential fluctuations recapitulate high-frequency activity cortical motifs. Nat Commun 6:1–12.

Chavez JC, LaManna JC (2002) Activation of hypoxia-inducible factor-1 in the rat cerebral cortex after transient global ischemia: potential role of insulin-like growth factor-1. J Neurosci 22:8922–8931.

Chen JL, Carta S, Soldado-Magraner J, Schneider BL, Helmchen F (2013a) Behaviour-dependent recruitment of long-range projection neurons in somatosensory cortex. Nature 499:336–340.

Chen Q, Cichon J, Wang W, Qiu L, Lee S-JR, Campbell NR, Destefino N, Goard MJ, Fu Z, Yasuda R, Looger LL, Arenkiel BR, Gan W-B, Feng G (2012a) Imaging neural activity using Thy1-GCaMP transgenic mice. Neuron 76:297–308.

Chen S, Mohajerani MH, Xie Y, Murphy TH (2012b) Optogenetic analysis of neuronal excitability during global ischemia reveals selective deficits in sensory processing following reperfusion in mouse cortex. J Neurosci 32:13510–13519.

Chen T-W, Wardill TJ, Sun Y, Pulver SR, Renninger SL, Baohan A, Schreiter ER, Kerr R a, Orger MB, Jayaraman V, Looger LL, Svoboda K, Kim DS (2013b) Ultrasensitive fluorescent proteins for imaging neuronal activity. Nature 499:295–300.

Cheng H, Duong TQ (2007) Simplified laser-speckle-imaging analysis method and its application to retinal blood flow imaging. Opt Lett 32:2188–2190.

Cheng MY, Wang EH, Woodson WJ, Wang S, Sun G, Lee a. G, Arac a., Fenno LE, Deisseroth K, Steinberg GK (2014) Optogenetic neuronal stimulation promotes functional recovery after stroke. Proc Natl Acad Sci 111.

Choi DW, Rothman SM (1990) The role of glutamate neurotoxicity in hypoxic-ischemic neuronal death. Annu Rev Neurosci 13:171–182.

Chow BY, Han X, Dobry AS, Qian X, Chuong AS, Li M, Henninger MA, Belfort GM, Lin Y,

Monahan PE, Boyden ES (2010) High-performance genetically targetable optical neural silencing by light-driven proton pumps. Nature 463:98–102.

Clarkson AN, Huang BS, Macisaac SE, Mody I, Carmichael ST (2010) Reducing excessive GABA-mediated tonic inhibition promotes functional recovery after stroke. Nature 468:305–309.

Clarkson AN, Overman JJ, Zhong S, Mueller R, Lynch G, Carmichael ST (2011) AMPA receptor-induced local brain-derived neurotrophic factor signaling mediates motor recovery after stroke. J Neurosci 31:3766–3775.

Colleoni S, Jensen AA, Landucci E, Fumagalli E, Conti P, Pinto A, De Amici M, Pellegrini-Giampietro DE, De Micheli C, Mennini T (2008) Neuroprotective effects of the novel glutamate transporter inhibitor (–)-3-hydroxy-4, 5, 6, 6a-tetrahydro-3aH-pyrrolo [3, 4-d]-isoxazole-4-carboxylic acid, which preferentially inhibits reverse transport (glutamate release) compared with glutamate reuptak. J Pharmacol Exp Ther 326:646–656.

Combs DJ, D'Alecy LG (1987) Motor performance in rats exposed to severe forebrain ischemia: effect of fasting and 1,3-butanediol. Stroke 18:503–511.

Constantinople CM, Bruno RM (2011) Effects and mechanisms of wakefulness on local cortical networks. Neuron 69:1061–1068.

Crain BJ, Westerkam WD, Harrison AH, Nadler J V (1988) Selective neuronal death after transient forebrain ischemia in the Mongolian gerbil: a silver impregnation study. Neuroscience 27:387–402.

Crick FH (1979) Thinking about the brain. Sci Am 241:219–232.

Crone NE, Crone NE, Miglioretti DL, Miglioretti DL, Gordon B, Gordon B, Sieracki JM, Sieracki JM, Wilson MT, Wilson MT, Uematsu S, Uematsu S, Lesser RP, Lesser RP (1998a) Functional mapping of human sensorimotor cortex with electrocorticographic spectral analysis. I. Alpha and beta event-related desynchronization. Brain 121 (Pt 1:2271–2299.

Crone NE, Miglioretti DL, Gordon B, Lesser RP (1998b) Functional mapping of human sensorimotor cortex with electrocorticographic spectral analysis. II. Event-related synchronization in the gamma band. Brain 121 (Pt 1:2301–2315.

Cui G, Jun SB, Jin X, Luo G, Pham MD, Lovinger DM, Vogel SS, Costa RM (2014) Deep brain optical measurements of cell type-specific neural activity in behaving mice. Nat Protoc 9:1213–1228.

Dai S, Bancej C, Bienek A, Walsh P, Stewart P, Wielgosz A (2009) Report summary Tracking heart disease and stroke in Canada 2009. Chronic Dis Inj Can 29.

Davidson BL, Stein CS, Heth JA, Martins I, Kotin RM, Derksen TA, Zabner J, Ghodsi A, Chiorini JA (2000) Recombinant adeno-associated virus type 2, 4, and 5 vectors: transduction of variant cell types and regions in the mammalian central nervous system. Proc Natl Acad Sci U S A 97:3428–3432.

DeFelipe J, López-Cruz PL, Benavides-Piccione R, Bielza C, Larrañaga P, Anderson S, Burkhalter A, Cauli B, Fairén A, Feldmeyer D (2013) New insights into the classification and nomenclature of cortical GABAergic interneurons. Nat Rev Neurosci 14:202–216.

Deng P, Xu ZC (2009) Brain Ischemia and Neuronal Excitability. :43–52.

Desai M, Kahn I, Knoblich U, Bernstein J, Atallah H, Yang A, Kopell N, Buckner RL, Graybiel AM, Moore CI, Boyden ES (2011) Mapping brain networks in awake mice using combined optical neural control and fMRI. J Neurophysiol 105:1393–1405.

Díez-García J, Akemann W, Knöpfel T (2007) In vivo calcium imaging from genetically specified target cells in mouse cerebellum. Neuroimage 34:859–869.

Ding JJ, Luo AF, Hu LY, Wang DC, Shao F (2014) Structural basis of the ultrasensitive calcium indicator GCaMP6. Sci China Life Sci 57:269–274.

Ding M-C, Wang Q, Lo EH, Stanley GB (2011) Cortical excitation and inhibition following focal traumatic brain injury. J Neurosci 31:14085–14094.

Dirnagl U, Iadecola C, Moskowitz MA (1999) Pathobiology of ischaemic stroke: An integrated view. Trends Neurosci 22:391–397.

Donnan GA, Fisher M, Macleod M, Davis SM (2008) Stroke.

Douglas HA, Callaway JK, Sword J, Kirov SA, Andrew RD (2011) Potent inhibition of anoxic depolarization by the sodium channel blocker dibucaine. J Neurophysiol 105:1482–1494.

Doyle KP, Simon RP, Stenzel-Poore MP (2008) Mechanisms of ischemic brain damage. Neuropharmacology 55:310–318.

Dreier JP (2011) The role of spreading depression, spreading depolarization and spreading ischemia in neurological disease. Nat Med 17:439–447.

Dreier JP, Woitzik J, Fabricius M, Bhatia R, Major S, Drenckhahn C, Lehmann TN, Sarrafzadeh A, Willumsen L, Hartings JA, Sakowitz OW, Seemann JH, Thieme A, Lauritzen M, Strong AJ (2006) Delayed ischaemic neurological deficits after subarachnoid haemorrhage are associated with clusters of spreading depolarizations. Brain 129:3224–3237.

Drew PJ, Shih AY, Driscoll JD, Knutsen PM, Blinder P, Davalos D, Akassoglou K, Tsai PS, Kleinfeld D (2010) Chronic optical access through a polished and reinforced thinned skull. Nat Methods 7:981–984.

Drongelen W van (2007) Signal Processing for Neuroscientists. Burlington, MA: Elsevier.

Duncan PW (2013) Outcome measures in stroke rehabilitation. Handb Clin Neurol 110:105–111.

Dunn AK, Bolay H, Moskowitz MA, Boas DA (2001) Dynamic imaging of cerebral blood flow using laser speckle. J Cereb Blood Flow Metab 21:195–201.

Engel SA, Rumelhart DE, Wandell BA, Lee AT, Glover GH, Chichilnisky EJ, Shadlen MN (1994) fMRI of human visual cortex. Nature 369:525.

Feldbauer K, Zimmermann D, Pintschovius V, Spitz J, Bamann C, Bamberg E (2009) Channelrhodopsin-2 is a leaky proton pump. Proc Natl Acad Sci U S A 106:12317–12322.

Feng G, Mellor RH, Bernstein M, Keller-Peck C, Nguyen QT, Wallace M, Nerbonne JM, Lichtman JW, Sanes JR (2000) Imaging neuronal subsets in transgenic mice expressing multiple spectral variants of GFP. Neuron 28:41–51.

Fenno L, Yizhar O, Deisseroth K (2011) The development and application of optogenetics. Annu Rev Neurosci 34:389–412.

Ferezou I, Haiss F, Gentet LJ, Aronoff R, Weber B, Petersen CCH (2007) Spatiotemporal Dynamics of Cortical Sensorimotor Integration in Behaving Mice. Neuron 56:907–923.

Fox MD, Greicius M (2010) Clinical applications of resting state functional connectivity. Front Syst Neurosci 4:19.

Fox MD, Zhang D, Snyder AZ, Raichle ME (2009) The global signal and observed anticorrelated resting state brain networks. J Neurophysiol 101:3270–3283.

Fox PT, Burton H, Raichle ME (1987) Mapping human somatosensory cortex with positron emission tomography. J Neurosurg 67:34–43.

Freund TF, Buzsáki G, Leon A, Baimbridge KG, Somogyi P (1990) Relationship of neuronal vulnerability and calcium binding protein immunoreactivity in ischemia. Exp Brain Res 83:55–66.

Fujii M, Hara H, Meng W, Vonsattel JP, Huang Z, Moskowitz MA (1997) Strain-related differences in susceptibility to transient forebrain ischemia in SV-129 and C57black/6 mice. Stroke 28:1805–1810; discussion 1811.

Fujioka H, Kaneko H, Suzuki SS, Mabuchi K (2004) Hyperexcitability-associated rapid plasticity after a focal cerebral ischemia. Stroke 35:e346–e348.

Fujioka M, Nishio K, Miyamoto S, Hiramatsu KI, Sakaki T, Okuchi K, Taoka T, Fujioka S (2000) Hippocampal damage in the human brain after cardiac arrest. Cerebrovasc Dis 10:2–7.

Funayama K, Minamisawa G, Matsumoto N, Ban H, Chan AW, Matsuki N, Murphy TH, Ikegaya Y (2015) Neocortical Rebound Depolarization Enhances Visual Perception. PLOS Biol 13:e1002231.

Gao TM, Pulsinelli W a, Xu ZC (1998) Prolonged enhancement and depression of synaptic transmission in CA1 pyramidal neurons induced by transient forebrain ischemia in vivo. Neuroscience 87:371–383.

Geocadin RG, Koenig MA, Jia X, Stevens RD, Peberdy MA (2008) Management of Brain Injury After Resuscitation From Cardiac Arrest. Neurol Clin 26:487–506.

Gerlai R, Thibodeaux H, Palmer JT, Van Lookeren Campagne M, Van Bruggen N (2000) Transient focal cerebral ischemia induces sensorimotor deficits in mice. Behav Brain Res 108:63–71.

Gharbawie OA, Gonzalez CLR, Williams PT, Kleim JA, Whishaw IQ (2005) Middle cerebral artery (MCA) stroke produces dysfunction in adjacent motor cortex as detected by intracortical microstimulation in rats. Neuroscience 130:601–610.

Ginsberg MD, Busto R (1989) Rodent models of cerebral ischemia. Stroke 20:1627–1642.

Gionet TX, Thomas JD, Warner DS, Goodlett CR, Wasserman EA, West JR (1991) Forebrain ischemia induces selective behavioral impairments associated with hippocampal injury in rats. Stroke 22:1040–1047.

Godefroy O (2013) The behavioral and cognitive neurology of stroke. Cambridge University Press.

Gong S, Zheng C, Doughty ML, Losos K, Didkovsky N, Schambra UB, Nowak NJ, Joyner A, Leblanc G, Hatten ME, Heintz N (2003) A gene expression atlas of the central nervous system based on bacterial artificial chromosomes. Nature 425:917–925.

Gordon JW, Chesa PG, Nishimura H, Rettig WJ, Maccari JE, Endo T, Seravalli E, Seki T, Silver J (1987) Regulation of Thy-1 gene expression in transgenic mice. Cell 50:445–452.

Gorski JA, Talley T, Qiu M, Puelles L, Rubenstein JLR, Jones KR (2002) Cortical excitatory neurons and glia, but not GABAergic neurons, are produced in the Emx1-expressing lineage. J Neurosci 22:6309–6314.

Gradinaru V, Thompson KR, Zhang F, Mogri M, Kay K, Schneider MB, Deisseroth K (2007) Targeting and readout strategies for fast optical neural control in vitro and in vivo. J Neurosci 27:14231–14238.

Gradinaru V, Zhang F, Ramakrishnan C, Mattis J, Prakash R, Diester I, Goshen I, Thompson KR, Deisseroth K (2010) Molecular and cellular approaches for diversifying and extending optogenetics. Cell 141:154–165.

Greer D, Scripko P, Bartscher J, Sims J, Camargo E, Singhal A, Furie K (2011) Serial MRI changes in comatose cardiac arrest patients. Neurocrit Care 14:61–67.

Grinvald A, Hildesheim R (2004) VSDI: a new era in functional imaging of cortical dynamics. Nat Rev Neurosci 5:874–885.

Grinvald A, Lieke E, Frostig RD, Gilbert CD, Wiesel TN (1986) Functional architecture of cortex revealed by optical imaging of intrinsic signals.

Grosenick L, Marshel JH, Deisseroth K (2015) Closed-Loop and Activity-Guided Optogenetic Control. Neuron 86:106–139.

Grubb MS, Burrone J (2010) Activity-dependent relocation of the axon initial segment fine-tunes neuronal excitability. Nature 465:1070–1074.

Grubb NR, O'Carroll R, Cobbe SM, Sirel J, Fox KA (1996) Chronic memory impairment after cardiac arrest outside hospital. BMJ 313:143–146.

Grynkiewicz G, Poenie M, Tsien RY (1985) A new generation of Ca2+ indicators with greatly

improved fluorescence properties. J Biol Chem 260:3440–3450.

Gunaydin L a, Grosenick L, Finkelstein JC, Kauvar I V, Fenno LE, Adhikari A, Lammel S, Mirzabekov JJ, Airan RD, Zalocusky K a, Tye KM, Anikeeva P, Malenka RC, Deisseroth K (2014) Natural neural projection dynamics underlying social behavior. Cell 157:1535–1551.

Guo Z V, Hart AC, Ramanathan S (2009) Optical interrogation of neural circuits in Caenorhabditis elegans. Nat Methods 6:891–896.

Guo Z V, Li N, Huber D, Ophir E, Gutnisky D, Ting JT, Feng G, Svoboda K (2014a) Flow of cortical activity underlying a tactile decision in mice. Neuron 81:179–194.

Guo Z V., Hires SA, Li N, O'Connor DH, Komiyama T, Ophir E, Huber D, Bonardi C, Morandell K, Gutnisky D, Peron S, Xu N, Cox J, Svoboda K (2014b) Procedures for Behavioral Experiments in Head-Fixed Mice Simon SA, ed. PLoS One 9:e88678.

Hacke W, Kaste M, Fieschi C, Toni D, Lesaffre E, von Kummer R, Boysen G, Bluhmki E, Höxter G, Mahagne MH (1995) Intravenous thrombolysis with recombinant tissue plasminogen activator for acute hemispheric stroke. The European Cooperative Acute Stroke Study (ECASS).

Haider B, Häusser M, Carandini M (2013) Inhibition dominates sensory responses in the awake cortex. Nature 493:97–100.

Hallett M (2000) Transcranial magnetic stimulation and the human brain. Nature 406:147–150.

Han X, Boyden ES (2007) Multiple-color optical activation, silencing, and desynchronization of neural activity, with single-spike temporal resolution. PLoS One 2:e299.

Han X, Qian X, Bernstein JG, Zhou H-H, Franzesi GT, Stern P, Bronson RT, Graybiel AM, Desimone R, Boyden ES (2009) Millisecond-timescale optical control of neural dynamics in the nonhuman primate brain. Neuron 62:191–198.

Hansen AJ, Nedergaard M (1988) Brain ion homeostasis in cerebral ischemia. Neurochem Pathol 9:195–209.

Harris KD, Mrsic-Flogel TD (2013) Cortical connectivity and sensory coding. Nature 503:51–58.

Harrison TC, Ayling OGS, Murphy TH (2012) Distinct cortical circuit mechanisms for complex forelimb movement and motor map topography. Neuron 74:397–409.

Harrison TC, Silasi G, Boyd JD, Murphy TH (2013) Displacement of sensory maps and disorganization of motor cortex after targeted stroke in mice. Stroke 44:2300–2306.

Hattox AM, Nelson SB (2007) Layer V neurons in mouse cortex projecting to different targets have distinct physiological properties. J Neurophysiol 98:3330–3340.

Haubensak W, Kunwar PS, Cai H, Ciocchi S, Wall NR, Ponnusamy R, Biag J, Dong H-W, Deisseroth K, Callaway EM, Fanselow MS, Lüthi A, Anderson DJ (2010) Genetic dissection of an amygdala microcircuit that gates conditioned fear. Nature 468:270–276.

Haustein MD, Kracun S, Lu XH, Shih T, Jackson-Weaver O, Tong X, Xu J, Yang XW, O'Dell TJ, Marvin JS, Ellisman MH, Bushong E a., Looger LL, Khakh BS (2014) Conditions and constraints for astrocyte calcium signaling in the hippocampal mossy fiber pathway. Neuron 82:413–429.

Heffner CS, Pratt CH, Babiuk RP, Sharma Y, Rockwood SF, Donahue LR, Eppig JT, Murray S a, Herbert Pratt C (2012) Supporting conditional mouse mutagenesis with a comprehensive cre characterization resource. Nat Commun 3:1218.

Hillman EMC (2015) Optical brain imaging in vivo: techniques and applications from animal to man. J Biomed Opt 12:051402.

Hippenmeyer S, Vrieseling E, Sigrist M, Portmann T, Laengle C, Ladle DR, Arber S (2005) A developmental switch in the response of DRG neurons to ETS transcription factor signaling. PLoS Biol 3:0878–0890.

Hira R, Honkura N, Noguchi J, Maruyama Y, Augustine GJ, Kasai H, Matsuzaki M (2009) Transcranial optogenetic stimulation for functional mapping of the motor cortex. J Neurosci Methods 179:258–263.

Hires SA, Zhu Y, Tsien RY (2008) Optical measurement of synaptic glutamate spillover and reuptake by linker optimized glutamate-sensitive fluorescent reporters. Proc Natl Acad Sci U S A 105:4411–4416.

Hofmeijer J, van Putten MJ a M (2012) Ischemic cerebral damage: an appraisal of synaptic failure. Stroke 43:607–615.

Holtmaat A, Bonhoeffer T, Chow DK, Chuckowree J, De Paola V, Hofer SB, Hübener M, Keck T, Knott G, Lee W-CA, Mostany R, Mrsic-Flogel TD, Nedivi E, Portera-Cailliau C, Svoboda K, Trachtenberg JT, Wilbrecht L (2009) Long-term, high-resolution imaging in the mouse neocortex through a chronic cranial window. Nat Protoc 4:1128–1144.

Holzer M, Bernard SA, Hachimi-Idrissi S, Roine RO, Sterz F, Mullner M, Collaborative Group on Induced Hypothermia for Neuroprotection After Cardiac A (2005) Hypothermia for neuroprotection after cardiac arrest: systematic review and individual patient data meta-analysis. Crit Care Med 33:414–418.

Hooks BM, Hires SA, Zhang YX, Huber D, Petreanu L, Svoboda K, Shepherd GMG (2011) Laminar analysis of excitatory local circuits in vibrissal motor and sensory cortical areas. PLoS Biol 9.

Horikawa K, Yamada Y, Matsuda T, Kobayashi K, Hashimoto M, Matsu-ura T, Miyawaki A, Michikawa T, Mikoshiba K, Nagai T (2010) Spontaneous network activity visualized by ultrasensitive Ca(2+) indicators, yellow Cameleon-Nano. Nat Methods 7:729–732.

Hossmann KA (1971) Cortical steady potential, impedance and excitability changes during and after total ischemia of cat brain. Exp Neurol 32:163–175.

Hossmann KA (2006) Pathophysiology and therapy of experimental stroke. Cell Mol Neurobiol 26:1057–1083.

Hossmann KA, Sato K (1970) Recovery of neuronal function after prolonged cerebral ischemia. Science 168:375–376.

Hossmann KA, Schmidt-Kastner R, Grosse Ophoff B (1987) Recovery of integrative central nervous function after one hour global cerebro-circulatory arrest in normothermic cat. J Neurol Sci 77:305–320.

Howells DW, Sena ES, O'Collins V, Macleod MR (2012) Improving the efficiency of the development of drugs for stroke. Int J Stroke 7:371–377.

Huang ZJ, Zeng H (2013) Genetic approaches to neural circuits in the mouse. Annu Rev Neurosci 36:183–215.

Huber D, Gutnisky D a, Peron S, O'Connor DH, Wiegert JS, Tian L, Oertner TG, Looger LL, Svoboda K (2012) Multiple dynamic representations in the motor cortex during sensorimotor learning. Nature 484:473–478.

Hughes PM, Allegrini PR, Rudin M, Perry VH, Mir AK, Wiessner C (2002) Monocyte chemoattractant protein-1 deficiency is protective in a murine stroke model. J Cereb Blood Flow Metab 22:308–317.

Hummel FC, Cohen LG (2006) Non-invasive brain stimulation: a new strategy to improve neurorehabilitation after stroke? Lancet Neurol 5:708–712.

Hunnicutt BJ, Long BR, Kusefoglu D, Gertz KJ, Zhong H, Mao T (2014) A comprehensive thalamocortical projection map at the mesoscopic level. Nat Neurosci 17:1276–1285.

Husson TR, Mallik AK, Zhang JX, Issa NP (2007) Functional imaging of primary visual cortex using flavoprotein autofluorescence. J Neurosci 27:8665–8675.

Iadecola C, Forster C, Nogawa S, Clark HB, Ross ME (1999) Cyclooxygenase-2 immunoreactivity in the human brain following cerebral ischemia. Acta Neuropathol 98:9–14.

Iadecola C, Zhang F, Casey R, Nagayama M, Ross ME (1997) Delayed reduction of ischemic brain injury and neurological deficits in mice lacking the inducible nitric oxide synthase gene. J Neurosci 17:9157–9164.

Ilie A, Ciocan D, Zagrean A-M, Nita DA, Zagrean L, Moldovan M (2006) Endogenous activation of adenosine A(1) receptors accelerates ischemic suppression of spontaneous electrocortical activity. J Neurophysiol 96:2809–2814.

Ilmoniemi RJ, Ruohonen J, Karhu J (1998) Transcranial magnetic stimulation--a new tool for functional imaging of the brain. Crit Rev Biomed Eng 27:241–284.

Issa JB, Haeffele BD, Agarwal A, Bergles DE, Young ED, Yue DT (2014) Multiscale Optical Ca2+ Imaging of Tonal Organization in Mouse Auditory Cortex. Neuron.

Jarvis CR, Anderson TR, Andrew RD (2001) Anoxic depolarization mediates acute damage independent of glutamate in neocortical brain slices. Cereb Cortex 11:249–259.

Jin L, Han Z, Platisa J, Wooltorton JRA, Cohen LB, Pieribone VA (2012) Single Action Potentials and Subthreshold Electrical Events Imaged in Neurons with a Fluorescent Protein Voltage Probe. Neuron 75:779–785.

Johansen FF, Tonder N, Zimmer J, Baimbridge KG, Diemer NH (1990) Short-term changes of parvalbumin and calbindin immunoreactivity in the rat hippocampus following cerebral ischemia. Neurosci Lett 120:171–174.

Johansen JP, Hamanaka H, Monfils MH, Behnia R, Deisseroth K, Blair HT, LeDoux JE (2010) Optical activation of lateral amygdala pyramidal cells instructs associative fear learning. Proc Natl Acad Sci U S A 107:12692–12697.

Johansson BB (2000) Brain plasticity and stroke rehabilitation. The Willis lecture. Stroke 31:223–230.

Kahn I, Desai M, Knoblich U, Bernstein J, Henninger M, Graybiel AM, Boyden ES, Buckner RL, Moore CI (2011) Characterization of the functional MRI response temporal linearity via optical control of neocortical pyramidal neurons. J Neurosci 31:15086–15091.

Kato HE, Zhang F, Yizhar O, Ramakrishnan C, Nishizawa T, Hirata K, Ito J, Aita Y, Tsukazaki T, Hayashi S (2012) Crystal structure of the channelrhodopsin light-gated cation channel. Nature 482:369–374.

Katsura K, Rodriguez de Turco EB, Folbergrová J, Bazan NG, Siesjö BK (1993) Coupling among energy failure, loss of ion homeostasis, and phospholipase A2 and C activation during ischemia. J Neurochem 61:1677–1684.

Kawai K, Nitecka L, Ruetzler CA, Nagashima G, Joó F, Mies G, Nowak TS, Saito N, Lohr JM, Klatzo I (1992) Global cerebral ischemia associated with cardiac arrest in the rat: I. Dynamics of early neuronal changes. J Cereb Blood Flow Metab 12:238–249.

Kellerman PS, Bogusky RT (1992) Microfilament disruption occurs very early in ischemic proximal tubule cell injury. Kidney Int 42:896–902.

Kirino T (1982) Delayed neuronal death in the gerbil hippocampus following ischemia. Brain Res 239:57–69.

Klapoetke NC et al. (2014) Independent optical excitation of distinct neural populations. Nat Methods 11:338–346.

Knöpfel T, Díez-García J, Akemann W (2006) Optical probing of neuronal circuit dynamics: Genetically encoded versus classical fluorescent sensors. Trends Neurosci 29:160–166.

Kobayashi Y, Hensch TK (2013) Germline recombination by conditional gene targeting with Parvalbumin-Cre lines. Front Neural Circuits 7.

Koh JY, Suh SW, Gwag BJ, He YY, Hsu CY, Choi DW (1996) The role of zinc in selective neuronal death after transient global cerebral ischemia. Science (80-) 272:1013–1016.

Konrad PE, Tacker WA, Levy WJ, Reedy DP, Cook JR, Geddes LA (1987) Motor evoked potentials in the dog: effects of global ischemia on spinal cord and peripheral nerve signals.

Neurosurgery 20:117–124.

Krakauer JW, Carmichael ST, Corbett D, Wittenberg GF (2012) Getting neurorehabilitation right: what can be learned from animal models? Neurorehabil Neural Repair 26:923–931.

Kralj JM, Douglass AD, Hochbaum DR, Maclaurin D, Cohen AE (2012) Optical recording of action potentials in mammalian neurons using a microbial rhodopsin. Nat Methods 9:90–95.

Kralj JM, Hochbaum DR, Douglass AD, Cohen AE (2011) Electrical spiking in Escherichia coli probed with a fluorescent voltage-indicating protein. Science 333:345–348.

Kravitz A V, Freeze BS, Parker PRL, Kay K, Thwin MT, Deisseroth K, Kreitzer AC (2010) Regulation of parkinsonian motor behaviours by optogenetic control of basal ganglia circuitry. Nature 466:622–626.

Kristián T, Siesjö BK (1998) Calcium in ischemic cell death. Stroke 29:705–718.

Krook-Magnuson E, Armstrong C, Oijala M, Soltesz I (2013) On-demand optogenetic control of spontaneous seizures in temporal lobe epilepsy. Nat Commun 4:1376.

Kuroiwa T, Bonnekoh P, Hossmann KA (1992) Laser doppler flowmetry in CA1 sector of hippocampus and cortex after transient forebrain ischemia in gerbils. Stroke 23:1349–1354.

Lagali PS, Balya D, Awatramani GB, Münch TA, Kim DS, Busskamp V, Cepko CL, Roska B (2008) Light-activated channels targeted to ON bipolar cells restore visual function in retinal degeneration. Nat Neurosci 11:667–675.

Lai TW, Zhang S, Wang YT (2014) Excitotoxicity and stroke: identifying novel targets for neuroprotection. Prog Neurobiol 115:157–188.

Lansberg MG, Bluhmki E, Thijs VN (2009) Efficacy and safety of tissue plasminogen activator 3 to 4.5 hours after acute ischemic stroke: a metaanalysis. Stroke 40:2438–2441.

Lay CC, Davis MF, Chen-Bee CH, Frostig RD (2011) Mild Sensory Stimulation Reestablishes Cortical Function during the Acute Phase of Ischemia. J Neurosci 31:11495–11504.

LeChasseur Y, Dufour S, Lavertu G, Bories C, Deschenes M, Vallee R, De Koninck Y (2011) A microprobe for parallel optical and electrical recordings from single neurons in vivo. Nat Methods 8:319–U63.

Lee JH, Durand R, Gradinaru V, Zhang F, Goshen I, Kim D-S, Fenno LE, Ramakrishnan C, Deisseroth K (2010) Global and local fMRI signals driven by neurons defined optogenetically by type and wiring. Nature 465:788–792.

Lee JM, Zipfel GJ, Choi DW (1999) The changing landscape of ischaemic brain injury mechanisms. Nature 399:A7–A14.

Lee S-H, Kwan AC, Zhang S, Phoumthipphavong V, Flannery JG, Masmanidis SC, Taniguchi H, Huang ZJ, Zhang F, Boyden ES, Deisseroth K, Dan Y (2012) Activation of specific interneurons improves V1 feature selectivity and visual perception. Nature 488:379–383.

Lemasters JJ, DiGuiseppi J, Nieminen A-L, Herman B (1987) Blebbing, free Ca2+ and

mitochondrial membrane potential preceding cell death in hepatocytes.

Leo AAP (1944) Spreading depression of activity in the cerebral cortex. J Neurophysiol 7:359–390.

Lesnick JE, Coyer PE, Michele JJ, Welsh FA, Simeone FA (1986) Comparison of the somatosensory evoked potential and the direct cortical response following severe incomplete global ischemia: selective vulnerability of the white matter conduction pathways. Stroke 17:1247–1250.

Lesnick JE, Michele JJ, Simeone FA, DeFeo S, Welsh FA (1984) Alteration of somatosensory evoked potentials in response to global ischemia. J Neurosurg 60:490–494.

Levine SR, Welch KM, Helpern JA, Chopp M, Bruce R, Selwa J, Smith MB (1988) Prolonged deterioration of ischemic brain energy metabolism and acidosis associated with hyperglycemia: human cerebral infarction studied by serial 31P NMR spectroscopy.

Lewis TL, Mao T, Svoboda K, Arnold DB (2009) Myosin-dependent targeting of transmembrane proteins to neuronal dendrites. Nat Neurosci 12:568–576.

Li B, Zhou F, Luo Q, Li P (2012) Altered resting-state functional connectivity after cortical spreading depression in mice. Neuroimage 63:1171–1177.

Li H, Siegel RE, Schwartz RD (1993) Rapid decline of GABA(A) receptor subunit mRNA expression in hippocampus following transient cerebral ischemia in the gerbil. Hippocampus 3:527–537.

Li N, Chen T, Guo Z V, Gerfen CR, Svoboda K (2015) A motor cortex circuit for motor planning and movement. Nature 519:51–56.

Li P, Murphy TH (2008) Two-photon imaging during prolonged middle cerebral artery occlusion in mice reveals recovery of dendritic structure after reperfusion. J Neurosci 28:11970–11979.

Li Y, Lei Z, Xu ZC (2009) Enhancement of inhibitory synaptic transmission in large aspiny neurons after transient cerebral ischemia. Neuroscience 159:670–681.

Liang R, Pang Z-P, Deng P, Xu ZC (2009) Transient enhancement of inhibitory synaptic transmission in hippocampal CA1 pyramidal neurons after cerebral ischemia. Neuroscience 160:412–418.

Lim C, Alexander MP, LaFleche G, Schnyer DM, Verfaellie M (2004) The neurological and cognitive sequelae of cardiac arrest. Neurology 63:1774–1778.

Lim DH, Ledue J, Mohajerani MH, Vanni MP, Murphy TH (2013) Optogenetic approaches for functional mouse brain mapping. Front Neurosci 7:54.

Lim DH, LeDue JM, Mohajerani MH, Murphy TH (2014) Optogenetic Mapping after Stroke Reveals Network-Wide Scaling of Functional Connections and Heterogeneous Recovery of the Peri-Infarct. J Neurosci 34:16455–16466.

Lim DH, Mohajerani MH, Ledue J, Boyd J, Chen S, Murphy TH (2012) In vivo Large-Scale Cortical Mapping Using Channelrhodopsin-2 Stimulation in Transgenic Mice Reveals Asymmetric and Reciprocal Relationships between Cortical Areas. Front Neural Circuits 6:11.

Lin JY (2011) A user's guide to channelrhodopsin variants: features, limitations and future developments. Exp Physiol 96:19–25.

Lin JY, Knutsen PM, Muller A, Kleinfeld D, Tsien RY (2013) ReaChR: a red-shifted variant of channelrhodopsin enables deep transcranial optogenetic excitation. Nat Neurosci 16:1499–1508.

Lin JY, Lin MZ, Steinbach P, Tsien RY (2009) Characterization of engineered channelrhodopsin variants with improved properties and kinetics. Biophys J 96:1803–1814.

Liu B, Liao M, Mielke JG, Ning K, Chen Y, Li L, El-Hayek YH, Gomez E, Zukin RS, Fehlings MG, Wan Q (2006) Ischemic insults direct glutamate receptor subunit 2-lacking AMPA receptors to synaptic sites. J Neurosci 26:5309–5319.

Liu RR, Murphy TH (2009) Reversible cyclosporin A-sensitive mitochondrial depolarization occurs within minutes of stroke onset in mouse somatosensory cortex in vivo: a two-photon imaging study. J Biol Chem 284:36109–36117.

Liu X, Ramirez S, Pang PT, Puryear CB, Govindarajan A, Deisseroth K, Tonegawa S (2012) Optogenetic stimulation of a hippocampal engram activates fear memory recall. Nature 484:381–385.

Liu Y, Wong TP, Aarts M, Rooyakkers A, Liu L, Lai TW, Wu DC, Lu J, Tymianski M, Craig AM, Wang YT (2007) NMDA receptor subunits have differential roles in mediating excitotoxic neuronal death both in vitro and in vivo. J Neurosci 27:2846–2857.

Lo EH (2008) A new penumbra: transitioning from injury into repair after stroke. Nat Med 14:497–500.

Lo EH, Dalkara T, Moskowitz M a (2003) Mechanisms, challenges and opportunities in stroke. Nat Rev Neurosci 4:399–415.

Locatelli F, Bersano A, Ballabio E, Lanfranconi S, Papadimitriou D, Strazzer S, Bresolin N, Comi GP, Corti S (2009) Stem cell therapy in stroke. Cell Mol Life Sci 66:757–772.

Macrez R, Ali C, Toutirais O, Le Mauff B, Defer G, Dirnagl U, Vivien Denis D (2011) Stroke and the immune system: From pathophysiology to new therapeutic strategies. Lancet Neurol 10:471–480.

Madisen L et al. (2012) A toolbox of Cre-dependent optogenetic transgenic mice for light-induced activation and silencing. Nat Neurosci 15:793–802.

Madisen L et al. (2015) Transgenic Mice for Intersectional Targeting of Neural Sensors and Effectors with High Specificity and Performance. Neuron 85:942–958.

Madisen L, Zwingman TA, Sunkin SM, Oh SW, Zariwala HA, Gu H, Ng LL, Palmiter RD,

Hawrylycz MJ, Jones AR, Lein ES, Zeng H (2010) A robust and high-throughput Cre reporting and characterization system for the whole mouse brain. Nat Neurosci 13:133–140.

Madl C, Holzer M (2004) Brain function after resuscitation from cardiac arrest. Curr Opin Crit Care 10:213–217.

Man HY, Lin JW, Ju WH, Ahmadian G, Liu L, Becker LE, Sheng M, Wang YT (2000) Regulation of AMPA receptor-mediated synaptic transmission by clathrin-dependent receptor internalization. Neuron 25:649–662.

Mancuso JJ, Kim J, Lee S, Tsuda S, Chow NBH, Augustine GJ (2011) Optogenetic probing of functional brain circuitry. Exp Physiol 96:26–33.

Mank M, Santos AF, Direnberger S, Mrsic-Flogel TD, Hofer SB, Stein V, Hendel T, Reiff DF, Levelt C, Borst A, Bonhoeffer T, Hübener M, Griesbeck O (2008) A genetically encoded calcium indicator for chronic in vivo two-photon imaging. Nat Methods 5:805–811.

Markounikau V, Igel C, Grinvald A, Jancke D (2010) A dynamic neural field model of mesoscopic cortical activity captured with voltage-sensitive dye imaging. PLoS Comput Biol 6.

Markram H, Toledo-Rodriguez M, Wang Y, Gupta A, Silberberg G, Wu C (2004) Interneurons of the neocortical inhibitory system. Nat Rev Neurosci 5:793–807.

Marvin JS, Borghuis BG, Tian L, Cichon J, Harnett MT, Akerboom J, Gordus A, Renninger SL, Chen T, Bargmann CI, Orger MB, Schreiter ER, Demb JB, Gan W, Hires SA, Looger LL (2013) An optimized fluorescent probe for visualizing glutamate neurotransmission. Nat Methods 10:162–170.

Matyas F, Sreenivasan V, Marbach F, Wacongne C, Barsy B, Mateo C, Aronoff R, Petersen CCH (2010) Motor control by sensory cortex. Science 330:1240–1243.

Mayford M, Bach ME, Huang YY, Wang L, Hawkins RD, Kandel ER (1996) Control of memory formation through regulated expression of a CaMKII transgene. Science 274:1678–1683.

McKhann GM, Borowicz LM, Goldsborough MA, Enger C, Selnes OA (1997) Depression and cognitive decline after coronary artery bypass grafting. Lancet 349:1282–1284.

Mercier L, Audet T, Hébert R, Rochette a, Dubois MF (2001) Impact of motor, cognitive, and perceptual disorders on ability to perform activities of daily living after stroke. Stroke 32:2602–2608.

Miesenböck G (2009) The optogenetic catechism. Science 326:395–399.

Miesenböck G (2011) Optogenetic Control of Cells and Circuits. Annu Rev Cell Dev Biol 27:731–758.

Minderer M, Liu W, Sumanovski LT, Kügler S, Helmchen F, Margolis DJ (2012) Chronic imaging of cortical sensory map dynamics using a genetically encoded calcium indicator. J Physiol 590:99–107.

Mohajerani MH, Aminoltejari K, Murphy TH (2011) Targeted mini-strokes produce changes in interhemispheric sensory signal processing that are indicative of disinhibition within minutes. Proc Natl Acad Sci U S A 108:E183–E191.

Mohajerani MH, Chan AW, Mohsenvand M, LeDue J, Liu R, McVea D a, Boyd JD, Wang YT, Reimers M, Murphy TH (2013) Spontaneous cortical activity alternates between motifs defined by regional axonal projections. Nat Neurosci 16:1426–1435.

Mohajerani MH, McVea DA, Fingas M, Murphy TH (2010) Mirrored bilateral slow-wave cortical activity within local circuits revealed by fast bihemispheric voltage-sensitive dye imaging in anesthetized and awake mice. J Neurosci 30:3745–3751.

Molitoris BA (1991) Ischemia-induced loss of epithelial polarity: potential role of the actin cytoskeleton. Am J Physiol Physiol 260:F769–F778.

Morris R (1985) Thy-1 in developing nervous tissue. Dev Neurosci 7:133–160.

Mostany R, Portera-Cailliau C (2011) Absence of large-scale dendritic plasticity of layer 5 pyramidal neurons in peri-infarct cortex. J Neurosci 31:1734–1738.

Mozaffarian D et al. (2014) Heart Disease and Stroke Statistics--2015 Update: A Report From the American Heart Association.

Murphy K, Birn RM, Handwerker D a, Jones TB, Bandettini P a (2009) The impact of global signal regression on resting state correlations: are anti-correlated networks introduced? Neuroimage 44:893–905.

Murphy TH, Corbett D (2009) Plasticity during stroke recovery: from synapse to behaviour. Nat Rev Neurosci 10:861–872.

Murphy TH, Li P, Betts K, Liu R (2008) Two-photon imaging of stroke onset in vivo reveals that NMDA-receptor independent ischemic depolarization is the major cause of rapid reversible damage to dendrites and spines. J Neurosci 28:1756–1772.

Nagel G, Ollig D, Fuhrmann M, Kateriya S, Musti AM, Bamberg E, Hegemann P (2002) Channelrhodopsin-1: a light-gated proton channel in green algae. Science 296:2395–2398.

Nagel G, Szellas T, Huhn W, Kateriya S, Adeishvili N, Berthold P, Ollig D, Hegemann P, Bamberg E (2003) Channelrhodopsin-2, a directly light-gated cation-selective membrane channel. Proc Natl Acad Sci U S A.

Nagy A (2000) Cre recombinase: The universal reagent for genome tailoring. Genesis 26:99–109.

Nedergaard M (1996) Spreading depression as a contributor to ischemic brain damage. Adv Neurol 71:75.

Nelles G, Spiekermann G, Jueptner M, Leonhardt G, Muller S, Gerhard H, Diener HC (1999) Reorganization of Sensory and Motor Systems in Hemiplegic Stroke Patients : A Positron Emission Tomography Study. Stroke 30:1510–1516.

Nelson SB, Sugino K, Hempel CM (2006) The problem of neuronal cell types: a physiological genomics approach. Trends Neurosci 29:339–345.

Nemoto EM, Snyder J V, Carroll RG, Morita H (1975) Global ischemia in dogs: cerebrovascular CO2 reactivity and autoregulation. Stroke 6:425–431.

Neumann-Haefelin T, Bosse F, Redecker C, Müller HW, Witte OW (1999) Upregulation of GABA(A)-receptor α1- and α2-subunit mRNAs following ischemic cortical lesions in rats. Brain Res 816:234–237.

Nguyen Q-T, Schroeder LF, Mank M, Muller A, Taylor P, Griesbeck O, Kleinfeld D (2010) An in vivo biosensor for neurotransmitter release and in situ receptor activity. Nat Neurosci 13:127–132.

Nitsch C, Scotti A, Sommacal A, Kalt G (1989) GABAergic hippocampal neurons resistant to ischemia-induced neuronal death contain the Ca2(+)-binding protein parvalbumin. Neurosci Lett 105:263–268.

Nolan JP, Morley PT, Vanden Hoek TL, Hickey RW, Kloek WGJ, Billi J, Böttiger BW, Okada K, Reyes C, Shuster M, Steen PA, Weil MH, Wenzel V, Carli P, Atkins D (2003) Therapeutic hypothermia after cardiac arrest. An advisory statement by the Advanced Life Support Task Force of the International Liaison Committee on Resuscitation. Resuscitation 57:231–235.

Nudo RJ (2006) Mechanisms for recovery of motor function following cortical damage. Curr Opin Neurobiol 16:638–644.

Nudo RJ, Wise BM, SiFuentes F, Milliken GW (1996) Neural substrates for the effects of rehabilitative training on motor recovery after ischemic infarct. Science 272:1791–1794.

Nunn J, Hodges H (1994) Cognitive deficits induced by global cerebral ischaemia: relationship to brain damage and reversal by transplants. Behav Brain Res 65:1–31.

O'Collins VE, Macleod MR, Donnan G a, Horky LL, van der Worp BH, Howells DW (2006) 1,026 Experimental Treatments in Acute Stroke. Ann Neurol 59:467–477.

O'Reilly SM, Grubb NR, O'Carroll RE (2003) In-hospital cardiac arrest leads to chronic memory impairment. Resuscitation 58:73–79.

Obeidat AS, Jarvis CR, Andrew RD (2000) Glutamate does not mediate acute neuronal damage after spreading depression induced by O2/glucose deprivation in the hippocampal slice. J Cereb Blood Flow Metab 20:412–422.

Oh SW et al. (2014) A mesoscale connectome of the mouse brain. Nature 508:207–214.

Okubo Y, Sekiya H, Namiki S, Sakamoto H, Iinuma S, Yamasaki M, Watanabe M, Hirose K, Iino M (2010) Imaging extrasynaptic glutamate dynamics in the brain. Proc Natl Acad Sci U S A 107:6526–6531.

Overman JJ, Clarkson AN, Wanner IB, Overman WT, Eckstein I, Maguire JL, Dinov ID, Toga AW, Carmichael ST (2012) A role for ephrin-A5 in axonal sprouting, recovery, and

activity-dependent plasticity after stroke. Proc Natl Acad Sci U S A 109:E2230–E2239.

Pala A, Petersen CCH (2014) In Vivo Measurement of Cell-Type-Specific Synaptic Connectivity and Synaptic Transmission in Layer 2/3 Mouse Barrel Cortex. Neuron:68–75.

Paller MS, Hoidal JR, Ferris TF (1984) Oxygen free radicals in ischemic acute renal failure in the rat. J Clin Invest 74:1156–1164.

Panahian N, Yoshida T, Huang PL, Hedley-Whyte ET, Dalkara T, Fishman MC, Moskowitz MA (1996) Attenuated hippocampal damage after global cerebral ischemia in mice mutant in neuronal nitric oxide synthase. Neuroscience 72:343–354.

Pang Z-P, Deng P, Ruan Y-W, Xu ZC (2002) Depression of fast excitatory synaptic transmission in large aspiny neurons of the neostriatum after transient forebrain ischemia. J Neurosci 22:10948–10957.

Pascual-Leone A, Freitas C, Oberman L, Horvath JC, Halko M, Eldaief M, Bashir S, Vernet M, Shafi M, Westover B (2011) Characterizing brain cortical plasticity and network dynamics across the age-span in health and disease with TMS-EEG and TMS-fMRI. Brain Topogr 24:302–315.

Paz JT, Christian CA, Parada I, Prince DA, Huguenard JR (2010) Focal cortical infarcts alter intrinsic excitability and synaptic excitation in the reticular thalamic nucleus. J Neurosci 30:5465–5479.

Peel AL, Klein RL (2000) Adeno-associated virus vectors: Activity and applications in the CNS. J Neurosci Methods 98:95–104.

Petersen CCH, Grinvald A, Sakmann B (2003) Spatiotemporal dynamics of sensory responses in layer 2/3 of rat barrel cortex measured in vivo by voltage-sensitive dye imaging combined with whole-cell voltage recordings and neuron reconstructions. J Neurosci 23:1298–1309.

Petito CK, Feldmann E, Pulsinelli WA, Plum F (1987) Delayed hippocampal damage in humans following cardiorespiratory arrest. Neurology 37:1281–1286.

Petreanu L, Huber D, Sobczyk A, Svoboda K (2007) Channelrhodopsin-2-assisted circuit mapping of long-range callosal projections. Nat Neurosci 10:663–668.

Pettersen KH, Devor A, Ulbert I, Dale AM, Einevoll GT (2006) Current-source density estimation based on inversion of electrostatic forward solution: effects of finite extent of neuronal activity and conductivity discontinuities. J Neurosci Methods 154:116–133.

Pfeffer CK, Xue M, He M, Huang ZJ, Scanziani M (2013) Inhibition of inhibition in visual cortex: the logic of connections between molecularly distinct interneurons. Nat Neurosci 16:1068–1076.

Pulsinelli WA, Brierley JB (1979) A new model of bilateral hemispheric ischemia in the unanesthetized rat. Stroke 10:267–272.

Pulsinelli WA, Brierley JB, Plum F (1982) Temporal profile of neuronal damage in a model of transient forebrain ischemia. Ann Neurol 11:491–498.

Qü M, Mittmann T, Luhmann HJ, Schleicher a, Zilles K (1998) Long-term changes of ionotropic glutamate and GABA receptors after unilateral permanent focal cerebral ischemia in the mouse brain. Neuroscience 85:29–43.

Quiroga RQ, Nadasdy Z, Ben-Shaul Y (2004) Unsupervised spike detection and sorting with wavelets and superparamagnetic clustering. Neural Comput 16:1661–1687.

Raha S, Robinson BH (2000) Mitochondria, oxygen free radicals, disease and ageing. Trends Biochem Sci 25:502–508.

Redecker C, Wang W, Fritschy J-M, Witte OW (2002) Widespread and Long-Lasting Alterations in GABAA-Receptor Subtypes After Focal Cortical Infarcts in Rats: Mediation by NMDA-Dependent Processes. J Cereb Blood Flow Metab 22:1463–1475.

Redondo RL, Kim J, Arons AL, Ramirez S, Liu X, Tonegawa S (2014) Bidirectional switch of the valence associated with a hippocampal contextual memory engram. Nature.

Ren JQ, Aika Y, Heizmann CW, Kosaka T (1992) Quantitative analysis of neurons and glial cells in the rat somatosensory cortex, with special reference to GABAergic neurons and parvalbumin-containing neurons. Exp brain Res 92:1–14.

Risher WC, Ard D, Yuan J, Kirov SA (2010) Recurrent spontaneous spreading depolarizations facilitate acute dendritic injury in the ischemic penumbra. J Neurosci 30:9859–9868.

Risher WC, Croom D, Kirov SA (2012) Persistent astroglial swelling accompanies rapid reversible dendritic injury during stroke-induced spreading depolarizations. Glia 60:1709–1720.

Risher WC, Lee MR, Fomitcheva I V, Hess DC, Kirov S a (2011) Dibucaine mitigates spreading depolarization in human neocortical slices and prevents acute dendritic injury in the ischemic rodent neocortex. PLoS One 6:e22351.

Roach GW, Kanchuger M, Mangano CM, Newman M, Nussmeier N, Wolman R, Aggarwal A, Marschall K, Graham SH, Ley C (1996) Adverse cerebral outcomes after coronary bypass surgery. Multicenter Study of Perioperative Ischemia Research Group and the Ischemia Research and Education Foundation Investigators. N Engl J Med 335:1857–1863.

Rose T, Goltstein PM, Portugues R, Griesbeck O (2014) Putting a finishing touch on GECIs. Front Mol Neurosci 7:88.

Rossi DJ, Oshima T, Attwell D (2000) Glutamate release in severe brain ischaemia is mainly by reversed uptake. Nature 403:316–321.

Ruan Y-W, Lei Z, Fan Y, Zou B, Xu ZC (2009) Diversity and fluctuation of spine morphology in CA1 pyramidal neurons after transient global ischemia. J Neurosci Res 87:61–68.

Runyan C a, Schummers J, Van Wart A, Kuhlman SJ, Wilson NR, Huang ZJ, Sur M (2010) Response features of parvalbumin-expressing interneurons suggest precise roles for subtypes of inhibition in visual cortex. Neuron 67:847–857.

Ruscher K, Shamloo M, Rickhag M, Ladunga I, Soriano L, Gisselsson L, Toresson H, Ruslim-

Litrus L, Oksenberg D, Urfer R, Johansson BB, Nikolich K, Wieloch T (2011) The sigma-1 receptor enhances brain plasticity and functional recovery after experimental stroke. Brain 134:732–746.

Sachidhanandam S, Sreenivasan V, Kyriakatos A, Kremer Y, Petersen CCH (2013) Membrane potential correlates of sensory perception in mouse barrel cortex. Nat Neurosci 16:1671–1677.

Schiene K, Bruehl C, Zilles K, Qü M, Hagemann G, Kraemer M, Witte OW (1996) Neuronal hyperexcitability and reduction of GABAA-receptor expression in the surround of cerebral photothrombosis. J Cereb Blood Flow Metab 16:906–914.

Schoenenberger P, Schärer Y-PZ, Oertner TG (2011) Channelrhodopsin as a tool to investigate synaptic transmission and plasticity. Exp Physiol 96:34–39.

Schölvinck ML, Maier A, Ye FQ, Duyn JH, Leopold D a (2010) Neural basis of global resting-state fMRI activity. Proc Natl Acad Sci U S A 107:10238–10243.

Schousboe A (2014) Glutamate Neurotoxicity Related to Energy Failure. In: Handbook of Neurotoxicity, pp 1299–1310. Springer.

Sheng H, Laskowitz DT, Pearlstein RD, Warner DS (1999) Characterization of a recovery global cerebral ischemia model in the mouse. J Neurosci Methods 88:103–109.

Shimamoto K, Lebrun B, Yasuda-Kamatani Y, Sakaitani M, Shigeri Y, Yumoto N, Nakajima T (1998) DL-threo-beta-benzyloxyaspartate, a potent blocker of excitatory amino acid transporters. Mol Pharmacol 53:195–201.

Shin HK, Dunn AK, Jones PB, Boas DA, Moskowitz MA, Ayata C (2006) Vasoconstrictive neurovascular coupling during focal ischemic depolarizations. J Cereb Blood Flow Metab 26:1018–1030.

Shoham D, Glaser DE, Arieli A, Kenet T, Wijnbergen C, Toledo Y, Hildesheim R, Grinvald A (1999) Imaging cortical dynamics at high spatial and temporal resolution with novel blue voltage-sensitive dyes. Neuron 24:791–802.

Shoykhet M, Simons DJ, Alexander H, Hosler C, Kochanek PM, Clark RSB (2012) Thalamocortical Dysfunction and Thalamic Injury after Asphyxial Cardiac Arrest in Developing Rats. J Neurosci 32:4972–4981.

Siesjö BK (1988) Acidosis and ischemic brain damage. Neurochem Pathol 9:31–88.

Siesjö BK, Ekholm A, Katsura K, Theander S (1990) Acid-base changes during complete brain ischemia. Stroke 21:III194–I199.

Silasi G, Boyd JD, Ledue J, Murphy TH (2013) Improved methods for chronic light-based motor mapping in mice: automated movement tracking with accelerometers, and chronic EEG recording in a bilateral thin-skull preparation. Front Neural Circuits 7:123.

Silasi G, Murphy TH (2014) Stroke and the Connectome: How Connectivity Guides Therapeutic Intervention. Neuron 83:1354–1368.

Sohal VS, Zhang F, Yizhar O, Deisseroth K (2009) Parvalbumin neurons and gamma rhythms enhance cortical circuit performance. Nature 459:698–702.

Squire LR (1992) Memory and the hippocampus: a synthesis from findings with rats, monkeys, and humans. Psychol Rev 99:195–231.

Steffensen AB, Sword J, Croom D, Kirov SA, MacAulay N (2015) Chloride Cotransporters as a Molecular Mechanism underlying Spreading Depolarization-Induced Dendritic Beading. J Neurosci 35:12172–12187.

Stroh A, Adelsberger H, Groh A, Rühlmann C, Fischer S, Schierloh A, Deisseroth K, Konnerth A (2013) Making Waves: Initiation and Propagation of Corticothalamic Ca2+ Waves In Vivo. Neuron 77:1136–1150.

Strong AJ, Anderson PJ, Watts HR, Virley DJ, Lloyd A, Irving EA, Nagafuji T, Ninomiya M, Nakamura H, Dunn AK (2007) Peri-infarct depolarizations lead to loss of perfusion in ischaemic gyrencephalic cerebral cortex. Brain 130:995–1008.

Strong AJ, Dardis R (2005) Depolarisation phenomena in traumatic and ischaemic brain injury. Adv Tech Stand Neurosurg 30:3–49.

Stuber GD, Stamatakis AM, Kantak PA (2015) Considerations when using Cre-driver rodent lines for studying ventral tegmental area circuitry. Neuron 85:439–445.

Szydlowska K, Tymianski M (2010) Calcium, ischemia and excitotoxicity. Cell Calcium 47:122–129.

Taniguchi H, He M, Wu P, Kim S, Paik R, Sugino K, Kvitsiani D, Kvitsani D, Fu Y, Lu J, Lin Y, Miyoshi G, Shima Y, Fishell G, Nelson SB, Huang ZJ (2011) A resource of Cre driver lines for genetic targeting of GABAergic neurons in cerebral cortex. Neuron 71:995–1013.

Tantama M, Hung YP, Yellen G (2012) Optogenetic reporters: Fluorescent protein-based genetically encoded indicators of signaling and metabolism in the brain. Prog Brain Res 196:235–263.

Taymans J-M, Vandenberghe LH, Haute C Van Den, Thiry I, Deroose CM, Mortelmans L, Wilson JM, Debyser Z, Baekelandt V (2007) Comparative analysis of adeno-associated viral vector serotypes 1, 2, 5, 7, and 8 in mouse brain. Hum Gene Ther 18:195–206.

Tecuapetla F, Patel JC, Xenias H, English D, Tadros I, Shah F, Berlin J, Deisseroth K, Rice ME, Tepper JM, Koos T (2010) Glutamatergic signaling by mesolimbic dopamine neurons in the nucleus accumbens. J Neurosci 30:7105–7110.

Tennant KA, Adkins DL, Donlan NA, Asay AL, Thomas N, Kleim JA, Jones TA (2011) The organization of the forelimb representation of the C57BL/6 mouse motor cortex as defined by intracortical microstimulation and cytoarchitecture. Cereb cortex 21:865–876.

Teplan M (2002) Fundamentals of EEG measurement. Meas Sci Rev 2:1–11.

Thompson RJ, Zhou N, MacVicar BA (2006) Ischemia opens neuronal gap junction hemichannels. Science 312:924–927.

Tian L, Andrew Hires S, Looger LL (2012) Imaging neuronal activity with genetically encoded calcium indicators. Cold Spring Harb Protoc 7:647–656.

Tian L, Hires SA, Mao T, Huber D, Chiappe ME, Chalasani SH, Petreanu L, Akerboom J, McKinney S a, Schreiter ER, Bargmann CI, Jayaraman V, Svoboda K, Looger LL (2009) Imaging neural activity in worms, flies and mice with improved GCaMP calcium indicators. Nat Methods 6:875–881.

Torrey EF, Barci BM, Webster MJ, Bartko JJ, Meador-Woodruff JH, Knable MB (2005) Neurochemical markers for schizophrenia, bipolar disorder, and major depression in postmortem brains. Biol Psychiatry 57:252–260.

Tortosa A, Ferrer I (1993) Parvalbumin immunoreactivity in the hippocampus of the gerbil after transient forebrain ischaemia: a qualitative and quantitative sequential study. Neuroscience 55:33–43.

Tran S, Chen S, Liu RR, Xie Y, Murphy TH (2011) Moderate or deep local hypothermia does not prevent the onset of ischemia-induced dendritic damage. J Cereb Blood Flow Metab:1–6.

Traversa R, Cicinelli P, Bassi A, Rossini PM, Bernardi G (1997) Mapping of motor cortical reorganization after stroke. A brain stimulation study with focal magnetic pulses. Stroke 28:110–117.

Traystman RJ (2003) Animal models of focal and global cerebral ischemia. ILAR J 44:85–95.

Tye KM, Deisseroth K (2012) Optogenetic investigation of neural circuits underlying brain disease in animal models. Nat Rev Neurosci 13:251–266.

van den Heuvel MP, Hulshoff Pol HE (2010) Exploring the brain network: a review on resting-state fMRI functional connectivity. Eur Neuropsychopharmacol 20:519–534.

van Kerkoerle T, Self MW, Dagnino B, Gariel-Mathis M-A, Poort J, van der Togt C, Roelfsema PR (2014) Alpha and gamma oscillations characterize feedback and feed- forward processing in monkey visual cortex. Proc Natl Acad Sci U S A 111:14332–14341.

Vanni MP, Murphy TH (2014) Mesoscale Transcranial Spontaneous Activity Mapping in GCaMP3 Transgenic Mice Reveals Extensive Reciprocal Connections between Areas of Somatomotor Cortex. J Neurosci 34:15931–15946.

Vidal M, Morris R, Grosveld F, Spanopoulou E (1990) Tissue-specific control elements of the Thy-1 gene. EMBO J 9:833–840.

Vlassenko AG, Vaishnavi SN, Couture L, Sacco D, Shannon BJ, Mach RH, Morris JC, Raichle ME, Mintun MA (2010) Spatial correlation between brain aerobic glycolysis and amyloid-β (Aβ) deposition. Proc Natl Acad Sci U S A 107:17763–17767.

Wang H, Peca J, Matsuzaki M, Matsuzaki K, Noguchi J, Qiu L, Wang D, Zhang F, Boyden E, Deisseroth K, Kasai H, Hall WC, Feng G, Augustine GJ (2007) High-speed mapping of synaptic connectivity using photostimulation in Channelrhodopsin-2 transgenic mice. Proc

Natl Acad Sci U S A 104:8143–8148.

Wang J-H (2003) Short-term cerebral ischemia causes the dysfunction of interneurons and more excitation of pyramidal neurons in rats. Brain Res Bull 60:53–58.

Wang YF, Tsirka SE, Strickland S, Stieg PE, Soriano SG, Lipton SA (1998) Tissue plasminogen activator (tPA) increases neuronal damage after focal cerebral ischemia in wild-type and tPA-deficient mice. Nat Med 4:228–231.

Warden MR, Cardin J a, Deisseroth K (2014) Optical Neural Interfaces. Annu Rev Biomed Eng 16:103–129.

White BC, Grossman LI, O'Neil BJ, DeGracia DJ, Neumar RW, Rafols J a., Krause GS (1996) Global brain ischemia and reperfusion. Ann Emerg Med 27:588–594.

White BR, Bauer AQ, Snyder AZ, Schlaggar BL, Lee J-M, Culver JP (2011) Imaging of functional connectivity in the mouse brain. PLoS One 6:e16322.

Wilson NR, Runyan C a, Wang FL, Sur M (2012) Division and subtraction by distinct cortical inhibitory networks in vivo. Nature 488:343–348.

Witten IB, Lin S-C, Brodsky M, Prakash R, Diester I, Anikeeva P, Gradinaru V, Ramakrishnan C, Deisseroth K (2010) Cholinergic interneurons control local circuit activity and cocaine conditioning. Science 330:1677–1681.

Wu D, Xiong W, Jia X, Geocadin RG, Thakor N V. (2012) Short- and long-latency somatosensory neuronal responses reveal selective brain injury and effect of hypothermia in global hypoxic ischemia. J Neurophysiol 107:1164–1171.

Xie Y, Chen S, Anenberg E, Murphy TH (2013) Resistance of optogenetically evoked motor function to global ischemia and reperfusion in mouse in vivo. J Cereb Blood Flow Metab 33:1148–1152.

Xie Y, Chen S, Murphy T (2012) Dendritic spines and pre-synaptic boutons are stable despite local deep hypothermic challenge and re-warming in vivo. PLoS One 7:e36305.

Xie Y, Chen S, Wu Y, Murphy TH (2014) Prolonged Deficits in Parvalbumin Neuron Stimulation-Evoked Network Activity Despite Recovery of Dendritic Structure and Excitability in the Somatosensory Cortex following Global Ischemia in Mice. J Neurosci 34:14890–14900.

Xie Y, Wang T, Sun GY, Ding S (2010) Specific disruption of astrocytic Ca2+ signaling pathway in vivo by adeno-associated viral transduction. Neuroscience 170:992–1003.

Xu Z, Pulsinelli W (1994) Responses of CA1 pyramidal neurons in rat hippocampus to transient forebrain ischemia: an in vivo intracellular recording study. Neurosci Lett 171:187–191.

Yamawaki N, Borges K, Suter BA, Harris KD, Shepherd GMG (2014) A genuine layer 4 in motor cortex with prototypical synaptic circuit connectivity. Elife 3:e05422.

Yang G, Pan F, Parkhurst CN, Grutzendler J, Gan W-B (2010) Thinned-skull cranial window

technique for long-term imaging of the cortex in live mice. Nat Protoc 5:201–208.

Yiu AP, Mercaldo V, Yan C, Richards B, Rashid AJ, Hsiang H-LL, Pressey J, Mahadevan V, Tran MM, Kushner SA, Woodin MA, Frankland PW, Josselyn SA (2014) Neurons Are Recruited to a Memory Trace Based on Relative Neuronal Excitability Immediately before Training. Neuron 83:722–735.

Yizhar O, Fenno LE, Prigge M, Schneider F, Davidson TJ, O'Shea DJ, Sohal VS, Goshen I, Finkelstein J, Paz JT, Stehfest K, Fudim R, Ramakrishnan C, Huguenard JR, Hegemann P, Deisseroth K (2011) Neocortical excitation/inhibition balance in information processing and social dysfunction. Nature 477:171–178.

Yonekura I, Kawahara N, Nakatomi H, Furuya K, Kirino T (2004) A model of global cerebral ischemia in C57 BL/6 mice. J Cereb Blood Flow Metab 24:151–158.

Yu SP, Canzoniero LMT, Choi DW (2001) Ion homeostasis and apoptosis. Curr Opin Cell Biol 13:405–411.

Zariwala H a., Borghuis BG, Hoogland TM, Madisen L, Tian L, De Zeeuw CI, Zeng H, Looger LL, Svoboda K, Chen T-W (2012) A Cre-Dependent GCaMP3 Reporter Mouse for Neuronal Imaging In Vivo. J Neurosci 32:3131–3141.

Zemelman B V., Lee G a., Ng M, Miesenböck G (2002) Selective photostimulation of genetically chARGed neurons. Neuron 33:15–22.

Zepeda A, Arias C, Sengpiel F (2004) Optical imaging of intrinsic signals: Recent developments in the methodology and its applications. J Neurosci Methods 136:1–21.

Zhan R-Z, Nadler JV, Schwartz-Bloom RD (2006) Depressed responses to applied and synaptically-released GABA in CA1 pyramidal cells, but not in CA1 interneurons, after transient forebrain ischemia. J Cereb Blood Flow Metab 26:112–124.

Zhang D, Raichle ME (2010) Disease and the brain's dark energy. Nat Rev Neurol 6:15–28.

Zhang F, Aravanis AM, Adamantidis A, de Lecea L, Deisseroth K (2007a) Circuit-breakers: optical technologies for probing neural signals and systems. Nat Rev Neurosci 8:577–581.

Zhang F, Gradinaru V, Adamantidis AR, Durand R, Airan RD, de Lecea L, Deisseroth K (2010) Optogenetic interrogation of neural circuits: technology for probing mammalian brain structures. Nat Protoc 5:439–456.

Zhang F, Wang L-P, Brauner M, Liewald JF, Kay K, Watzke N, Wood PG, Bamberg E, Nagel G, Gottschalk A, Deisseroth K (2007b) Multimodal fast optical interrogation of neural circuitry. Nature 446:633–639.

Zhang H, Schools GP, Lei T, Wang W, Kimelberg HK, Zhou M (2008) Resveratrol attenuates early pyramidal neuron excitability impairment and death in acute rat hippocampal slices caused by oxygen-glucose deprivation. Exp Neurol 212:44–52.

Zhang S, Boyd J, Delaney K, Murphy TH (2005) Rapid reversible changes in dendritic spine structure in vivo gated by the degree of ischemia. J Neurosci 25:5333–5338.

Zhang S, Murphy TH (2007) Imaging the impact of cortical microcirculation on synaptic structure and sensory-evoked hemodynamic responses in vivo. PLoS Biol 5:e119.

Zhang Y, Deng P, Li Y, Xu ZC (2006) Enhancement of excitatory synaptic transmission in spiny neurons after transient forebrain ischemia. J Neurophysiol 95:1537–1544.

Zhao S, Cunha C, Zhang F, Liu Q, Gloss B, Deisseroth K, Augustine GJ, Feng G (2008) Improved expression of halorhodopsin for light-induced silencing of neuronal activity. Brain Cell Biol 36:141–154.

Zhao S, Ting JT, Atallah HE, Qiu L, Tan J, Gloss B, Augustine GJ, Deisseroth K, Luo M, Graybiel AM, Feng G (2011) Cell type–specific channelrhodopsin-2 transgenic mice for optogenetic dissection of neural circuitry function. Nat Methods 8:745–752.

Zingg B, Hintiryan H, Gou L, Song MY, Bay M, Bienkowski MS, Foster NN, Yamashita S, Bowman I, Toga AW, Dong H-W (2014) Neural networks of the mouse neocortex. Cell 156:1096–1111.

Zola-Morgan S, Squire LR, Amaral DG (1986) Human amnesia and the medial temporal region: enduring memory impairment following a bilateral lesion limited to field CA1 of the hippocampus.